Earth-Science Reviews 237 (2023) 104275

Contents lists available at ScienceDirect

Earth-Science Reviews

journal homepage: www.elsevier.com/locate/earscirev

The forearc ophiolites of California formed during trench-parallel spreading: Kinematic reconstruction of the western USA Cordillera since the Jurassic

Cemil Arkula [a,b,*], Nalan Lom [a], John Wakabayashi [c], Grant Rea-Downing [d], Abdul Qayyum [a], Mark J. Dekkers [a], Peter C. Lippert [d], Douwe J.J. van Hinsbergen [a,**]

[a] Department of Earth Sciences, Utrecht University, Princetonlaan 8A, 3584, CB, Utrecht, the Netherlands
[b] School of Earth and Climate Sciences, University of Maine, 5790 Bryand Global Sciences Center, Orono, ME 04469, USA
[c] California State University, Fresno, Department of Earth and Environmental Sciences, 2576 East San Ramon Avenue, Mailstop ST-24, Fresno, 93740-8039, CA, USA
[d] Department of Geology and Geophysics, University of Utah, Salt Lake City, UT, USA

ARTICLE INFO

Keywords:
North America
Cordillera
Coast Range Ophiolite
Franciscan Complex
San Andreas Fault
Paleo-ridge
paleomagnetism
GPlates

ABSTRACT

Ophiolites, fragments of oceanic lithosphere exposed on land, are typically found as isolated klippen in intensely deformed fold-thrust belts spanning hundreds to thousands of kilometers along-strike. Ophiolites whose geochemistry indicates that they formed above subduction zones, may have been relics of larger, once-coherent, oceanic lithosphere tracts that formed the leading edge of an upper plate below which subduction occurred; such tracts were subsequently dismembered by deformation and erosion during orogenesis and uplift. However, to what extent the first-order original coherence is maintained between ophiolitic klippen is difficult to assess. Here, we aim to evaluate whether the Jurassic forearc ophiolites overlying subduction complex rocks in California, now scattered over 1000 km and dismembered by the wider San Andreas Fault Zone, still maintain their original lithospheric coherence. To this end we (i) compile available crustal ages from all ophiolite klippen exposed in the Jurassic ophiolite belt of the western United States; (ii) review and kinematically reconstruct post-middle Jurassic deformation that occurred between the modern western coast and the stable North American craton to restore the original positions of the ophiolite fragments relative to each other and to North America, and (iii) perform a paleomagnetic analysis of a sheeted dyke sections of the Mt. Diablo and Josephine ophiolites to estimate the orientation of the spreading axis at which the Jurassic Californian forearc ophiolites formed. The latter analysis reveals that the original ridge orientation likely trended ~080–260°, near-perpendicular to the orientation of the trench along the western margin of the ophiolite belt. We show that with these constraints, a straightforward ridge-transform system can explain the age distributions of the ophiolites with spreading rates of 6–7 cm/a. Our analysis shows that the Jurassic ophiolites of California may be considered klippen of a single sheet of oceanic lithosphere that accreted at a supra-subduction zone spreading ridge. In addition, we show that kinematic and paleomagnetic analysis of ophiolite belts may provide novel constraints on the kinematic evolution of accretionary orogens and the plates now lost to subduction.

1. Introduction

Much of our understanding of the chemical and physical dynamics of plate tectonics comes from the study of ophiolites – fragments of ocean floor that have become tectonically uplifted and are exposed on land (e.g., Dewey, 1976). Ophiolite records provide invaluable sources of information on the formation and evolution of all types of plate boundaries in all main geodynamic environments (Dilek and Furnes, 2011; Furnes and Dilek, 2022). They have been instrumental in identifying mantle and oceanic crustal composition, rheology, melting, and mineralization (Dilek and Furnes, 2011; Moores et al., 2000; Shervais, 2001). Geochemical and geochronological data have revealed ophiolites that formed at mid-ocean ridges far away from subduction zones (Piccardo et al., 2014; Rollinson, 2017), but also in forearcs during

* Corresponding author at: School of Earth and Climate Sciences, University of Maine, 5790 Bryand Global Sciences Center, Orono, ME, 04469, USA.
** Corresponding author at: Department of Earth Sciences, Utrecht University, Princetonlaan 8A, 3584 CB, Utrecht, the Netherlands.
E-mail addresses: cemil.arkula@maine.edu (C. Arkula), d.j.j.vanhinsbergen@uu.nl (D.J.J. van Hinsbergen).

https://doi.org/10.1016/j.earscirev.2022.104275
Received 11 July 2022; Received in revised form 11 November 2022; Accepted 29 November 2022
Available online 6 January 2023

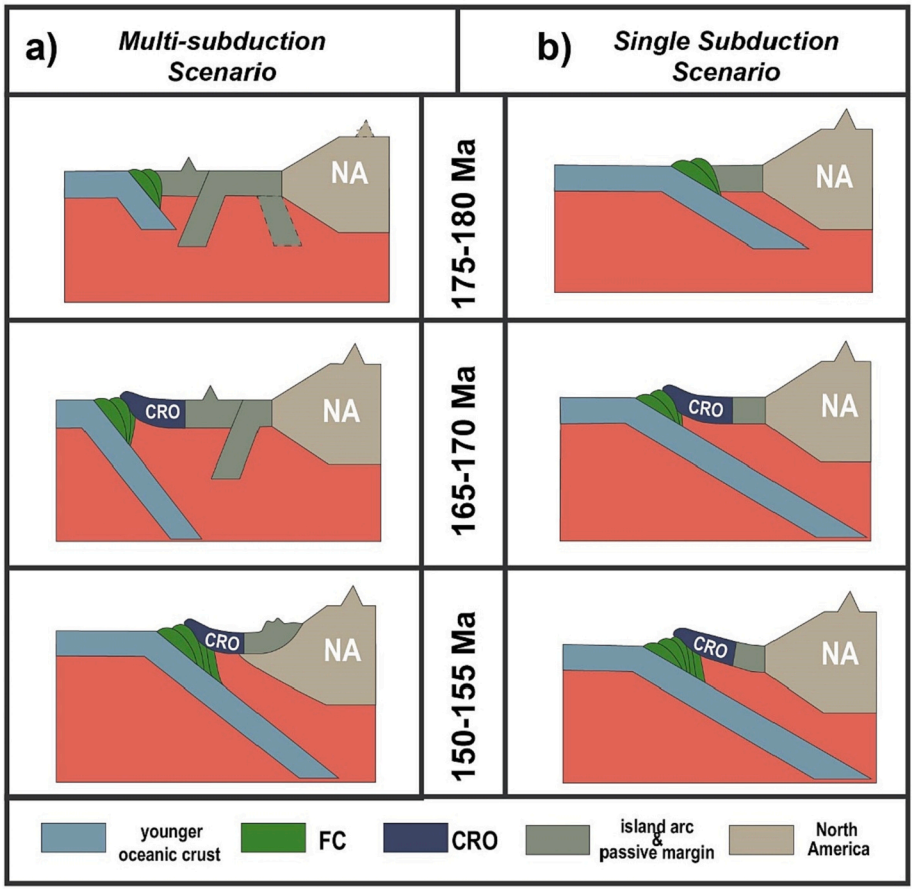

Fig. 1. Schematic diagram illustrating views on possible geodynamic settings for the origin of the Middle to Late Jurassic Californian ophiolites (Coast Range Ophiolites). Left panel (a) is the simplified version of the scenarios in which the ophiolites were formed following eastward subduction initiation in the back-arc of an older, west-dipping subduction zone. Right panel (b) is the simplified version of the scenario in which the ophiolites were formed in the forearc of an eastward subduction zone in which the North American plate was the upper plate. The abbreviations: CRO, Coast Range Ophiolite; FC, Franciscan Comlex, NA, North America.

subduction zone infancy (Pearce et al., 1984; Stern et al., 2012; Stern and Bloomer, 1992). Ophiolites not only contain records of spreading ridges, but also relics of subduction interfaces in the form of metamorphic soles (Guilmette et al., 2018; Hacker et al., 1996), as well as transform faults (Allerton, 1989; Morris and Maffione, 2016). But because ophiolites form and are uplifted at plate boundaries, they typically are dismembered, displaced, and eroded klippen that form the structurally highest thrust sheet in fold-thrust belts (e.g., Maffione et al., 2015b; Porkoláb et al., 2021; Robertson, 2002). With rare exceptions such as in the Semail ophiolite of Oman that covers an area of >20,000 km^2 (Nicolas et al., 2000), the original coherence of these klippen as an ocean floor cannot be directly established from field observations. As a result, it is difficult to establish whether geochemical and temporal variation in ophiolite belts represent a gradual evolution of spreading at a single ridge system, or a sequence of formation in different tectonic settings separated by plate boundary reorganizations (e.g., Hébert et al., 2012; Hopson et al., 2008; Kapp and DeCelles, 2019; Maffione and van Hinsbergen, 2018; Wakabayashi and Dilek, 2003; Wakabayashi and Shimabukuro, 2022).

The Middle to Upper Jurassic ophiolites of California and southern Oregon in the western United States are a prime example of a strongly dismembered, displaced, eroded, and highly incomplete record of ophiolite klippen that lack significant burial metamorphism (Fig. 3). These ophiolites form fragments, each smaller than 150 km^2, scattered along a N-S distance of >1000 km, have crustal ages ranging from ~170 to ~160 Ma and geochemical signatures signaling formation in the forearc above a (nascent) subduction zone (Choi et al., 2008; Harper, 2003; Shervais and Kimbrough, 1985; Snortum and Day, 2020). The isolated ophiolite klippen have been proposed to be part of a once-coherent ocean floor in a supra-subduction zone position, whose formation was underway by ~170 Ma (Harper et al., 1996; Shervais et al., 2005; Shervais and Kimbrough, 1985; Stern and Bloomer, 1992). During their formation, the ophiolites were already in an upper plate position relative to the Franciscan subduction zone to the west as shown by the oldest accreted, metamorphic sole rocks in the Franciscan accretionary prism of ~180 Ma (Mulcahy et al., 2018), but perhaps also to an older subduction zone to the east that was in its waning stages. This older subduction zone was proposed to have consumed the 'Mezcalera Ocean' between the ophiolites and North America, and the arc records of this subduction zone continue until ~150 Ma (Dickinson, 2008) (Fig. 1a). The Jurassic to Neogene tectonic and erosional history has fragmented much of this ocean floor: the ophiolites were uplifted due to formation of an accretionary prism known as the Franciscan Complex whose formation started shortly after subduction initiation and continued until subduction arrest (Wakabayashi, 2015, 2021a). This subduction arrest occurred when the Farallon-Pacific spreading ridge entered the trench in the Oligocene (Atwater, 1989), and was superseded by Pacific-North American plate transform motion, most of which was along dextral faults of the San Andreas fault system in western California. This change in tectonic regime was associated with regional uplift and exposure of the ophiolites, the underlying accretionary prism, and the overlying marine fore-arc basins. This dextral strike-slip fault zone displaced ophiolite klippen relative to each other and relative to cratonic North America over hundreds of kilometers (McLaughlin et al., 1988; McQuarrie and Wernicke, 2005; Suppe, 1970).

In this paper, we attempt to evaluate whether the isolated, dismembered, and displaced klippen of Middle to Upper Jurassic ophiolites of California can simply be interpreted as the product of spreading at a single ridge-transform system. To this end, we first kinematically restore the deformation that affected the western United States since the Jurassic. As a basis, we use the detailed reconstruction of Eocene and younger deformation of McQuarrie and Wernicke (2005).

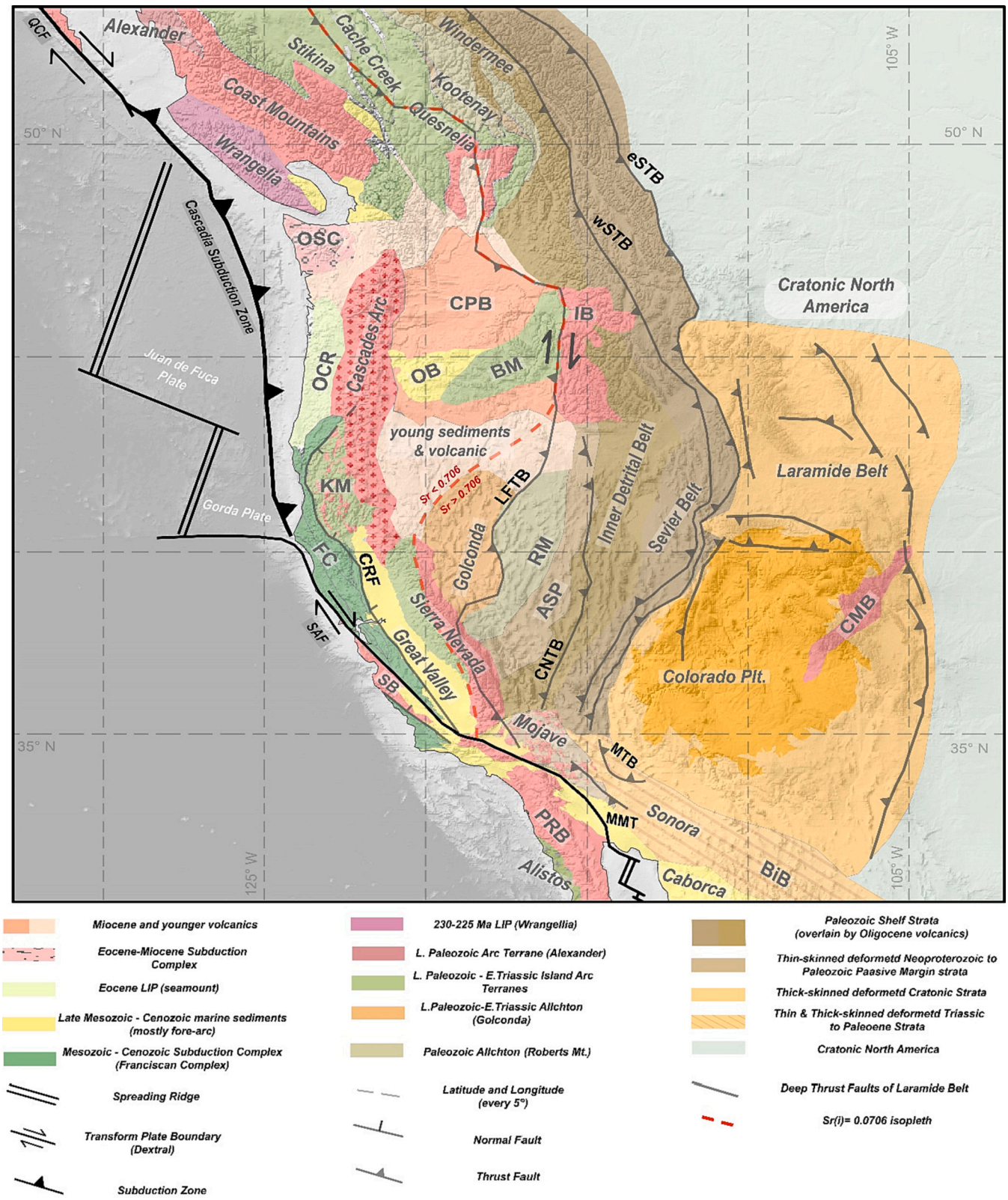

Fig. 2. fore-arc basins (modified from Yonkee and Weil (2015) and Hildebrand (2013)). The gray bold texts are the names of the blocks, which are occasionally written by abbreviations. The abbreviations for block names: ASP, Antler Shelf Platform; BiB, Bisbee Basin; BM, Blue Mountains; CMB, Colorado Mineral Belt; CPB, Columbia Plateau Basalts; FC, Franciscan Complex; IB, Idaho Batholith; KM, Klamath Mountain; MMT, Mule Mountain Thrust; MTB, Maria Thrust Belt; OB, Ochoco Basin; OCR, Oregon Coast Range; OSC, Olympic Subduction Complex; PRB, Peninsula Range Batholith; and RM, Roberts Mountains. The bold black text are the abbreviations for faults: CNTB, Central Nevada Thrust Belt; CRF, Coast Range Fault; eSTB, eastern Seveier Thrust Belt; LFTB, Luning-Fencemaker Thrust Belt; SAF, San Andreas Fault; QSF, Queen Charlotte Fault; and wSTB, western Sevier Thrust Belt.

Their reconstruction, however, was mostly focused on extension in the Basin and Range province. Here we add more details to the kinematic evolution of the San Andreas fault system with the consequent relative motions between ophiolite klippen. In addition, we restore the deformation that accumulated from Jurassic to Eocene time; we also include the more regional deformation of western North America, associated with the Sevier and Laramide orogens (DeCelles, 2004; Yonkee and Weil, 2015). Through this methodology, we restore the positions of the Middle to Upper Jurassic ophiolites relative to each other and to North America. We then evaluate whether the ophiolites and underlying accretionary prism formed in the North American forearc (Shervais et al., 2004), or instead represent an allochthonous and far-traveled complex, relics of which are detected in seismic tomographic images of the lower mantle below the eastern Pacific Ocean and North American continent (Clennett et al., 2020; Sigloch and Mihalynuk, 2013; van der Meer et al., 2010, 2012, 2018).

We present new paleomagnetic results of sheeted dyke complexes and pillow lava sequences from two ophiolitic klippen: the Mt. Diablo and Josephine ophiolites (Fig. 3). We collected these data to reconstruct the paleo-dyke strike using a so-called net tectonic rotation analysis (Allerton and Vine, 1987; MacDonald, 1980), which we then use as a proxy for the forearc ridge orientation. Finally, we place North America and the reconstructed forearc in a paleomagnetic reference frame and use the reconstructed paleo-ridge orientation to model a ridge-transform system that obeys the age distribution of the ophiolites. If such a reconstruction is possible and leads to a reasonable full-spreading rate [i.e., typically not more than ~10 cm/a, with exceptions up to 20 cm/a (Rioux et al., 2013; Wu et al., 2022; Zahirovic et al., 2015)], then the interpretation that the ophiolites represent relics of a coherent upper plate is permissible. Finally, we discuss implications of our study for the causes of ophiolite dismemberment and opportunities to learn about intra-plate geochemical and temporal variation. These variations prompted previous studies to suggest that the ophiolites were derived from more than one generation of oceanic lithosphere (e.g., Hopson et al., 2008; Kosanke, 2000). We also use our results to evaluate which parts of the subduction systems that existed in the eastern Panthalassa Ocean may reside in the western USA, and which parts may be better sought in the Canadian Cordillera to the north, or in the Caribbean region to the South.

2. Kinematic restoration of Mesozoic-Cenozoic deformation in the western USA

2.1. Approach

The first step in our analysis is to reconstruct the relative positions of the Middle to Upper Jurassic Californian ophiolites. To this end, we kinematically restore orogenic deformation in the western USA back to ~170 Ma, the approximate time of ophiolite formation. Our reconstruction was made in GPlates plate reconstruction software (Müller et al., 2018) following reconstruction protocols for restoring orogenic architecture detailed in Boschman et al. (2014) and van Hinsbergen et al. (2020). This protocol restores tectonic deformation within context of (i) a plate circuit, followed by restoration of (ii) continental extension; (iii) strike-slip faulting and (iv) continental shortening, after which (v) a geometrically sound restoration is made that is then (vi) tested against paleomagnetic data for rotations and paleo-latitudinal motions. After all of this, (vii) plates are defined that are surrounded by plate boundaries ending in stable triple junctions.

Because we are concerned with the deformation of the western North American margin, and we do not reconstruct the paleogeography of the downgoing plate from accreted units, our reconstruction here is not dependent on a plate circuit. We also do not attempt to reconstruct all intra-oceanic subduction zones that must have existed in the eastern Panthalassa Ocean to the west of North America in the Mesozoic according to seismic tomographic images of slab remnants, because this requires also reconstructing the accretionary records of the Canadian Cordillera and Alaska (Clennett et al., 2020; Johnston, 2001, 2008; Sigloch and Mihalynuk, 2013; Torsvik et al., 2012; van der Meer et al., 2018). In this paper, we only evaluate the deformation recorded in (i) the ophiolites and underlying accretionary prism, (ii) the North American continental margin and evaluate (iii) whether the Californian ophiolites are far-traveled relative to north America and correlated to-distant intra-oceanic subduction in the Panthalassa Ocean (Clennett et al., 2020), or formed locally in the North American forearc (Pavlis et al., 2019).

As a starting point for our reconstruction of the western North American margin, we adopt the kinematic restoration of the Basin and Range province since 36 Ma of McQuarrie and Wernicke (2005), which was put into GPlates format by Boschman et al. (2018b). We adopt the simple reconstruction of western Mexico as outlined in Boschman et al. (2018b), in which the geology of Baja California and the Guerrero arc is explained in an upper plate setting relative to Farallon Plate subduction. The Guerrero arc formed on a Triassic accretionary prism consisting of North America-derived continental clastic sediments and was separated and subsequently merged with North America by the Jurassic to early Cretaceous (~170–120 Ma) opening and late Cretaceous closure of a narrow oceanic Arperos back-arc basin (Boschman et al., 2018a; Martini et al., 2014). This back-arc basin was part of the extensional system that led to the formation of the Bisbee Basin that lies to the east of that in Mexico and extends into southern New Mexico and Arizona (Dickinson and Lawton, 2001b; Lawton et al., 2020). However, our reconstruction of the western USA margin ends to the north of this basin system and is not dependent on reconstruction choices made for Mexico, where also models of far-traveled allochthony of the Guerrero arc have been proposed (Clennett et al., 2020; Dickinson and Lawton, 2001a).

To restore the relative positions of the Jurassic ophiolites of the western USA, we increase the detail of McQuarrie and Wernicke (2005) reconstruction for the various branches of the San Andreas fault system. To this end, we divided the study area into blocks bounded by faults and reconstruct these using published slip estimates from field correlations. Strike-slip deformation in California is intense and distributed over more faults that we can reconstruct. We therefore simplified the tectonic architecture by modeling deformation distributed over parallel faults separated by less than ~30 km spacing as a single fault. We ignored faults that accumulated fewer than 10 km of documented slip during their activity span. Finally, we restore the deformation history prior to the extension of the Basin and Range province by compiling and restoring strike-slip and shortening estimates in the various fold-thrust belts of the western USA. Our reconstruction retro-deforms a pattern defined by pre-Jurassic geological architecture of western North America, whose geological characteristics are reviewed below.

2.2. Review

2.2.1. Geological architecture of the western USA

The western United States exposes litho-tectonic units characterized by internally coherent stratigraphy and geological evolution separated by major faults, which comprise, from west to east (i) a Mesozoic-Cenozoic subduction-accretion complex (Franciscan Complex) and structurally overlying Middle-Upper Jurassic ophiolites; (ii) Paleozoic to Lower Mesozoic arc complexes (Blue Mountains, Klamath Mountains, and Sierra Nevada); (iii) Paleozoic subduction-accretion complexes (Golconda and Roberts Mountains); (iv) the 'Cordilleran Miogeocline' (Antler Shelf, the Inner Detrital Belt, Sevier Belt, and Laramide Foreland Belt); and (v) the North American Craton (Fig. 2). These belts and their boundaries were intruded by Mesozoic subduction-related batholiths [e.g., Idaho, Siera Nevada, Peninsula Range batholiths, or Colorado Mineral Belt (Fig. 2)].

The Middle to Late Jurassic ophiolites of California and southern Oregon occasionally preserve all elements of the Penrose sequence, but the remnants also frequently miss one or more of the Penrose component

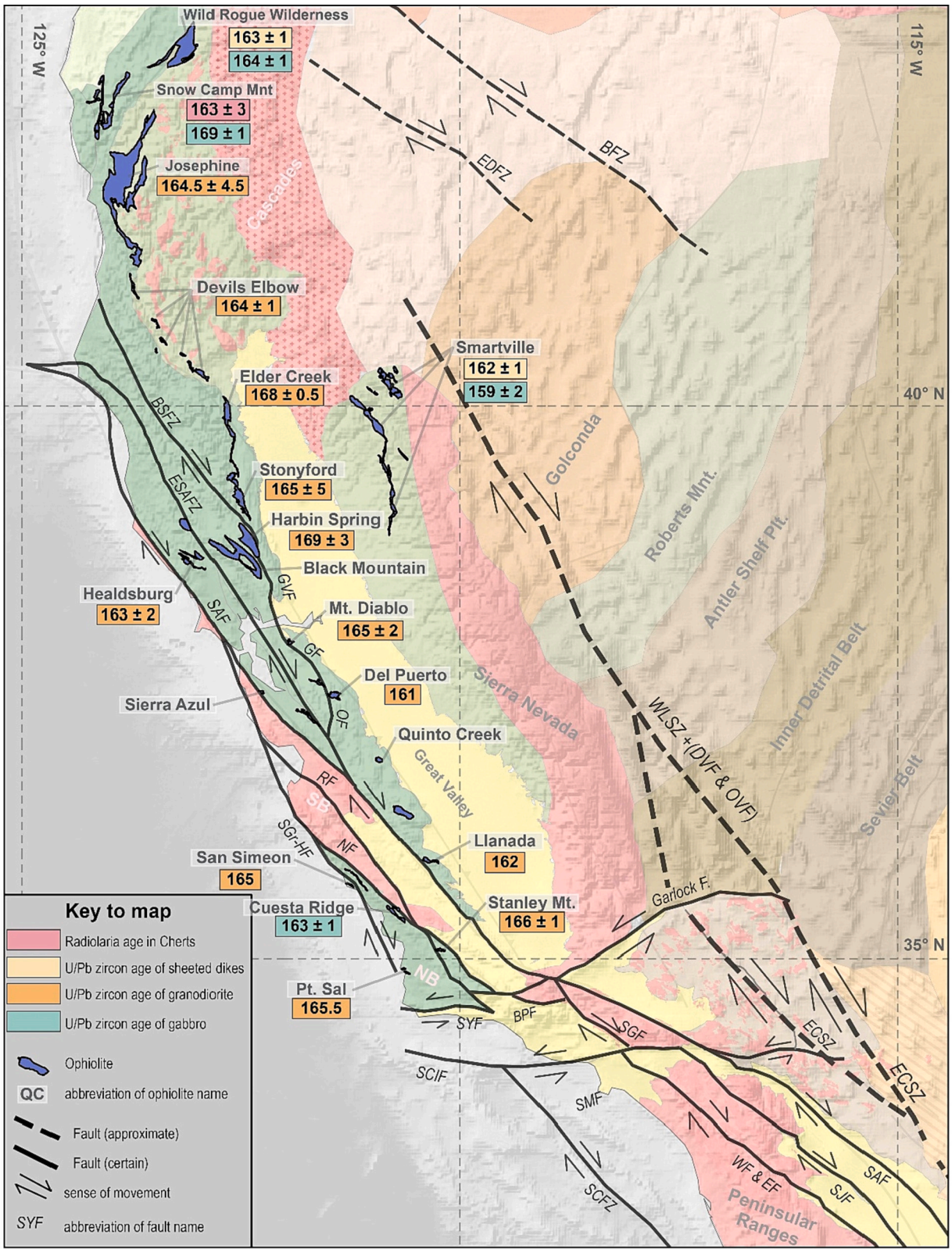

Fig. 3. Middle to Late Jurassic ophiolites with their names and crystallization ages and (block bounding) faults of California and southern Oregon. The exact crystallization ages are in Table 1. The gray bold text are the names of the blocks. The italic abbreviations are the fault names; BFZ, Brothers Fault Zone BPF, Big Pine Fault; BSF, Bartlett Spring Fault; CF, Calavares Fault; DVF, Death Valley Fault; ECSZ, Eastern California Shear Zone EDFZ, Eugene-Denio Fault Zone EF, Elsinore Fault.; EHF, Eastern Huasna Fault; GVF, Green Valley Fault; KCF, Kern Canyon Fault; NB, Nacimiento Block; NF, Nacimiento Fault; OVF, Owens Valley Fault; PRB, Peninsula Range Batholith; RCF, Roger Creek Fault; SB, Salinian Block; SCIF, Santa Cruz Island Fault;; SGF, San Gabriel Fault; SMF, Santa Monica Fault; SYF, Santa Ynez Fault; WF, Whitter Fault; WLSZ, Walker Lane Shear Zone; and WWF, White Wolf Fault.

Table 1
The crystallization and paleontologic ages of Middle to Late Jurassic ophiolites. The youngest zircon uranium-led ages of the Granodiorite and/or sheeted dyke components are written in bold numbers. These components are dated in most of the remnants and are used for our ridge configuration. We paid attention to use dates from sections of ophiolite during our ridge configuration. Abbreviations; Ar, Argon; K, Potassium; Pb, led.

0phiolite	Dated rock type	Age	Method	Reference
Wild Rogue Wilderness	Diorite intrusion in pillow lava sequence	157.2 ± 2 Ma	Hornblende Ar-Ar	Saleeby written commun. 1999 in Kosanke (2000)
	Diorite intrusion in pillow lava sequence	159 ± 1 Ma	Zircon U-Pb	Saleeby written commun. 1999 in Kosanke (2000)
	Diorite intrusion in pillow lava sequence	160 ± 1 Ma	Zircon U-Pb	Saleeby written commun. 1999 in Kosanke (2000)
	Sheeted Dyke Complex	**163 ± 1 Ma**	Zircon U-Pb	Saleeby written commun. 1999 in Kosanke (2000)
	Metagabbro (Part of Ophiolite?)	171.4 ± 3.1 Ma	Hornblende Ar-Ar	Heizler pers. commun. 1998 in Kosanke (2000)
	Metatonalite (High-level Gabbro)	**164 ± 1 Ma**	Zircon U-Pb	Saleeby written commun. 1999 in Kosanke (2000)
Snow Camp Mountain	ages of radiolaria in Chert	**~166–160 Ma**	*Paleontology*	Pessagno et al. (1996)
	Gabbro	**169 ± 1 Ma**	Zircon U-Pb	Saleeby et al. (1984)
Josephine	Plagiogranite (Gabbro-Sheeted dyke complex transition)	162 Ma	Zircon U-Pb	Harper et al. (1994)
	Plagiogranite (Gabbro-Sheeted dyke complex transition)	162 Ma	Zircon U-Pb	Harper et al. (1994)
	Plagiogranite (Gabbro-Sheeted dyke complex transition)	163 ± 5 Ma	Zircon Pb-Pb	Harper et al. (1994)
	Plagiogranite clast in ophiolitic brecia	160 ± 2.5 Ma	Hornblende $Ar^{-}Ar$	Harper et al. (1994)
	Plagiogranite (Gabbro-Sheeted dyke complex transition)	**162 + 7/−2**	Recalculated U-Pb data of Harper et al., 1994	Pálfy et al. (2000)
	Gabbro clast in ophiolitic brecia	164.5 ± 5 Ma	Hornblende ^{40}Ar-^{39}Ar	Harper et al. (1994)
	Gabbro intruded by diabase dykes	165.3 ± 5 Ma	Hornblende Ar-Ar	Harper et al. (1994)
Devils Eldow Remnant	Plagiogranite	**164 ± 1 Ma**	Zircon U/Pb	Wyld and Wright, (1988)
Elder Creek	Plagiogranite	169.7 ± 4.1 Ma	Concordia plots (^{238}U-^{206}Pb vs ^{235}U-^{207}Pb)	Shervais et al. (2005)
	Plagiogranite	**167.9 ± 0.4**	Zircon U-Pb	Mattinson et al. (2008)
	Intruded Qtz diorite sills between gabbro and SDC	172 ± 4 Ma	Concordia plots (^{238}U-^{206}Pb vs ^{235}U-^{207}Pb)	Shervais et al. (2005)
	Gabbro	154 ± 5 to 163 ± 5 Ma	Hornblende K-Ar	McDowell et al. (1984)
Stonyford	Quartz diorote dyke that crosscuts isotropic gabbro	**164.8 ± 4.8 Ma**	Concordia plots (^{238}U-^{206}Pb vs ^{235}U-^{207}Pb)	Shervais et al. (2005)
	Quartz diorote block in melange	163.5 ± 3.9 Ma	Concordia plots (^{238}U-^{206}Pb vs ^{235}U-^{207}Pb)	Shervais et al. (2005)
Smartville	Sheeted Dyke Complex	**162 ± 1 Ma**	Zircon U-Pb	Saleeby et al. (1989)
	Zoned gabbro diorite body intruded in diabese and dykes	159 ± 2 Ma	U-Pb	Day and Bickford (2004)
	Granodiorite body intruded in upper volcanic units	158 ± 3 Ma	Zircon U-Pb	Day and Bickford (2004)
	K-tonalite body intruded in gabbro-diorite & diabase	156 ± 3 Ma	Zircon ^{238}U-^{206}Pb	Day and Bickford (2004)
Harbin Spring	Plagiogranite	**169 ± 3 Ma**	Zircon U-Pb	Mattinson, written commun. 1981 in McLaughlin and Ohlin (1984)
Healdsburg	Plagiogranite	**163 ± 2 Ma**	Zircon U-Pb	Hopson et al. (1981)
Mount Diablo	Late-stage differentietestiates of diabase screen intruded by SDC	165 Ma	Zircon U-Pb	Mattinson pers. commun. 1982 in Mankinen et al. (1991)
	Plagiogranite in Gabbro	**165 ± 2 Ma**	Zircon U-Pb	Mattinson pers. commun. in (Williams, 1983)
Del Puerto	Plagiogranite vein in quartz diorite	**161.1 ± 0.1**	Zircon U-Pb	Mattinson et al. (2008)
	Plagiogranite vein in quartz diorite	**161.2 ± 0.1**	Zircon U-Pb	Mattinson et al. (2008)
	Tonalite related to the cumulates	157 ± 2 Ma	Hornblende ^{40}Ar-^{39}Ar	Evarts et al. (1992)
	dykes cuting the cumulates	150 ± 6 Ma & 149 ± 5 Ma	Hornblende ^{40}Ar-^{39}Ar	Evarts et al. (1992)
	Plagiogranite porphyry that cuts hornblend diorite	155 ± 2 Ma	Zircon U-Pb	Hopson et al. (1981)
Llanada	Albitite	164 ± 3 Ma	Zircon U-Pb	Hopson et al. (1981)
	Albitite	**162.2 ± 0.1**	Zircon U-Pb	Mattinson et al. (2008)
Cuesta Ridge	Plagiogranite	152.5 ± 2.5 Ma	Zircon U-Pb	Hopson et al. (1981)
		166 ± 4 Ma	–	Mattinson and Hopson, 1992 in Dickinson et al. (1996a)
	Gabbro	**163.3 ± 1.1 Ma**	U-Pb, apatite-feldspar isochron	Mattinson pers. commun. 2007, in Hopson et al. (2008)
Stanley Mountain	Plagiogranite	**166 ± 1 Ma**	Zircon U-Pb	Mattinson reported in Hull and Pessagno (1994)
Point Sal & San Simon	Plagiogranite	**165.6 ± 0.01 Ma**	Zircon U-Pb	Mattinson et al. (2008)
Ingalls Ophiolite	Radiolarian Ages	Oxfordian or Kimmeridgian (163–152 Ma)		Miller et al. (1993)
	Gabbro	155 Ma	Zircon U/Pb	Miller et al. (1993)
	Gabbro	161 ± 1 Ma	Zircon U/Pb	Miller et al. (2003)

(s) due to erosion, tectonic dismemberment, or the prevailing conditions during seafloor spreading (Hopson et al., 1981, 2008; Shervais et al., 2004). The ophiolites are scattered klippen and the best-described ones include from north to south the Wild Rogue Wilderness, Snow Camp Mountain, Josephine, Devil's Elbow, Smartville, Elder Creek, Stonyford, Harbin Springs, Geyser Peak (or Black Mountain), Healdsburg, Mount Diablo, Del Puerto, Sierra Azul, Quinto Creek, Llanada, Cuesta Ridge, Stanley Mountain, San Simeon, and Point Sal ophiolites (Dickinson et al., 1996a; Hopson et al., 1981, 2008; Shervais et al., 2004) (Fig. 3). Most of these ophiolites experienced only metamorphism interpreted as seafloor hydrothermal alteration ranging from zeolite to greenschist-grade (Evarts and Schiffman, 1983; Harper et al., 1996; Xenophontos and Bond, 1978).

The Smartville Ophiolite and the Josephine Ophiolite (and its outliers) are often considered as separate belts from the rest of the Californian ophiolites, due to their associations with arc rocks (Hopson et al., 2008; Kosanke, 2000). The Smartville Ophiolite formed in an intra-arc setting (Saleeby et al., 1989) and the Josephine Ophiolite formed in a back arc setting (Harper et al., 1996; Kosanke, 2000). The geodynamic setting of other Californian ophiolites (known as the Coast Range Ophiolite) based on geochemical interpretations have been interpreted as a nascent fore-arc (Shervais et al., 2004) (Fig. 1b) back-arc basin (Dickinson et al., 1996b) (Fig. 1a)—which both indicate supra-subduction zone setting— or at a mid-ocean ridge (Hopson et al., 2008), but geochemical analyses of the last 15 years consistently converge to a supra-subduction zone environment (Choi et al., 2008; Snortum and Day, 2020). This interpretation is consistent with volumetrically minor but widespread HT-HP metamorphic rocks of the Franciscan Complex structurally below the ophiolites that are interpreted as remnants of a metamorphic sole that yield ages overlapping with and predating (~6 Ma) the crystallization ages of magmatic sections of the ophiolites (Anczkiewicz et al., 2004; Harper et al., 1990, 1996; Mulcahy et al., 2018; Rutte et al., 2020; Wakabayashi and Dilek, 2003).

The ages of the ophiolites range between ~160 and ~170 Ma and are derived from U/Pb zircon geochronology on mostly plagiogranites and quartz diorites and some $^{40}Ar/^{39}Ar$ hornblende ages (Table 1) (Fig. 3). We will use these ages to determine whether the Middle-Late Jurassic ophiolites, that may have formed in different positions relative to arc and trench, after reconstruction into their original configuration corrected for post-Jurassic deformation, may straightforwardly be explained by spreading at a single SSZ ridge-transform system.

Most of the Middle to Upper Jurassic ophiolites of California are structurally underlain by the Franciscan Accretionary Complex that formed by episodic accretion of ocean plate stratigraphy (Wakabayashi, 2015), i.e. pillow lavas, oceanic pelagic sediments, and trench fill continental clastic sedimentary rocks that form the typical stratigraphy of oceanic crust approaching a trench (Isozaki et al., 1990) (Fig. 2 & 3). The oldest accreted material of Franciscan Complex comprises amphibolites, garnet-amphibolites, eclogites, and coarse blueschists (with amphibolite or eclogite relics), that likely formed during early stages of oceanic subduction (Cloos, 1985; Platt, 1975; Wakabayashi, 1992; Wakabayashi and Dumitru, 2007). These rocks have yielded Lu-Hf garnet ages ranging from 153 to 176 Ma, U-Pb metamorphic zircon ages of ca.157 to 176 Ma and Ar-Ar hornblende ages of ca. 155–168 Ma (Mulcahy et al., 2018; Ross and Sharp, 1988; Rutte et al., 2020; Shervais et al., 2011; Wakabayashi and Dumitru, 2007). The ca. 176 Ma Lu-Hf garnet and U-Pb zircon ages of Mulcahy et al. (2018) suggest initiation of Franciscan subduction 6 Ma before the earliest crystallization ages of the overlying Coast Range ophiolite. Such time lags between subduction and upper plate spreading and sole cooling have recently also been uncovered from ophiolites in the Tethyan realm (Turkey, Oman, Tibet) and may be common in subduction zone infancy (Guilmette et al., 2018; Pourteau et al., 2019). The extended time span of Franciscan high-temperature metamorphism is longer than that recorded in other metamorphic soles and subduction complexes, with the possible exception of the Sanbagawa Belt of Japan (Wakabayashi and Shimabukuro, 2022).

The trench fill clastic rocks form ~90% of the volume of the Franciscan Complex, and the youngest depositional ages in the accreted sequences, which approximate the age of accretion (Isozaki et al., 1990; Wahrhafting, 1984) where rocks are too insufficiently metamorphosed to yield datable minerals (Dumitru et al., 2010, 2015, 2018). The ages of accretion decrease structurally downward and westward in the Franciscan Complex, from ~180 to ~12 Ma (Dumitru et al., 2015, 2018; Ernst, 2011; Wakabayashi, 2015, 2021b; Mulcahy et al., 2018). The total structural thickness of the accreted tectonic stack, as well as the ages of accretion of units and their lithologic character vary significantly along strike (Wakabayashi, 2022). Collectively, the Franciscan complex is interpreted to reflect the incomplete accretionary record of a continuous subduction history from the Jurassic to the Miocene, but with alternating and along-strike varying episodes of accretion and non-accretion/subduction erosion (Raymond, 2018; Wakabayashi, 2015, 2021b), a common phenomenon in accretionary systems (Isozaki et al., 1990, 2010; van Hinsbergen and Schouten, 2021).

Along most of the western North American margin, accretion involved 300 to 700 m thick ocean plate stratigraphy (OPS) sequences of the Franciscan complex, which were thickened by imbrication (Wakabayashi, 2021b). An exception is the Siletzia terrane that accreted around 50 Ma to the north of California, from Oregon to southern British Columbia, as a large, coherent accreted domain (Fig. 2 & 5). The Siletzia terrane (~55–50 Ma) consists of basalts interpreted as a large igneous province (LIP) that formed on subducting oceanic crust of the Farallon Plate from a presumed mantle plume around ~55 Ma, not far from the subduction zone below North America. Accretion of the Silezia LIP to the western North American orogen occurred around ~50 Ma (McCrory and Wilson, 2013; Snavely et al., 1968; Wells et al., 2014) (Fig. 5b & 5c).

In the Mojave Desert region of southern California, accretionary prism rocks known as Pelona-Orocopia-Rand (POR) and related schists consist of OPS that were metamorphosed typically under greenschist to amphibolite grade and at some locations (e.g., at San Emigdio SE of Sierra Nevada batholith) under lower granulite facies i.e. at higher temperature conditions than in the Franciscan Complex to the north, and are now exposed in tectonic windows (Chapman, 2017; Chapman et al., 2016). These rocks are not shown on our figures because they occupy only small areas. Along the central California coast is the Nacimiento Belt, which is commonly considered as part of the Franciscan Complex (Ernst, 1980). Recent studies, interpreted the Nacimiento Belt as the northwestward displaced (together with Salinian Pluton) up-dip correlative of Pelona-Orocopia-Rand schists based on identical detrital zircon age populations of clastic rocks (Chapman, 2017; Chapman et al., 2016) (Fig. 3). Metamorphic and accretion ages of Nacimiento Belt rocks overlap with those of the Franciscan Complex and they are interpreted to have formed at the same subduction plate boundary (Chapman et al., 2011, 2016; Jacobson et al., 1996, 2011; Kidder and Ducea, 2006).

The Middle to Upper Jurassic ophiolites are unconformably overlain by clastic sedimentary rocks of the Great Valley Group that is interpreted as a series of forearc basin deposits (DeGraaff-Surpless et al., 2002; Surpless et al., 2006; Williams and Graham, 2013). The oldest rocks of the Great Valley Group yielded maximum depositional ages constrained from detrital zircon geochronology of ~153–148 Ma (Orme and Surpless, 2019). Sediment provenance studies of the Great Valley Group, in Jurassic as well as Cretaceous clastic sedimentary rocks, have shown that detrital zircon age spectra are straightforwardly explained by a provenance from the North American margin to the east (DeGraaff-Surpless et al., 2002; Orme and Surpless, 2019; Williams and Graham, 2013). Detrital zircon spectra from trench fill clastics in the Franciscan Complex reveal maximum depositional ages of mostly ~120 Ma and younger. They are also consistent with a sediment provenance from the North American margin to the east, including its cratonic basement and accreted magmatic arcs (Sierra Nevada, Klamath Mountain, and Idaho) (Dumitru et al., 2015). The Cretaceous (ca. 113–86 Ma) Ochoco basin around the accreted Siletzia terrane, is likely the northward

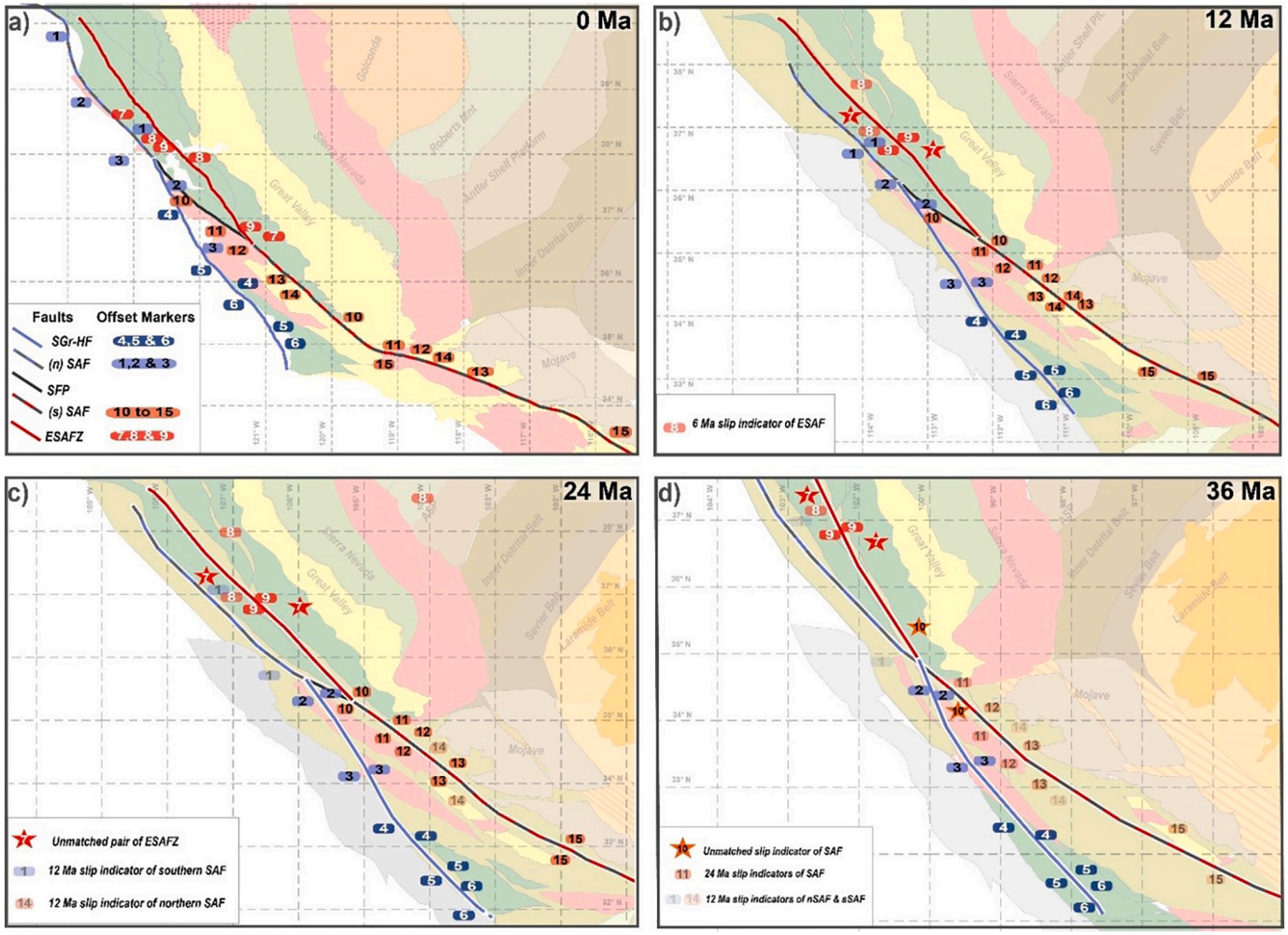

Fig. 4. (a) Offset Markers of San Andreas Fault System at present, and at (b)12 Ma, (c) at 24 Ma, and (d) at 36 Ma. The offset markers that record a part of the whole slip are shown semi transparently, and the offset markers that miss match are shown by stars. The details of the offset Markers are given in Table 2.

continuation of the Great Valley forearc basin (Surpless and Gulliver, 2018).

Structurally above the Franciscan Complex, and east of the Middle to Upper Jurassic ophiolites, two Upper Paleozoic to Jurassic island arc complexes with mélange units are exposed in the Blue Mountains, the Klamath Mountains, the northern Sierra Nevada range and the western Foothills of southern Sierra Nevada. These units are correlated with units in the Intermontane Belt of Canada (Dickinson, 2008; Ernst et al., 2008; Schwartz et al., 2011) (Fig. 2). The interpretations of these arc complexes vary between authors and between outcrops, but these arc complexes contain the youngest evidence for possible subduction east of the Franciscan complex, that could have accommodated convergence between the North American continental margin and the Franciscan complex and overlying Middle to Upper Jurassic ophiolites. If the Blue Mountains-Klamath Mountains and Sierra Nevada arc units represent intra-oceanic arc complexes, then they were located during their activity west of the North American continental margin above a west-dipping subduction zone, perhaps alongside a second subduction zone that dipped east below the continental margin (Dickinson, 2008; Ernst et al., 2008; Schwartz et al., 2011; Wakabayashi et al., 2010) (Fig. 1a). The timing of emplacement of the intra-oceanic arc complexes over the western North American margin estimated from deformation and sediment provenance studies (e.g., of the Great Valley Group, see above) varies along strike and may be diachrounous, or laterally irregular. At the Intermontane Belt of Canada (a northern equivalent of the system), Blue Mountains, Klamath Mountains, and Sierra Nevada (entire northern range and western foothills of the southern part), the emplacement is estimated between Middle Jurassic (~169 Ma) and ~150 Ma at the youngest (Fig. 5e) (Dickinson, 2008; Edelman and Sharp, 1989; LaMaskin et al., 2022; Schwartz et al., 2011). A detailed analysis of the pre-late Jurassic history of accretionary orogenesis of the Cordillera is beyond the scope of our paper and not essential for our analysis, but it is important to note that the Middle to Late Jurassic ophiolites of California may have formed in the waning stages of westward subduction below the Klamath-Blue Mountain-Sierra Nevada Foothills, during a subduction polarity reversal (Wakabayashi et al., 2010). The Smartville and possibly Josephine ophiolite complexes may preserve relics of this older oceanic arc system, within which Middle-Late Jurassic seafloor spreading formed the Middle to Upper Jurassic Californian ophiolites (Yule et al., 2006). In this case, it is possible that until ~150 Ma, the upper plate in which the Middle-Upper Jurassic Californian Ophiolites formed was mobile relative to the continental margin to the east (Fig. 1a & 5f). After this time, the only known record of subduction-accretion is to the west of and structurally below the ophiolites in the Franciscan Complex. From at least ~150 Ma onward, the Middle to Upper Jurassic ophiolites formed the underpinnings of the North American forearc basin that was gradually filled during the Late Jurassic, and spilled into the trench leading to accretion of the oldest North America-derived clastic sedimentary rocks below the ophiolites in Early Cretaceous time (Orme and Surpless, 2019).

To the east of the accreted intra-oceanic arcs, the Golconda and Roberts Mountains Allochthons represent OPS units derived from

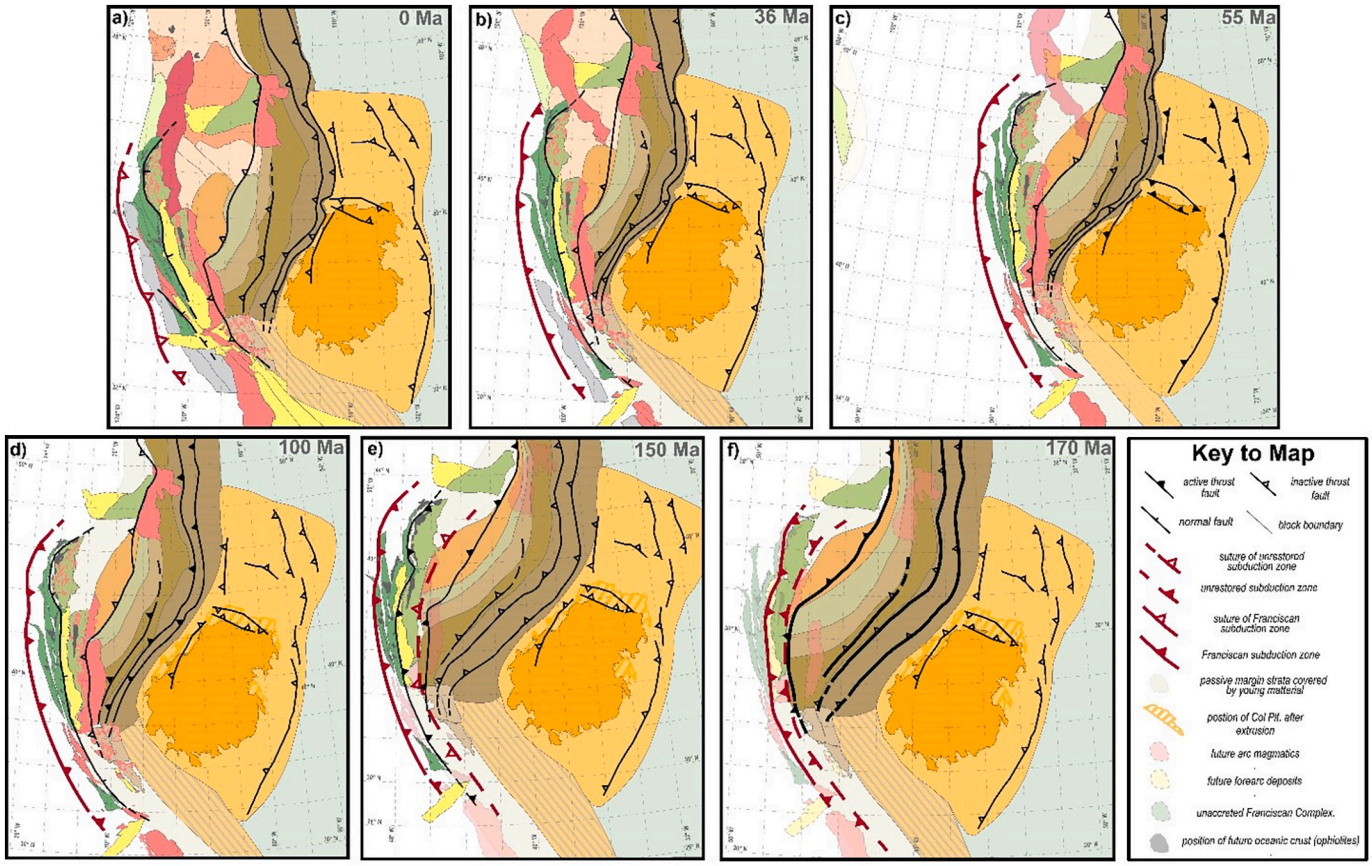

Fig. 5. The geological map of western United States (the reconstruction area) at present day, and the reconstructed geological maps at (b) 36 Ma, (c) 55 Ma, (d) 100 Ma, (e) 150 Ma, (f) 170 Ma in global frame. See the legend of Fig. 2 for the names of the blocks and faults. The red dashed west dipping suture and subduction zone in (e) and (f) are the probable locations of pre-150 Ma Mezcalara subduction zone (see text for further explanation).

Paleozoic ocean floor that accreted to the continental margin units in Late Paleozoic to Triassic time (Dickinson et al., 2000). This continental margin comprises Ordovician-Devonian shelf strata known as the Antler Shelf Platform (Fig. 2), which is widely regarded as part of the North American Cordilleran passive margin (or miogeocline) (Speed and Sleep, 1982; Yonkee and Weil, 2015). Models that aim to explain anomalously low paleomagnetic inclinations that are systematically found in the Canadian Cordillera have suggested that the Antler Shelf may have been part of a kinematically independent ribbon continent that may have moved relative to North America until well into the Cretaceous (Hildebrand, 2009; Johnston, 2008). There is, however, currently no known geological record of post-Jurassic subduction anywhere between the Middle to Upper Jurassic ophiolites of California and the North American Craton, and whether and how the anomalously low Cordilleran inclinations are tectonically explained remains enigmatic (Pavlis et al., 2019).

East and south of the Antler Shelf are the Inner Detrital Belt, the Sevier Thrust Belt, and the Laramide Foreland Belt, which contain polydeformed Paleozoic strata, high-grade metamorphic rocks, and Neoarchean crystalline basement (Hildebrand, 2013; Yonkee and Weil, 2015). These units have similar lithologies and the boundaries of the belts are defined by the style of *E*-W shortening that occurred in Late Jurassic to Cenozoic time. The Laramide Foreland Belt is characterized by thick-skinned, basement-involved thrusting (Allmendinger, 1992; Erslev et al., 1993), while thrusting in the Sevier Thrust Belt was thin-skinned, and the Detrital Belt escaped major shortening (Allmendinger, 1992; Armstrong, 1968; DeCelles and Coogan, 2006).

The litho-tectonic belts described above are intruded by the Sierra Nevada, Idaho, and Peninsular Range Batholiths (Fig. 2). These plutonic rocks are interpreted as a Mesozoic magmatic arc related to the eastward subduction that is recorded in the Franciscan accretionary complex (Gaschnig et al., 2011; Yonkee and Weil, 2015) (Fig. 2 & 5). The Sierra Nevada Batholith is the most prominent of these and consists of approximately north-south striking zones that display a gradual variation from dioritic to more felsic composition between 140 and 80 Ma (Balgord et al., 2021; Kistler et al., 2014; Nadin and Saleeby, 2008; Saleeby et al., 2008).

Geochemical analyses have recognized a marked transition in the Mesozoic arc (Idaho, Sierra Nevada, Peninsula Range Batholiths) where the initial $^{87}Sr/^{86}Sr$ (Sr_i) isotope ratios to the west are lower and to the east are higher than 0.706. This boundary is interpreted to result from crustal contamination, signaling a change from ocean-derived (OPS, ophiolite) accreted rocks allochthonous to the North American continent to the west, to continental lithosphere in the east (Gaschnig et al., 2011; Kistler et al., 2014; Saleeby et al., 2008) (Fig. 2).

The Salinian plutons exposed in southwestern California (Fig. 3 & 4a) are currently flanked to the east and west by rocks of the Franciscan accretionary complex and overlying ophiolites, but their Sr isotopes signatures suggests that they are underlain by continental lithosphere of the North American margin. These plutonic rocks are commonly interpreted as intruded in the North American margin and displaced by post-Middle Cretaceous strike-slip dissection (Fig. 3 & 4) (Graham, 1978). Another anomaly to the overall trend of the Mesozoic Arc is the Colorado Mineral Belt (75–43 Ma), which is located ~1200 km farther inboard than other arc-related magmatic rocks (Fig. 2) (Chapin, 2012). Explanations for this outlying arc are commonly sought in anomalous Late Cretaceous flat slab subduction (Chapin, 2012).

In Washington and Oregon, the litho-tectonic belts described above are intruded and overlain by the upper Cenozoic Cascades Arc and Columbia River Basalts (Fig. 2). Magmatism of the Cascades Arc occurs

Table 2
The estimated displacements for the faults of San Andreas Fault System. The offset markers (1 to 15) of these estimates are shown in Fig. 4.

Faults	Offset Marker	Slip & timing of slip	Evidence	Reference
ESAFZ	**ESAFZ (7)**	230–250 km since 12–13 Ma	Lithological Similarities/oldest fault related basin	Wakabayashi (1999b);Wakabayashi and Dumitru (2007)
ESAFZ	**ESAFZ (9)**	160–170 km since 11.1 Ma	correlation of volcanic units	McLaughlin et al. (1996); and Ford et al. (2003)
ESAFZ	**ESAFZ (8)**	50–70 km Post 6 Ma	lithological correlations	McLaughlin et al. (1996)
ESAFZ	**ESAFZ (8)**	40–45 km [1]; >30 km [2]Post 8 Ma	lithological correlations	Wagner et al. (2005) [1]& Ford et al. (2003)[2]
ESAFZ &SAF	**SAF (10)**	~320 km Post Eocene	stratigraphic, paleoenviromental and lithologic correlations	Clarke (1973); Graham et al. (1989); &Dickinson et al. (2005)
ESAFZ &SAF	**SAF (11)**	305–320 km since 24 Ma	clast source relation, magmatic anomaly, lithologic correlation	Sims (1993); Griscom et al. (1990); & other refferences in Burnham, 2009
San Andreas Fault	**SAF (12)**	315 ± 5 km Post 23.5 Ma	correlation of volcanic units	Matthews, (1976)
San Andreas Fault	**SAF (13)**	300 km Post 23 Ma	Magmatic anomaly	Griscom et al. (1990)
San Andreas Fault	**SAF (14)**	216 km Post 12 Ma	clast-source relation	Sims (1993)
San Andreas Fault	**SAF (15)**	310 km btween 23.7 & 1.6 Ma	Gravity high and lithological correlation	Griscom et al. (1990)
San Andreas Fault	**(n)SAF(1)**	228 ± 13 km since 7 Ma	Lithological correlation	McLaughlin et al. (2005) in Burnham (2009)
SGr-(n)SAF	**SGr-northern SAF (2)**	180 ± 5 km Post Eocene Ma	Lithological and stratigraphic correlations, magmatic anomaly	Burnham (2009) and the refferences there in
SGr-(n)SAF	**SGr-northern SAF (3)**	~ 150 km Post 12–11 Ma & 180 km Post Eocene	clast source relation, lithologic and geochemical correlations	Burnham (2009) and the refferences there in
SGr-HF	**SGr-HF (4)**	155 km Post 11 Ma	magmatic anomaly and stratigraphic correlations	Dickinson et al. (2005); and Langenheim et al. (2013)
SGr-HF	**SGr-HF (5)**	122 km	magmatic anomaly and stratigraphic correlations	Graham and Dickinson (1978)Langenheim et al. (2013)
SGr-HF	**SGr-HF (6)**	90 km Post 16 Ma	magmatic anomaly and stratigraphic correlations	Burnham (2009) and refferences there in; & Langenheim et al. (2013)

above the still-active Cascade subduction zone, where the Juan de Fuca plate subducts beneath North America (Fig. 2). The arc has been active for >40 Ma, since the accretion of the Siletzia LIP (du Bray and John, 2011). The Middle to Upper Miocene Columbia River Basalts to the east are interpreted as products of the same mantle plume that formed the Siletzia LIP. This plume migrated beneath the upper plate of the Cordilleran subduction system due to the ongoing absolute westward motion of North America and associated slab retreat (Camp and Hanan, 2008; Hooper et al., 2007).

2.2.2. *Kinematic constraints on Post-Middle Jurassic deformation*

2.2.2.1. San Andreas fault system. The youngest prominent deformation phase affecting the western US is the transform motion along the San Andreas-Gulf of California fault system. This deformation mostly affected the geological units located west of the Mesozoic magmatic arc and the Great Valley Basin (Fig. 4 & 5). The transform regime originated when the Farallon plate entirely subducted beneath North America due to arrival of the Farallon-Pacific spreading ridge in the trench; Pacific-North America motion was nearly parallel to the former trench inducing transform motion, but with an extensional component (Atwater, 1989). It is possible that dextral strike-slip motion was present prior to the arrest of subduction, as reconstructed North America-Farallon convergence had a dextral oblique component (Burnham, 2009; Sharman et al., 2013). During the last stages of Farallon subduction in the late Eocene and Oligocene, the western US underwent widespread extension forming the Basin and Range province, exhuming a large mosaic of metamorphic core complexes. The impact area of this extension reached east of the Colorado Plateau, including almost all units east of the Mesozoic continental magmatic arc described above (McQuarrie and Wernicke, 2005; Wernicke, 1981; Wernicke et al., 1992). Absolute plate motion models (e.g., Doubrovine et al., 2012) show that North America was moving westward relative to the mantle throughout this time window, and Basin and Range extension must thus have resulted from slab roll-back that outpaced upper plate advance (Boschman et al., 2018b). This was perhaps facilitated by the decreasing width of the slab upon the arrival of ridge segments in the trench (Schellart et al., 2010).

The reconstruction of McQuarrie and Wernicke (2005) that we use as basis for our reconstruction mostly focused on restoring the extension in the Basin and Range province. In their reconstruction, the dextral component of the San Andreas system was modeled as a single San Andreas Fault, which accommodated 315 ± 10 km dextral motion since 16 Ma. Because the ophiolites of California are located between numerous branches of the San Andreas Fault System, we increase the detail of the McQuarrie and Wernicke's (2005) reconstruction by partitioning the total displacement of the San Andreas Fault over the main branches. The reconstructed faults are described below from west to east, and details and references are provided in Table 2, 3, 4, 5 and 6.

The westernmost onshore faults in the central part of the reconstructed area are the San Gregio and Hosgri Faults (SGHF), which we simplify to a single block-bounding fault, due to their proximity and parallelism, between the NW corner of Western Transverse Range and the San Andreas Fault at Point Reyes (Fig. 3 & 4). The SGHF separates the Point Reyes and Gualala Blocks, located west of the San Andreas Fault, from the Salinian Block (Fig. 3 and 4) (Table 2). Offset markers (O.M.s) suggest a southward decreasing amount of displacements for the San Gregio-Hosgri Fault (Fig. 4) (Table 2). The decrease in slip suggests that the smaller-offset markers may have formed after fault initiation or may result from erroneous offset-marker identification. A re-evaluation of the southernmost offset markers, Pt. Sal and San Simeon (Fig. 4; O.M. 6) that consist of identical Coast Range Ophiolite remnants covered by Miocene strata, did not suggest a dextral tectonic displacement prior to Miocene (Colgan and Stanley, 2016).

Between the San Gregio-Hosgri Fault and the San Andreas Fault, dextral deformation has been partitioned over the Rinconada, Eastern Huasna, and Nacimiento Faults (Fig. 3) (Table 3). The Nacimiento Fault forms the boundary between displaced continental margin arc plutons of the Salinian Block and the Nacimiento subduction-accretion assemblage (Chapman et al., 2016; Ingersoll, 2019; Johnston et al., 2018). Each of these faults has several tens of km of displacement (Table 3).

The most prominent of the Californian dextral faults is the San Andreas Fault whose clearest offset markers are the Neenach and Pinnacles Volcanics (both 23.5 Ma), which have been offset by ~310 km

Table 3
The estimated applied displacements for Cenozoic dextral faults (except San Andreas Fault System).

Fault Zone	Applied Slip	Estimated Slip	Evidence	Reference
Eastern ECSZ (Ludlow and Bistol Mnt. Fault)	**36 km since 4 Ma/ e-ECSZ**	36 km (12 + 24) Post Miocene	Magmatic Anomaly & field relations	Jachens et al. (2002); &Lease et al. (2009),
Central Mojave ECSZ - Pisgah&Rodman, Blackwater&Calico, Camp Rock, Lenwood, and Heledale Fault	**25 km since 4 Ma/ CM-ECSZ**	25 km since likely since 6–8 Ma	Magmatic Anomaly & field relations	Dixon and Xie (2018); &Dokka and Travis (1990b)
Eastern California Shear Zone	**65 km since 4 Ma/ ECSZ**	53 ± 6 km	Revision of structural data	McQuarrie and Wernicke (2005)
Eastern California Shear Zone	**65 km since 4 Ma ECSZ**	between 65 & 100 km	Stratigraphic and structural correlations	Dokka and Travis (1990b); & Oldow et al., 2008
Walker Lane Shear Zone	**65 km since 4 Ma/ WLSZ**	20–30 km since 9–3 Ma	Oligocene Paleovalley	Faulds et al. (2005)
Walker Lane Shear Zone	**65 km since 4 Ma/ WLSZ**	100 ± 10 km	Revision of Structural data	McQuarrie and Wernicke, 2005
WLSZ Stateline & Hunter Mountain-Panamit Valley Faults	**65 km since 4 Ma/ WLSZ**	30 ± 4 km Post 13 Ma & 9.3 km Post 4 Ma	Lithologic correlations	Guest et al., 2007; and Gourmelen et al. (2011)
Death Valley Fault Zone	**65 km since 4 Ma/ WLSZ**	<8 km	Late Precambrian isopach data	Wright and Troxel (1966) in Butler et al. (1988)
Death Valley Fault Zone	**65 km since 4 Ma/ WLSZ**	35 km Post Miocene	matching gravels of alluvial fan	Butler et al. (1988)
Death Valley Fault Zone	**65 km since 4 Ma/ WLSZ**	50 km	reinterpreation of the Late Precambrian isopach data	Hamilton and Myers (1966)
Death Valley Fault Zone	**65 km since 4 Ma/ WLSZ**	80 km	reinterpreation of the Late Precambrian isopach data	Stewart (1967)
Ortigalita & Greenville	**10 km since 18 Ma/ Of-GF-GVF-BSFZ**	12 km & 6 to 10 km slip	Lithological correlations	Wakabayashi, 1999b
Bartlett Spring Fault Zone	**11 km since 18 Ma/ Of-GF-GVF-BSFZ**	47–53 km Post Cretaceous (?)	Lithological correlations	Ohlin et al. (2010)
Rinconada Fault	**44 km since 16 Ma/ RF**	39–43 km since early Miocene	magmatic anomaly & Miocene paleo-isobaths	Langenheim et al. (2013);
Rinconada Fault		18 km slip since Pliocene	Gravity anomaly and lithologic correlations	Langenheim et al. (2013) and refferences there in
Rinconada Fault		64–72 km Post Cretaceous	lithologic correlations	Schwade et al., 1958; and Diblee 1976 in Langenheim et al. (2013)
Pilarcitos	**0 km**	250 km [1]; 155 – 122 km [2] since Miocene	regional correlations	Powell (1993) [1]; Griscom et al. (1990);McLaughlin et al. (1996) [2]
Pilarcitos	**0 km**	<7 km	field relations	Wakabayashi (1999b)
Nacimiento Fault	**73 km since 36 Ma / NF**	>90 km Post-Eocene	lithologic correlations	Vedder et al. (1991)
Easter Huasna Fault	**17 km since 12 Ma/ EHF**	25 km	magmatic anomaly	Langenheim et al. (2013)
San Gabriel Fault	**70 km since 11 Ma /SGF**	~45 km Post 13 Ma	regional correlations and field relations	Powell and Weldon (1992)
San Jacinto Fault	**24 km since 11 Ma /SJF**	25 km	lithologic correlations	Sharp (1981)
Elsinore Fault Zone	**44 km since 11 Ma/ EFZ**	37 km	fluvial valley trends	Abbott et al. (1983)
San Clemente Fault Zone	**68 km since 18 Ma/ SCFZ**	60 km since Neogene	Middle Miocene circular crater structures	Goldfinger et al., 2000

Table 4
The estimated and applied displacements for Cenozoic Faults sinistral faults.

Fault Zone	Applied Slip	Estimated Slip	Evidence	Refference
Garlock Fault	63 km since 11 Ma/ GF	btween 48 & 64 km Post 17 Ma (likely since 11 Ma)	correlations of bedrock and structural features	Hatem and Dolan (2018); and the refferences there in
Pinto Mountain Fault	22 km since 16 Ma/ PMF	16 km Post Cretaceous	lithologic correlations	Powell (1981) and the references therein
Blue Cut Fault	Considered as PMF	~5 – 6.5 km	lithologic correlations	Powell (1981) and the references therein
Big Pine Fault	50 km since 12 Ma/ northern boundary of WTR	14 km Post Miocene	correlation of structural features (fault, syncline)	Hill and Dibblee (1953)
Santa Ynes Fault	51 km since 12 Ma/ n boundary of Western Transverese Range	37 km Post 22 Ma	lithologic correlation	McCulloh (1981)
Santa Monica and Santa Cruz Island Fault's	90 km since 16 Ma/ southern boundary of WTR	60 km since Middle Miocene	correlation of stratigraphic features (paleocurrent)	Truex (1976)
Santa Monica and Santa Cruz Island Fault's	90 km since 16 Ma/ southern boundary of WTR	90 km since Mioce	correlation of stratigraphic boundaries	Campbell and Yerkes, 1976

Table 5
The estimated and applied displacements in the literature for Mesozoic dextral deformation.

Shear Zone	Applied Slip	Estimated Slip	Evidence	Refference
Eastern Colorado Shear Zone	85 km between 89 and 67 Ma/ ECSZ and Laramide Belt	between 5&–20 km [1]/ 33 & 110 km [2]	Interpretation of Mesozoic Stratigraphic features	Woodward et al. (1997) [1]/ Cather et al. (2006) [2]
Eastern Colorado Shear Zone	85 km between 89 and 67 Ma/ ECSZ and Laramide Belt	between 55 & 90 km [1]/ 60 & 120 km [2]/ 100 & 170 km [3]	lithologic correlations	Cather et al. (2006) [1]; Cather (1999) [2]; & Karlstrom and Daniel (1993) [3]
Eastern Colorado Shear Zone	85 km between 89 and 67 Ma/ ECSZ and Laramide Belt	60 to 120 km /~85 km	Regional Correlations (NS shortening at north)	Cather (1999) and refferences there in
Western Idaho Batholith S.Z.	75 km between 90 and 60 Ma/ WIBSZ (along LFTB)	between 15 & 90 km	finite strain estimates from numerical models	Giorgis et al. (2005)
Western Idaho Batholith S.Z.		btween 30 & 75 km	Correlation of structural features	Stetson-Lee (2015)
Owens Valley Fault	75 km between 90 and 60 Ma/ WLSZ (along LFTB)	65 ± 5 km km Post 83 Ma (5–10 km post L. Pliocene)	Stratigraphic and Lithologic correlations	Bartley et al. (2007)
Sierra Crest Shear Zone (to south (proto) Kern Canyon F.)	75 km between 90 and 60 Ma/ WLSZ (along LFTB)	~27 km Late Cretaceous	convetional structural analysis	Nadin and Saleeby (2008)
Mojave-Snow Lake Fault	200 km between 145 and 102 Ma (max. Disp. Scenario)	400 km slip between ~145 & ~ 102 Ma	Stratigraphic correlations	Wyld and Wright (2001)
Mojave-Snow Lake Fault	200 km between 145 and 102 Ma (max. Disp. Scenario)	200 km slip between ~145 & ~ 102/ 87 Ma	offset of Sri 0.706 line	Memeti et al. (2010)
Mojave-Snow Lake Fault	no slip minimum displacement scenario	no slip		Chapman et al. (2015)

Table 6
The estimated displacements in the literature for Mesozoic east-west shortening.

Thrust Belt	Faults	Applied & Estimated Offset	Evidence	Reference
Sevier Belt-eastern part of Central Utah Salient	Pavant, Paxton & Gunnison Thrust's	10 km btween 65&75 Ma, 20 km btween 75&84 Ma, 70 km btween 86&110 Ma	structural correlations, seismic and well data	DeCelles and Coogan (2006) and the refferences there in
Sevier Belt-western part of Central Utah Salient	Canyon Range Thrust	115 km btween 145 & 110 Ma	structural correlations	Currie (2002); DeCelles and Coogan (2006)
Sevier Belt-eastern part of Wyoming Salient	Crawford, Absaroka & Hogsbach Thrusts	21 km 50&56 Ma, 30 km btween 75&84 Ma, 33 km btween 84 & 92 Ma	structural correlations	DeCelles, 1994; Yonkee et al. (2019)
Sevier Belt-western part Wyoming Salient	Willar, Paris & Meade Thrusts	60 km btween 125 Ma and 92 Ma	structural correlations	Yonkee et al. (2019); Yonkee and Weil (2015)
Sevier B-Montana Distributed Belt	Lewis, Eldorado, Hoadley, Libby Thrusts	140 km btween 74 and 58 Ma (west), & 25 km btw 110 &85 Ma (east)	stratigraphic and structural correlations	Sears (2001)
Western Idaho Batholith Shear Zone	–	80 km btween 90 & 105 Ma	geochemical studies and finite strain analysis	Giorgis et al. (2005, 2008))
Central Nevada Thrust Belt	–	15 km btween 105 & 90 Ma	structural correlations	Taylor (2003) personal commun. in DeCelles and Coogan (2006)
Luning-Fencemaker Thrust Belt	–	100 km between 170 & 145 Ma		(DeCelles and Coogan (2006); & Wyld (2002)

(Fig. 4; O.M. 12) (Table 2). Stratigraphic constraints from these displaced markers reveal that slip initiated sometime between 23 and 18 Ma (Atwater and Stock, 1998; Sims, 1993). Prior to this Neogene ~310 km dextral slip, an additional 100 to 200 km of dextral deformation is suggested by aligning the Middle Cretaceous arc rocks of the Salinian Block with the rest of the Sierra Nevada arc system (Dickinson et al., 2005; Wakabayashi, 1999a). There is no consensus about the timing or about the structures that accommodated this additional pre-Neogene slip, but the detrital zircon studies of Sharman et al. (2015, 2013) indicated that at least 50–75 km (and most likely 100 km) of this required dextral slip occurred between 38 Ma and 23 Ma.

A series of faults branch off the San Andreas Fault towards the east in northern California, which we here summarize as the Eastern San Andreas Fault Zone (Fig. 3) (Table 2). The ages of fault-related basins suggest that the movement initiated around 12 Ma (Buising and Walker, 1995). The Volcanic units with similar age (~11.6 Ma), the Burdell Mountain Volcanics and Quien Sabe Volcanics (Fig. 4; O.M. 9), are displaced ~170 km by the main faults of this zone (i.e., Calaveras-Hayward-Rogers Creek and Maacama Fault's) (Table 2) (Ford et al., 2003; McLaughlin et al., 1996). An older offset marker, the Skaggs Spring Schist's (Fig. 4; O.M. 7), suggests 230–250 km dextral slip (Wakabayashi, 1999b). The difference between these two estimates is not necessarily reflecting an additional slip prior to 12 Ma, because the schists are exposed at wider scope and thereby likely record post 12 Ma slips of faults east and west of the volcanic units (e.g., Ortigalita Fault) (Wakabayashi, 2022).

In the eastern Coast Ranges are, from north to south and roughly in each other's continuation, the Concord, Tesla, Ortigalita, Greenville, and Green Valley Faults (Fig. 3). Slip estimates for these faults are around 10 km accommodated in the late Cenozoic (Wakabayashi, 1999b) (Table 3). Therefore, we applied 10 km dextral slip since 18 Ma to these faults that are the most eastern remnants of the San Andreas Fault system. The Bartlett Spring Fault to the north of this system accommodated 47–53 km of slip in the late Cenozoic (Ohlin et al., 2010).

The Walker Lane-Eastern California Shear Zone is the easternmost structure partitioning dextral slip between the Pacific and North

American plates. This shear zone extends from southern California, where it diverges from the San Andreas Fault (SAF) and continues until the latitude of the Mendocino triple junction. The Walker Lane-Eastern California Shear Zone accommodates 20% of the current dextral plate motion (Dokka and Travis, 1990a; Faulds et al., 2008; Stewart and Ernst, 1988; Wesnousky, 2005) (Fig. 3). The shear zone consists of a network of discontinuous structures in which the overall displacement estimates vary between 30 and 110 km (Dokka and Travis, 1990b; Faulds et al., 2005; McQuarrie and Wernicke, 2005).

In southern California, the dextral San Andreas fault system is crosscut by several sinistral strike-slip faults, which include the Garlock and Pinto Mountain faults located south of Sierra Nevada Batholith and east of San Andreas Fault, and the Santa Ynez and Santa Monica faults which form the northern and southern boundary of the Western Transverse range (Table 4) (Fig. 3). Our reconstruction of these faults follows McQuarrie and Wernicke (2005), and we refer the reader to that paper for details.

2.2.2.2. Cenozoic East-West Extension. McQuarrie and Wernicke (2005) divided the Basin and Range province into three latitudinal zones [northern (between 39° and 42° N lat.), central (between 35° and 39° N lat.) and southern (32° and 35° N lat.)]. Their reconstruction of the northern and central parts reveals a total of up to ~235 km extension with variable distribution, that took place in the last ~36 Ma. For the southern part, they estimated the cumulative extension, accommodated by multiple core complexes at ~195 km since ~30 Ma. We revised the reconstruction of the Northern Basin and Range province, by adding ~30 km of extension between 50 and 36 Ma, i.e. preceding the timeframe of McQuarrie and Wernicke (2005), estimated from the Ruby Mountains–East Humboldt Range and Wood Hills–Pequop Mountains core complexes (Cassel et al., 2020; Gans et al., 1983) (Fig. 5c).

McQuarrie and Wernicke (2005) modeled extension solely south of the northern California boundary and we expanded the reconstruction farther north, albeit with much less detail. North of California, the magnitude of Cenozoic extension decreases. The most prominent extensional structure is the 50–60 km wide, 100 km long, north-south trending Oregon-Idaho (*syn*-volcanic) graben (Cummings et al., 2000). It is likely that the region experienced more extension but the widespread coverage by young volcanics of the Cascadia Arc and the Middle to Upper Miocene Columbia River and Snake River Plain basalts may obscure much of this pre-late Neogene extensional record (Geist and Richards, 1993; Rodgers et al., 1990; Takahahshi et al., 1998). North of the Cascadia Arc, in southern Canada, where pre-Neogene rocks are well exposed, Neogene extensional structures are rare. An abrupt northward change in the amount of extension would require accommodation along *E*-W striking dextral transform faults, and some may exist (Olympic–Wallowa lineament, Brothers, Eugene-Denio and Mount McLoughlin Faults), but estimated slip magnitudes are negligible compared to the documented extension in the Basin and Range (Reidel et al., 2013, 2021). In our reconstruction, we therefore assume that the area between latitudes 42° N and 47° N (including Oregon and Washington) accommodated a gradually northward decreasing extension from ~235 km at the California-Oregon boundary to non-extended southern Canada in the last 36 Ma (the time span of reference model). In its simplest form, this predicts a gradual, late Eocene to Miocene clockwise rotation of ~15° of the Cascadia arc region relative to stable North America.

The area east of the Columbia River basalts exposes a record of extension in the Anaconda and Bitter Root core complexes that occurred between ~53 and 38 Ma (Foster et al., 2007, 2010). The estimated magnitude of extension is between 80 and 95 km (Constenius, 1996; Foster et al., 2007). North of the Anaconda and Bitter Root extensional province is the dextral Lewis and Clark Fault Zone that transfers the extension towards the northwest, where it gradually decreases through the Sushwap extensional complex towards southern Canada (Foster et al., 2007; Wallace et al., 1990). We reconstruct the extension as gradually decreasing towards the southern Canadian Rockies to north and the southern Idaho Batholith to south, where no extension is documented.

Finally, some *E*-W extension was also accommodated in the Franciscan complex in California and Oregon, where the unmetamorphosed Coast Range Ophiolite and Great Valley Group sediments are separated from high-grade metamorphic Franciscan units by an east-dipping fault that is shown as Coast Range Fault in Fig. 2 (Jayko et al., 1987; Platt, 1986; Schmidt and Platt, 2018; Wakabayashi, 2015). The structure accommodates a metamorphic gap with an estimated vertical omission of at least 15 km that has been proposed to have formed by Neogene *syn*-subduction extension (Jayko et al., 1987; Platt, 1986; Schmidt and Platt, 2018; Wakabayashi, 2015, 2021a; but see "Ring and Brandon, 1994" for an alternative proposal advocating shortening). There is no detailed estimate of extension, and we did not include it in our reconstruction, which as a result may lead to an overestimation of the width of the pre-Neogene Californian forearc by perhaps 20 km.

2.2.2.3. Late Jurassic to Paleogene East-West Shortening. Prior to Basin and Range extension, the western North American margin underwent shortening above the Farallon subduction zone from the Middle Jurassic to the Paleocene, most of the east-west shortening was accommodated by multiple east-directed thrusts (Yonkee and Weil, 2015). These thrust belts are from east to west the Laramide Thrust Belt, the Sevier Thrust Belt, the Western Idaho Batholith Shear Zone, the Central Nevada Thrust Belt, and the Luning-Fencemaker Thrust Belt (Table 6) (Fig. 2 & 5). The Laramide Belt consists of discontinuous thrust that accommodated thick-skinned thrusting. Shortening in the Laramide Belt has mostly been constructed based on vertical axis rotations estimated from paleomagnetic data (Bird, 1998; Weil et al., 2016; Yonkee and Weil, 2015), and is relatively minor, some ~30 km of east-west shortening.

In the area affected by latitudinally heterogeneous variable Basin and Range extension, the crust was shortened by thin-skinned deformation accommodated by multiple fold-and-thrust belts. We restored these thrust belts by dividing them into three latitudinal zones roughly as analogous to the zones of Basin and Range extension described above. This was necessary to accurately restore the overprinting younger deformation, which varies latitudinally, and for precisely applying shortening estimates that vary along strike (Table 6).

The Sevier Thrust Belt is the easternmost thin-skinned structure and is represented in the reconstruction with two faults (Fig. 2 & 5). Both faults in the reconstruction (eSTB and wSTB) represents multiple structures that are closely spaced (e.g, the Paris and Meade thrusts; and the Crawford, Absaroka and Hogsback thrusts) or aligned with each other (e.g., Willard and Meade trusts). The shortening difference along the strike of the Sevier Belt is reflected in opposite vertical axis rotations causing oroclinal bending (Fig. 2 & 5a). Paleomagnetic data suggest that 75% of the modern curvature of the Sevier Thrusts was acquired by bending, with maximum shortening in the center of eastward convex bends (Weil et al., 2010; Yonkee and Weil, 2010). These bends include from north to south the Montana Distributed Belt, the Wyoming Salient, and the Central Utah Salient, and accommodated 165 km, 144 km, and 227 km shortening, respectively, between 145 and 58 Ma (Table 6).

Farther to west, the Western Idaho Batholith Shear Zone in the north, and the Central Nevada Thrust Belt in the south accommodated 90 km and 15 km of shortening, respectively (Table 6). We assume a gradual change between these belts, by applying 65 km of shortening in the intervening region part at the latitude of the Wyoming Salient (the central convex bend of Sevier Belt) (Fig. 2).

The westernmost (thin-skinned) east-directed thrust belt is the "Luning-Fencemaker Thrust Belt", which accommodate 50 to 75% shortening between 168 and 145 Ma (Wyld, 2002). Wyld (2002) does not specify whether these estimates represent an uncertainty, or an along-strike variation. We applied the minimum amount of shortening corresponding to 100 km, which is also consistent with the minimum

value determined by DeCelles (2004) based on the study of Wyld (2002).

To the south, simultaneous thin and thick-skinned shortening affected North American continental crust in northern Mexico and southern edge of US (e.g., along the San Marcos and La Babia Faults (Fig. 2 & 5) (Chávez-Cabello et al., 2007), however, strong overprinting of Basin and Range extension precludes accurate shortening estimates (DeCelles, 2004). The most southern part of our reconstruction area contains the Maria and Mule Mountain thrust systems (Fig. 2) (Knapp and Heizler, 1990; Tosdal, 1990), but there are no detailed estimates of displacement. Farther south, in central Mexico, Cretaceous to Paleocene shortening is reportedly of similar magnitude to that of the Sevier Belt (Fitz-Díaz et al., 2011, 2018) (Table 6).

2.2.2.4. Late Mesozoic Dextral Strike-Slip Faults. In addition to the *E*-W shortening, the coastal units of western North America moved northward relative to cratonic North America during the Mesozoic (Table 5). This movement is estimated from dextral shear zones located east of the Colorado Plateau and in the Sierra Nevada, close to the Walker Lane-Eastern California Shear Zone (Fig. 2, 3 & 5).

East of the Colorado Plateau, the roughly east-west striking lineaments of 1.4 Ga structures observed in aeromagnetic data are dextrally separated between 55 and 90 km (Cather et al., 2006) (Table 5). Towards the south, similar offsets were estimated [e.g., 70 and 110 km in southern New Mexico by Cather et al., 2002]. To the north, this deformation was accommodated by ~85 km of north-south shortening along east-west striking reverse/thrust faults (e.g., the Uinta, Owl Creek, and Wind River thrusts). Collectively, these constraints together with the Eastern Colorado Plateau Shear Zone were interpreted to indicate, northward extrusion of the Colorado Plateau (Cather, 1999; Karlstrom and Daniel, 1993). We applied 80 km of northward movement by extruding the Colorado Plateau northward between 75 and 45 Ma. We note that the timing of the dextral deformation east of the Colorado Plateau is debated. Scenarios with less northward movement during this time span are possible (Cather et al., 2006; Woodward et al., 1997), but these have little influence on our final reconstruction of the Californian forearc.

To the west, approximately along strike with each other, are the Idaho Batholith Shear Zone (IBSZ), and Kern Canyon-Owens and Death Valley Faults (Southeastern Sierra Nevada) (Fig. 2). Between 30 and 75 km of dextral slip from 90 to 60 Ma is estimated for IBSZ (Giorgis et al., 2005; Stetson-Lee, 2015). The estimated overall post-Late Cretaceous dextral slip in the south-eastern Sierra Nevada is around 100 km (Memeti et al., 2010) (Table 5). The 70 to 25 km difference in dextral slip between these two zones is accommodated by the Walker Lane-Eastern California Shear Zone, the dextral shear zone that formed in the late Neogene and ends at latitudes of the Mendocino triple junction, which deforms the eastern part of the Sierra Nevada (Bartley et al., 2007). Finally, significant dextral strike-slip motion may have been accommodated between 145 and 102 Ma, along Mojave Desert-Snow Lake Fault overprinted by the Luning-Fencemaker Thrust and by the Eastern California Shear Zone. Dextral slip estimates based on structural and stratigraphic correlations range as high as 500 km (Lahren and Schweickert, 1989; Wyld and Wright, 2001), to less than ~200 km dextral slip based on recent detrital zircon studies (Chapman et al., 2015; Memeti et al., 2010), others argues that there may not have been any strike-slip displacement (Chapman et al., 2015). We will return to this uncertainty in the next section.

3. Reconstruction

We present our reconstruction of the kinematic history of the western U.S.A. and provide reconstruction snapshots at 36, 55, 100, 150 and 170 Ma (Fig. 5). These time frames coincide with marked changes in the deformation history. We chose to reconstruct maximum displacement estimates if these were not in direct conflict with (later) observations. GPlates reconstruction files that form the foundation of the maps in Fig. 5 are provided in the supplementary information. The aim of our reconstruction is to ascertain the positions of the Jurassic Californian ophiolites relative to each other, and relative to North America, and the uncertainties therein. This reconstruction forms the basis for the interpretation of our paleomagnetic information pertaining to the orientation of the spreading ridge that will follow in the next section.

The reconstruction at 36 Ma shows the reconstructed position of the ophiolites of California prior to the deformation of the wider San-Andreas system (Fig. 4). Reconstructing 310 km dextral slip of San Andreas Fault (Neogene), and the smaller displacements of the adjacent faults summarized above (Table 2). An additional 100 km dextral slip of proto–San Andreas Fault (Late Eocene and Oligocene) restored the Salinian arc plutons to its southeastern origin and aligned the Coast Range Fault and Sur-Nacimiento faults (Fig. 5b). This reconstruction restores the Jurassic Californian ophiolites southward relative to North America. The westernmost ophiolite remnants (i.e., Point Sal) are reconstructed 500 km southward, whereas the easternmost ophiolite (Smartville) is displaced <100 km.

We note that not all displacement estimates are consistent, and in our reconstruction we favored estimates that are kinematically consistent. Altering our reconstruction to fit the maximum and minimum estimates, particularly for the western branch (SGHF), and eastern branch (ESAFZ) of the San Andreas Fault system (Fig. 4) would change the relative positions of a few ophiolites by up to 60 km. Because the affected ophiolites lack well contrained ages, these uncertainties do not impact our interpreted ridge configuration of spreading rate estimates.

In addition to the strike-slip deformation, restoring the extension in Basin and Range province moved the Californian coastal framework (south of latitude 40° N) ~200 km inboard (eastward) (Fig. 5b). To the north, the amount of extension decreased gradually through Oregon and southern Washington (between latitudes 40° and 45° N) to non-extended northern Washington and Canada (north of latitude 50°N). This northward gradual decrease of extension rotated the southern Cascades Arc and Oregon Coast Range into a westward convex orocline. Our reconstruction thus removed the westward bulge, leading to an originally nearly straight western North American margin.

Deformation between 55 and 36 Ma was mostly concentrated in the northern part of the reconstructed area, in which the southernmost deformation was ~30 km of extension in the northern Basin and Range province (at present-day between latitudes 39° and 42° N). We restore ~100 km E-W extension at northern Oregon and Washington. This bends the northward continuation of the Mesozoic arc, passive margin, and fore-arc sediments eastward. We reconstruct accretion of the Siletzia LIP to North America at 50 Ma and connect it to Farallon prior to this time.

From 55 Ma back to 100 Ma, the entire coastal framework is reconstructed westward relative to North America to account for the restoration of (retro-arc) shortening. Superimposed on this shortening, the coastal units are moved southward due to the restoration of the northward extrusion of Colorado Plateau and the dextral Western Idaho Batholith Shear Zone and ~ north-south striking dextral faults within or proximal to the Sierra Nevada Batholith (e.g., Kern Canyon Fault, Owens Valley Fault).

To arrive at the configuration at 170 Ma, we reconstruct the pre-100 Ma shortening in the Sevier Belt and the Luning-Fencemaker Thrust Belt (Table 6). The restoration of this shortening separated the coastal units from the Sierra Nevada Batholith and units east of it (e.g., Golconda, Roberts Mnt.), which increased the width of the Middle Jurassic oceanic arc complexes (e.g., Klamath Mountain, Blue Mountains, foothills of Sierra Nevada). We note, given the ongoing controversy, that we have reconstructed no dextral displacement on the Mojave Desert-Snow Lake Fault in the Early Cretaceous, as suggested by Chapman et al. (2015) and Memeti et al. (2010). If the alternative estimate of up to 500 km of displacement between 145 and 102 Ma is correct as suggested by Lahren and Schweickert (1989) and Wyld and Wright (2001), the reconstructed

position of the Jurassic ophiolites of California would shift ~4–5° farther southward. Finally, field evidence shows that subduction between the Klamath-Blue Mountains-Sierra Nevada foothills arc and the North American continent may have continued until 165–150 Ma (Fig. 5e & 5f) (Dickinson, 2008; Edelman and Sharp, 1989; LaMaskin et al., 2022; Schwartz et al., 2011). Our reconstruction at 170 Ma has not taken this motion into account, as there are no direct kinematic constraints on the timing and magnitude of associated displacements. The approximate location of this unrestored west dipping subduction zone is shown in Fig. 5f. Because the Jurassic Californian ophiolites are located to the west of the collision zone between those arcs and North America, this added uncertainty must be considered when interpreting the paleogeography at the timing of formation of the ophiolites in the next sections.

4. Paleomagnetic and Net tectonic rotation analysis of Mt. Diablo Ophiolite

4.1. Previous work

A mid-ocean-ridge origin close to the paleo-equator for the Coast Range Ophiolite has been suggested by some paleomagnetic studies: at Stanley Mountain by McWilliams and Howell (1982); at Point Sal, and Llanada by Beebe (1986) and Pessagno et al. (1996). In contrast, other paleomagnetic studies identified origins with paleolatitudes concordant with North America (Hagstrum and Jones, 1998; Hagstrum and Murchey, 1996; Mankinen et al., 1991). Hagstrum and Murchey (1996) defined two stable components of the natural remnant magnetization (NRM); one of them had the inclinations as the present day, one of them had inclinations that suggested a paleo-equatorial latitudes as origin. Hagstrum and Murchey (1996) assumed that the paleo-equatorial origin referring direction was an overprint, based on lacked reversed magnetic polarity in ophiolite unlike the overlying cherts. They conclude that the direction with dual polarity, which indicated a 32° ± 8° N paleolatitude origin, was the primary direction. Furthermore, the sheeted intrusive complexes and pillow lavas of the Mount Diablo remnant were analyzed by Hagstrum and Jones (1998) and Mankinen et al. (1991). They both suggested an origin close to North America, although they assumed paleohorizontal orientations that are perpendicular to each other for the same intrusive complex (interpreting as sheeted sill complex and as sheeted dyke complex).

4.2. Sampling

The Mount Diablo Ophiolite is the only remnant of Coast Range Ophiolite with a well-developed sheeted dyke complex, exposing a crustal section consisting of diabase screens, sheeted dykes, pillow basalts and basalt flows, and it is overlain by Upper Jurassic Great Valley Group fore-arc basin clastic sediments (Hopson et al., 2008; Williams, 1984) (Fig. AP1). This sequence is in tectonic contact with underlying rocks of the Franciscan Complex (Hopson et al., 2008; Wakabayashi, 2021a) (Fig. AP1a). The only age data from Mount Diablo Ophiolite is a 165 ± 2 Ma U-Pb zircon age obtained from dykes that are interpreted to be a late stage differentiate of diabase that intruded into the sheeted dyke complex (Hopson et al., 2008; Mankinen et al., 1991).

The Mount Diablo is proper part of an anticlinorium formed at a restraining step-over between the Greenville and Concord faults of the San Andreas fault system and is undergoing active uplift (Unruh et al., 2007; Wakabayashi et al., 2004). The fastest uplift rates are recorded in the south of the anticlinorium (Bürgmann et al., 2006; Unruh et al., 2007), whereas our sampling locations are in the north, where late Neogene uplift rates have been proposed to be higher, but have since declined (Wakabayashi et al., 2004). The sampled area is thus part of a still actively tilting, south verging anticline.

Samples were collected from three locations in the Mt. Diablo ophiolite: 33 samples were collected from a pillow lava section exposed in Mitchell Rock, in the northeastern part of the Mt. Diablo anticlinorium. Samples were collected spanning the maximum exposed stratigraphic thickness of approximately 40 m. We collected one core per lava pillow to optimize the chance of sampling a separate spot reading of paleosecular variation with each core (see Gerritsen et al., 2022). The sampled pillows were slightly altered, and we sampled the least altered centers of the pillows (Fig. AP1b). The sheeted dyke section of the ophiolite is well-exposed in two quarries on the north side of Mt. Diablo (Fig. 7). We collected 55 and 38 samples from sheeted dyke sections in the Hanson and Cemex quarries, respectively, ~1250 m to the northwest of Mitchell Rock.

The sampled section in Hanson Quarry lies approximately 1 km west of the sections sampled in Cemex Quarry (Fig. 7). Dykes are typically 0.5–1.5 m wide, and we collected one sample per dyke to optimize the chance that our samples represent paleosecular variation (cf. Gerritsen et al., 2022). These dykes were not affected by significant alteration or ductile deformation and contained the typical grading of sheeted dyke complexes with single chilled margins, coarser grained at one side and finer grained at the other side (Fig. AP1c). The chilled margins (finer grained sides) were located on the northwest side of the dykes suggesting that the ridge was located to the southeast (in modern coordinates). Dyke orientations from Cemex and Hanson quarries are similar, and the average pole-to-dyke orientation is 153/50, $\alpha 95 = 3.4$, $n = 21$.

The Josephine Ophiolite contains an oceanic crustal section that was dated 163 ± 1 Ma (Harper et al., 1994) (Table 1). From the Josephine Ophiolite, we sampled a sheeted dyke section south of Idlewild Maintain Station on Highway 199 (Fig. AP2). The approximate strike of the dykes was roughly parallel to the road cliff and therefore it was difficult to define the number of dykes and their true width, which we estimated at ~0.5–1 m. We collected 13 samples from at least 10 different dykes. The chilled margins of the dykes were at the SE edge of the dykes, suggesting the ridge was located to the NW (in modern coordinates). Pillow lavas were sampled in a road section close to Snake River Fork, 1.8 km to the S-SW of the sampled sheeted dykes. The pillows were intensely fractured making collection of paleomagnetic cores challenging, but the pillow shapes were preserved. Some pillows were up to 70 cm -– 1 m in width and the tops of the pillows were systematically younging up-dip, towards the SE. We collected 20 samples from the pillows, one per lava pillow.

4.3. Methods

We used a water-cooled portable rock drill, magnetic and sun compasses for sampling and orienting the samples. The primary layering of pillow lavas and the orientation of dykes that contained a single chilled margin were measured for Net Tectonic Rotation Analysis. All field measurements were corrected for the local magnetic declination at the time of sampling (13°E; www.ngdc.noaa.gov).

The texture and mineralogical assemblage of samples were determined by studying polished thin sections under an optical microscope and a table-top scanning electron microscope (JEOL JCM-6000) that was coupled with an energy-dispersive X-ray detector (Earth Simulation Lab – Utrecht University, The Netherlands). The main purposes of these analyses were: (i) defining the ferromagnetic minerals with their nature and distribution, and (ii) ensuring that the samples were not foliated, an observation that would indicate ductile deformation.

Remanence components were analyzed using: stepwise progressive alternating field (AF) demagnetization, in 14 steps up to 120 mT; and thermal demagnetization, in 18 steps up to 585 °C. The demagnetization and remanence measurement were operated by a robotized superconducting quantum interference device (SQUID) magnetometer installed at the Paleomagnetic laboratory “Fort Hoofddijk” of Utrecht University (Mullender et al., 2016). Zijderveld diagrams (Zijderveld, 1967) were interpreted using principle component analysis (Kirschvink, 1980) or, in case of two components decaying simultaneously,

remagnetization great circles (McFadden and McElhinny, 1988). Data interpretation was performed using software available on Paleomagnetism.org (Koymans et al., 2016, 2020). All paleomagnetic data and interpretations are available in the supplementary information, and are included in paleomagnetic databases MagIC (Jarboe et al., 2012; Tauxe et al., 2016) as well as Paleomagnetism.org (Koymans et al., 2020).

In contrast to sedimentary or volcanic rocks that often contain bedding, sheeted dykes do not preserve indications of a paleohorizontal. Instead, the dominant magmatic fabric of sheeted dykes forms parallel to the paleo-orientation of the dyke, which is typically thought to be vertical. A restoration of a dyke back to vertical, however, leaves a tilt component around an axis normal to the dyke unresolved. The Net Tectonic Rotation (NTR) analysis overcomes this problem (Allerton and Vine, 1987; MacDonald, 1980). If the original paleomagnetic inclination is known by approximation through plate tectonic reconstruction cast in a paleomagnetic reference frame, or constrained by independent paleomagnetic data, then a primary magnetic vector may be restored to the original vector through a single, net rotation around an inclined axis. If the angle between the primary magnetic vector and dyke strike has remained constant and assuming that the dyke intruded vertically, this analysis restores the dyke to its original position. The NTR analysis gives up to four possible solutions for initial dyke orientation: the dyke may be overturned or not, and the magnetic polarity can be normal or reversed. Each of these four solutions comes with a predicted rotation axis orientation and rotation amount, from which the present-day orientation of the paleohorizontal may be computed. Regional architecture of the ophiolite (general dip direction, is it overturned or not, etc) may then be used to further limit the options (see e.g., Allerton and Vine, 1987; Maffione et al., 2015a; Morris et al., 1998). For our analysis, we used the software to perform NTR Analysis and to estimate associated uncertainties in primary dyke strike; this routine is available at www.paleomagnetism.org (Koymans et al., 2016, 2020).

Whether the characteristic remanent magnetization of the dykes is primary should follow from standard paleomagnetic and rock magnetic data interpretation. The primary inclination of the sampled ophiolites may be estimated from the kinematic reconstruction of western North America presented in the previous section, whereby we consider that in the first ~10 Ma after their formation the ophiolites may still have undergone unresolved motion relative to North America accommodated by subduction between the Klamath-Blue Mountains-Sierra Nevada foothills arc. In addition, the primary inclination may be estimated from pillow lava sections of the ophiolites. The assumption that dykes emplace vertically is important: if that assumption is false by a few tens of degrees, then the results of the NTR analysis are invalid (Titus and Davis, 2021). However, sheeted dykes preserve only half of the original dyke that became split in their center upon ongoing horizontal plate spreading, inviting the intrusion of the next dyke, and it is not likely nor ever documented that such dykes form systematically at an angle that deviates significantly from the paleo-vertical.

To independently support the measured orientation of the dykes, we performed an anisotropy of magnetic susceptibility (AMS) measurements to define the magma flow fabric in 16 samples from different dykes of Mount Diablo and ten samples from likely eight dykes of Josephine Ophiolite. The samples of Josephine showed a roughly vertical flow (parallel to the dyke orientation). The magma flow was most likely vertical and a parallelism between magma flow and dyke orientations will lend strength to of the assumption that the dykes intruded vertically, as the perpendicularity of dyke orientation with the proximal pillow lavas orientations also suggest. During AMS analysis, we follow the steps that Staudigel et al. (1992) and Tauxe et al. (1998) followed in their studies for ophiolites in Cyprus.

4.4. Results

4.4.1. Petrology

In total ten thin sections were analyzed from cores, two from each sampling location of sheeted dyke and pillow lava section from the Mt. Diablo and Josephine ophiolites. The dyke samples contain mostly plagioclase, clinopyroxene, hornblende, and opaque minerals (Fig. 8a & 8d). The plagioclase and clinopyroxene are also seen in abundance in the pillow lavas (Fig. 8g & 8j). The textures of samples are purely magmatic, showing no evidence of a deformation fabric (Fig. 8). The presence of some chlorite and prehnite overgrowing magmatic minerals, previously also observed by Williams (1984), is best interpreted as low temperature seafloor alteration shortly after emplacement, which is common in ophiolites and is not likely to have affected the magnetization (e.g., Morris et al., 2017; van Hinsbergen et al., 2019). Magnetite grains with sizes ranging from ~5–500 μm in dykes and ~ 10–100 μm pillow lavas are observed with scanning electron microscope (SEM) coupled with EDX (Fig. 8b & 8h).

4.4.2. Magmatic fabrics in dykes from anisotropy of magnetic susceptibility (AMS) analysis

We performed AMS analysis to evaluate whether magmatic flow fabrics are in line with our dyke orientation estimates. When magma flows into a dyke, the elongated particles (including iron bearing minerals) will imbricate, producing an anisotropy, in which the axis of maximum magnetic susceptibility occurs along the long axis of the grains (Tauxe et al., 1998 and the references therein).

All samples from Josephine Ophiolite show a pattern that indicates roughly vertical flow (parallel to the dyke orientation) as it was expected (Fig. AP 3c and 3d). Ten of sixteen samples of Mount Diablo show a pattern that indicates parallel flow to the dyke orientation (vertical flow) (Fig. AP3a). Six other samples of Mount Diablo indicate a flow direction perpendicular to the dyke orientation (Fig. AP3b). Such so-called reverse, or inverse trends have also been observed by Staudigel et al. (1992) and Tauxe et al. (1998), and are caused by rolling of elongated particles in the flow field, post emplacement modifications, or fabric variation of particles. Staudigel et al. (1992) suggested that the inverse trends indicate horizontal magma flow as result of fast spreading rates and the inverse trend may become more likely away from the chilled margin. The distance of our sample to the chilled margin varied – we merely chose the freshest part of a dyke irrespective of the position within the dyke, and the AMS fabrics are thus within the expected orientation and of the expected types for sheeted dykes. This confirms the overall dyke orientation, as well as the absence of a significant tectonic fabric in the dyke sections.

4.4.3. Paleomagnetic results

A total of 35 specimens of the pillow lavas at Mitchell Rock were demagnetized, 29 with AF and 6 with thermal demagnetization. Demagnetization diagrams reveal a viscous overprint that is removed at low coercivity (0–15 mT) or temperature (0–180 °C), after which most specimens show coherent demagnetization towards the origin at between 15 and 50 mT or ~ 210–500 °C (Fig. 9a & 9b). We interpret this latter component as the Characteristic Remanent Magnetization. The low-T or low-coercivity component is slightly offset towards a smaller northerly declination between the high-T/coercivity component and the present-day field and is interpreted as another minor recent-field overprint. In some cases, a small component is left after demagnetization such that decay is not converging towards the origin, causing great circle trajectories with NW-SE strikes (Fig. 9c). Demagnetization diagrams suggest the presence of a southeast-down component that co-defines these great-circles, but no samples provide a well-resolved direction. The north-down component is well-resolved and yields well-clustered direction. Applying a 45° cutoff to eliminate outliers eliminated nine directions, giving $D \pm \Delta D_x = 14.4° \pm 9.7°$, $I \pm \Delta I_x = 67.6 \pm 4.4°$, $K = 23.3$, $A95 = 6.1$, $N = 25$ in geographic coordinates. This cluster passes the reliability envelope of (Deenen et al., 2011), suggesting their scatter represent paleosecular variation. This inclination is approximately 10° steeper than the expected inclination for the recent paleomagnetic field in the study region.

Table 7
Paleomagnetic results from sheeted dyke section and pillow lava sections of Mount Diablo and Josephine Ophiolite.

Collection	Latitude (°N)	Longitude (°W)	N(45° cutoff)	Ns	D	ΔDx	I	ΔIx	K	A95	A95Min	A95Max
Mt Diablo ophiolite												
MR (pillows) - overprint	37.91	121.94	25	34	14.5	9.7	67.6	4.4	23.3	6.1	3.3	10.8
CQ (dykes) - overprint	37.93	121.95	39	39	7.5	9.8	68.7	4.2	15.6	6.0	2.8	8.2
HQ (dykes) - overprint	37.92	121.96	25	34	25.2	10.3	54.2	8.6	12.7	8.5	3.3	10.8
HQ + CQ - overprint	37.93	121.95	63	73	15.6	7.4	64.2	4.1	13.0	5.2	2.3	6.0
HQ + CQ without great circle	37.93	121.95	63	65	117.6	4.3	20.0	7.6	19.3	4.2	2.3	6.0
HQ + CQ.col - primary (with great circle analysis)	**37.92**	**121.96**	**85**	**88**	**116.7**	**3.5**	**20.4**	**6.3**	**20.6**	**3.5**	**2.0**	**5.0**
Josephine Ophiolite												
SF (pillows)	41.9	123.8	–	8	–	–	–	–	–	–	–	–
IDL (dykes) - overprint	41.9	123.8	13	18	348.9	18.7	64,3	10.1	11.4	12.8	4.3	16.3

A total of 35 specimens were demagnetized from the Cemex Quarry (CQ), 7 with thermal demagnetization and 28 with AF demagnetization. Demagnetization diagrams often reveal two components, with a low-coercivity or low-temperature component isolated between 5 and 15–20 mT or 80 and 210 °C differing from a component that decays towards the origin between ~20 and 50 mT or 240 and 570 °C (Fig. 9d & 9e). Interpreting these components separately, however, yields two data clusters that are statistically indistinguishable, with a declination coinciding with north and a steep inclination of ~70°. This is steeper than the expected inclination for the present-day location of Mt. Diablo (57°) but is close to the low-coercivity and low-temperature component of the pillow lavas of Mitchell Rock (MR). In three specimens, a southeast-down component is overprinted by a north-down low-coercivity component that is part of the low-coercivity components that cluster around 0/70° (Fig. 9f). The overprint and interpreted original direction (ChRM) span a great circle that cuts through the datacloud of the north-directed overprint component and a southwest-down component that is observed in a few samples (e.g., Fig. 9g).

From Hanson Quarry (HQ), 73 specimens were demagnetized. Their majority reveal a southwest-down high-temperature (240–570 °C) or high-coercivity (20–50 mT) component (interpreted as ChRM) that decays towards the origin (Fig. 9h & 9j). Most samples also contain a low-coercivity (5–15 mT) or low-temperature (80–210 °C), north-down component that is close to the overprint direction recorded in the CQ samples, and the direction recorded in MR.

Combining all three sampling locations, we interpret that the north-down component that is the only component found in the pillow lavas of Mitchell Rock, represents the strong overprint component. This component dominates the dykes of Cemax Quarry, and forms the low-temperature or coercivity overprint in the dykes of Hanson Quarry, as a secondary, remagnetized component. The inclination of the remagnetized component is plunging ~10° steeper towards the north than the modern paleomagnetic field direction. We interpret this as the effect of the ongoing formation of the Mt. Diablo restraining bend that is causing northward tilting of the northern part of Mt. Diablo where our sampling region is located (Bürgmann et al., 2006; Unruh et al., 2007; Wakabayashi, 2021a; Wakabayashi et al., 2004).

The southwest-down component that defines the Characteristic Remanent Magnetization in Hanson Quarry and that is also found in Cemex Quarry, yields a scatter that is randomly distributed as may be expected for paleosecular variation (PSV) (e.g., Cromwell et al., 2018). The scatter yields a K-value of 19.3 and 20.6 without and with adding directions interpreted from remagnetization great circles, respectively. A95 values for both clusters fall within the reliability envelope of Deenen et al. (2014, 2011) (Table 7), suggesting that the scatter may be straightforwardly explained by PSV alone. We interpret this direction as the primary direction, and use the value that includes great circle analysis, with slightly smaller uncertainty values owing to a larger dataset, for our further analysis.

The overprinting of the pillow lavas of Mitchell Rock precludes a direct paleomagnetic estimate of the paleolatitude at which the Mt. Diablo ophiolite formed. However, because the magnetizations of the three localities reveal similar behavior, it seems likely that they form a coherent body with a similar original magnetization and a similar overprint. In the absence of primary paleomagnetic directions from MR and CQ to directly evaluate whether differential tilting or rotation has occurred between the pillow lavas of Mitchell Rock and the sheeted dykes of the Cemex and Hanson Quarries, we plotted the great circle trajectories between the common overprint direction and the presumed original magnetization (Fig. 10). The great circle trajectories of CQ and HQ appear to overlap with the cluster of interpreted ChRM components from HQ. The great circles of MR, however, suggest that the unresolved component that generates the great circle trajectories is rotated clockwise relative to the ChRM components identified from HQ. Such a rotation may result from folding around a north-dipping fold axis consistent with the estimates that our sampling locations are located in the northern part, north-dipping upright limb of the Mt. Diablo anticlinorium (Wakabayashi, 2021a). Hence, we cannot reliably use the paleomagnetic direction estimated from CQ and HQ to estimate a primary paleolatitude of the pillow lavas at MR and we have no direct paleomagnetic control on the paleolatitude at which the Mt. Diablo ophiolite formed.

Paleomagnetic results from the Josephine ophiolite did not yield meaningful directions. The pillow lavas of Snake River Fork yielded noisy demagnetization diagrams without a consistent demagnetization pattern between samples (Fig. 9k) and no paleomagnetic direction was interpreted from these samples. The dykes of the Idlewild section generated better-defined components that often do not decay towards the origin (Fig. 9l). The resulting data scatter is large but overlaps with the recent paleomagnetic field (Table 7). Remagnetization great circles do not yield a common intersection, and we do not interpret a primary magnetization from the Idlewild dykes.

4.4.4. Net Tectonic Rotation Analysis

Our paleomagnetic analysis above isolated a characteristic remanent magnetization that we interpret as the primary magnetization of the sheeted dyke sequence with $D/I = 116.7 \pm 3.5° / 20.4 \pm 6.3°$, in geographic coordinates. Average orientation is well-defined at 153/50 with $\alpha 95 = 3.4$. A successful NTR analysis further requires an estimate of the primary inclination. We cannot constrain this inclination directly from our own data, and previous estimates yielded disparate results, varying from equatorial latitudes to latitudes expected if the ophiolites had always been part of the North American Plate [~30°N for Mt. Diablo in our reconstruction cast in the paleomagnetic reference frame of Torsvik et al., 2012]. We may use these two endmembers as options in our initial exploration of NTR results. We note, however, that from our kinematic restoration of the western USA Cordillera, the only fault with unresolved motion after the formation of the Mt. Diablo ophiolite at 165 Ma is the suture between the Klamath Mountains – Blue Ridge Mountains – Sierra Nevada Foothills arc and the youngest age ascribed to termination of significant motion is ~150 Ma (Fig. 1a, 5e & 5f) (Dickinson, 2008; Edelman and Sharp, 1989; LaMaskin et al., 2022; Schwartz

Table 8
Results of the Net Tectonic Rotation Analysis [Allerton and Vine, 1987] for Mount Diablo Ophiolite.

Solution	Reference vector		Magnetization vector		Pole to dyke			Rotation pole				Initial dyke		Paleohorizontal after rotation
	D	I ± Δix	D ± DΔx	I ± Δix	Azimuth	Plunge	α95	Azimuth	plunge	angle	sense	strike	dip	
A (1)	0	40 ± 5	116.7 ± 3.5	20.4 ± 6.3	153	50	3.4	63.8	37.7	161.7	CCW	100.8	90.0	169/103 W
B (2)	0	40 ± 5	116.7 ± 3.5	20.4 ± 6.3	153	50	3.4	60.2	24.9	140.4	CCW	79.2	90.0	191/117 W
C (3)	180	-40 ± 5	116.7 ± 3.5	20.4 ± 6.3	153	50	3.4	220.3	39.1	84.5	CCW	280.7	90.0	010/62 E
D (4)	**180**	**-40 ± 5**	**116.7 ± 3.5**	**20.4 ± 6.3**	**153**	**50**	**3.4**	**194.8**	**28.9**	**91**	**CCW**	**259.3**	**90.0**	**348.6/77 E**

et al., 2011). Plate reconstructions of the Panthalassa Ocean suggest that the eastern Panthalassa subduction zones accommodated a northward motion component of the Farallon Plate relative to North America in the Jurassic (Boschman et al., 2021). Hence, some more northward motion of the Californian ophiolites relative to the North American continent may have occurred between 165 and 150 Ma than indicated in our reconstruction, but it is unlikely that this amounted thousands of kilometers as this would yield unrealistically high plate motion rates.

We performed our initial NTR analysis assuming a paleolatitude of ~25°N, corresponding to a paleo-inclination of ~40°, which is on the lower end of the predicted paleolatitude range for our reconstruction of Mt. Diablo in the paleomagnetic reference frame of Torsvik et al. (2012). This analysis yields four possible restorations of the initial dyke orientation to the paleovertical (Table 8). The two normal polarity options require that the sampled part of the Mt. Diablo ophiolite should be overturned, dipping steeply eastwards. This is clearly at odds with the present-day architecture of the ophiolites that shows an EN*E*-ward tilt in the study area, but with the higher pseudostratigraphic units east of the lower one. Also, the bedding measurements of pillows in the Mitchell Rock and on the eastern margin of Cemex quarry show the ophiolite is

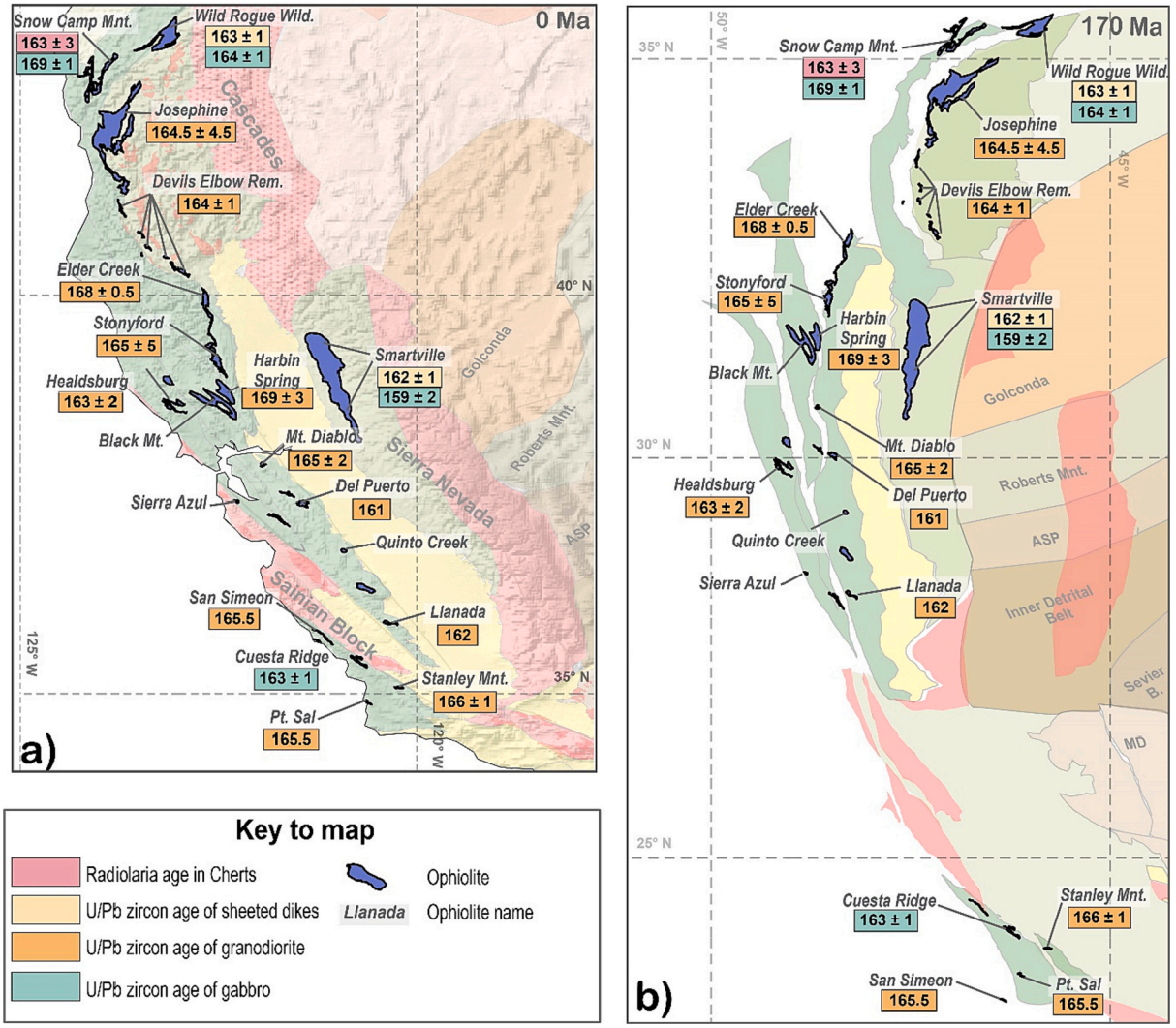

Fig. 6. **(a)** The current position of the ophiolites and **(b)** the position of ophiolites after restoration of post Jurassic deformation phases, at 170 Ma.

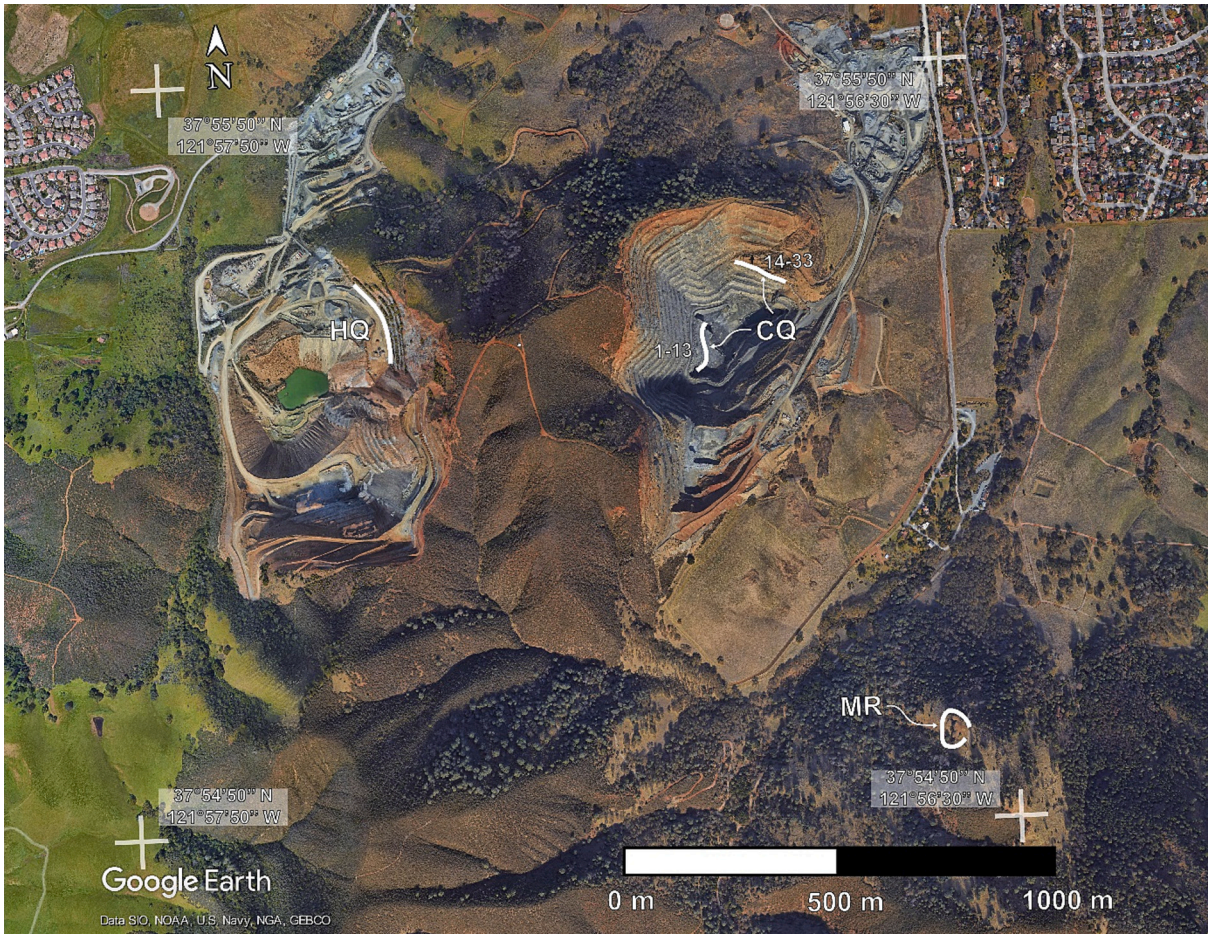

Fig. 7. Google Earth Picture of sampling sites of pillow lava (MR) and sheeted dyke sections (CQ &HQ).

upright (not overturned). We therefore discard these two solutions that require an overturned ophiolite. The two reversed-polarity options predict that the ophiolite is tilted ~60° to the ESE (option C) or 77° to the ENE (option D). The dip of option C coincides best with the measured orientation of the pillow lavas at Mitchell Rock as well as the regional structure mapped by Wakabayashi (2021a), and the strike of option D mimics the strike of the ophiolite and dykes best and suggests a slightly higher tilt, by ~15°. Option D predicts an initial dyke orientation of ~260°, whereas option C predicts ~280°. Because the tilt of the ophiolite is typically more difficult to assess directly than its better resolved strike, we prefer option D that correctly identifies the strike and generates a dip close to the measured dip.

The main uncertainty of the analysis is the initial paleo-inclination, so we explore to what extent options C and D would change if we changed the initial inclination. When the inclination is steepened, corresponding to a higher paleolatitude, the NTR analysis provides no solution, i.e., it is not possible to align the measured and initial magnetic directions while generating a vertical dyke orientation. This could either mean that the initial dyke orientation was systematically tilted, for which we see no evidence, or that there was some northward motion of the ophiolites in the Jurassic, as explained above. Nonetheless, the initial dyke orientation would not significantly change. Decreasing the initial inclination, corresponding to more southerly and eventually near-equatorial latitudes, changes the initial dyke strikes to 299° with an inclination of 30° (~16.1° paleolatitude), and to 306° with an inclination of 20° (~10.3° paleolatitude). However, these solutions also require a larger tilt of the ophiolite to vertical, or overturned, respectively, which is inconsistent with the modern architecture of the ophiolite.

We therefore use option D (Fig. 11, Table 8) as basis for our further analysis. The initial dyke strike of 260° shows that the paleo-spreading direction of the Mt. Diablo ophiolite was almost N-S, nearly parallel to the reconstructed subduction zone and north American margin.

5. Discussion

5.1. Ridge configuration and spreading rate in the Jurassic Californian forearc

We now evaluate whether the Jurassic ophiolites of California may have formed at a single ridge-transform system and may represent remnants of a single oceanic lithospheric sheet structurally overlying the Franciscan Complex. To this end, we use as input (i) the relative positions of the ophiolites prior to post-Jurassic deformation that follows from our kinematic reconstruction and their position relative to stable North America (Fig. 5); (ii) the global apparent polar wander path of Torsvik et al. (2012) to place the reconstruction in the paleomagnetic frame of reference; (iii) the paleoridge orientation that we obtained from the Mt. Diablo ophiolite (260°); and (iv) the formational ages (preferably U-Pb zircon) of the Jurassic ophiolites of California (Fig. 6) (Table 1). We attempted to find a ridge-transform configuration in which the ages of the ophiolites are explained by a near-constant spreading rate perpendicular to the reconstructed paleoridge orientation.

Uncertainties that must be considered are the error in the paleomagnetic reference frame that allows for deviations in declination of a few degrees, errors in the paleo-dyke orientation (Fig. 11a), uncertainties in the reconstruction of the kinematic reconstruction, particularly of the wider San Andreas fault system that affect the relative

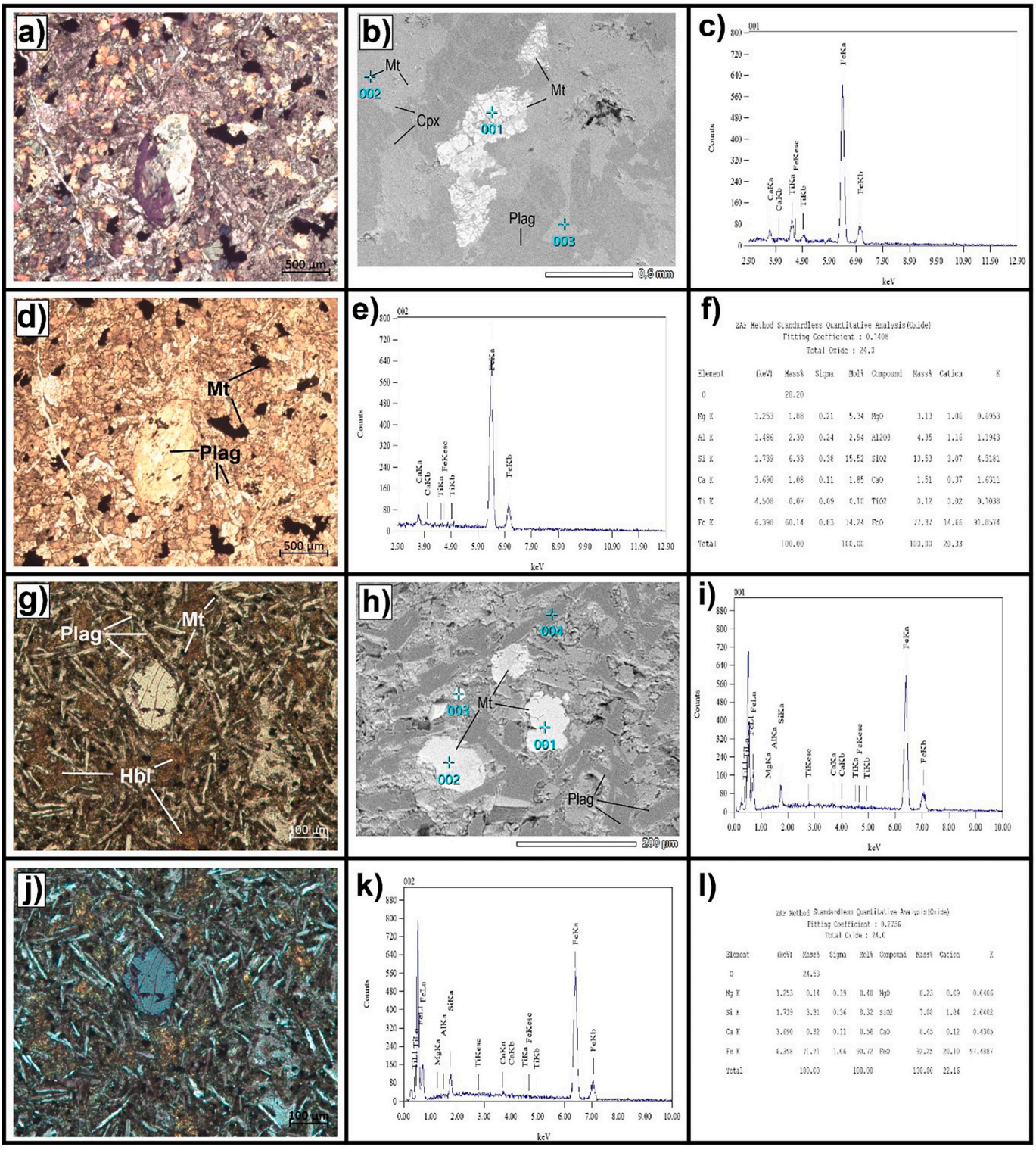

Fig. 8. Photomicrographs of two representative thin sections from sheeted dyke and pillow lava sections of the Mount Diablo Ophiolite under (a & g) normal and (d & j) polarized light, and (b, e & h) scanning electron microscope (SEM). (c, e, i, & k) EDX element analysis graphs of ferromagnetic grains. Quantitative results for grain 1 in sheeted dyke (f), and grain 2 in pillow lava (l), using the standardless ZAF quantification method. Abbreviations for mineral names: Cpx, clinopyroxene; Hbl, hornblende; Mt, magnetite; Plag, plagioclase.

positions of the ophiolites. These uncertainties permit a variation in the paleo-spreading direction relative to the ophiolites up to 10° and may change the reconstructed spreading rate by <10%. Within these uncertainties, we find two possible configurations which differ by a factor 2 in spreading rate (see below). The most important uncertainty comes from the unknown motion that the Californian forearc and the incipient Franciscan Complex may have undergone during final subduction between the Blue Mountains-Klamath Mountains-Sierra Nevada arcs and North America during the formation of the Californian ophiolites between ~170 and 160 Ma (Fig. 5e & 5f). We assume that this motion may

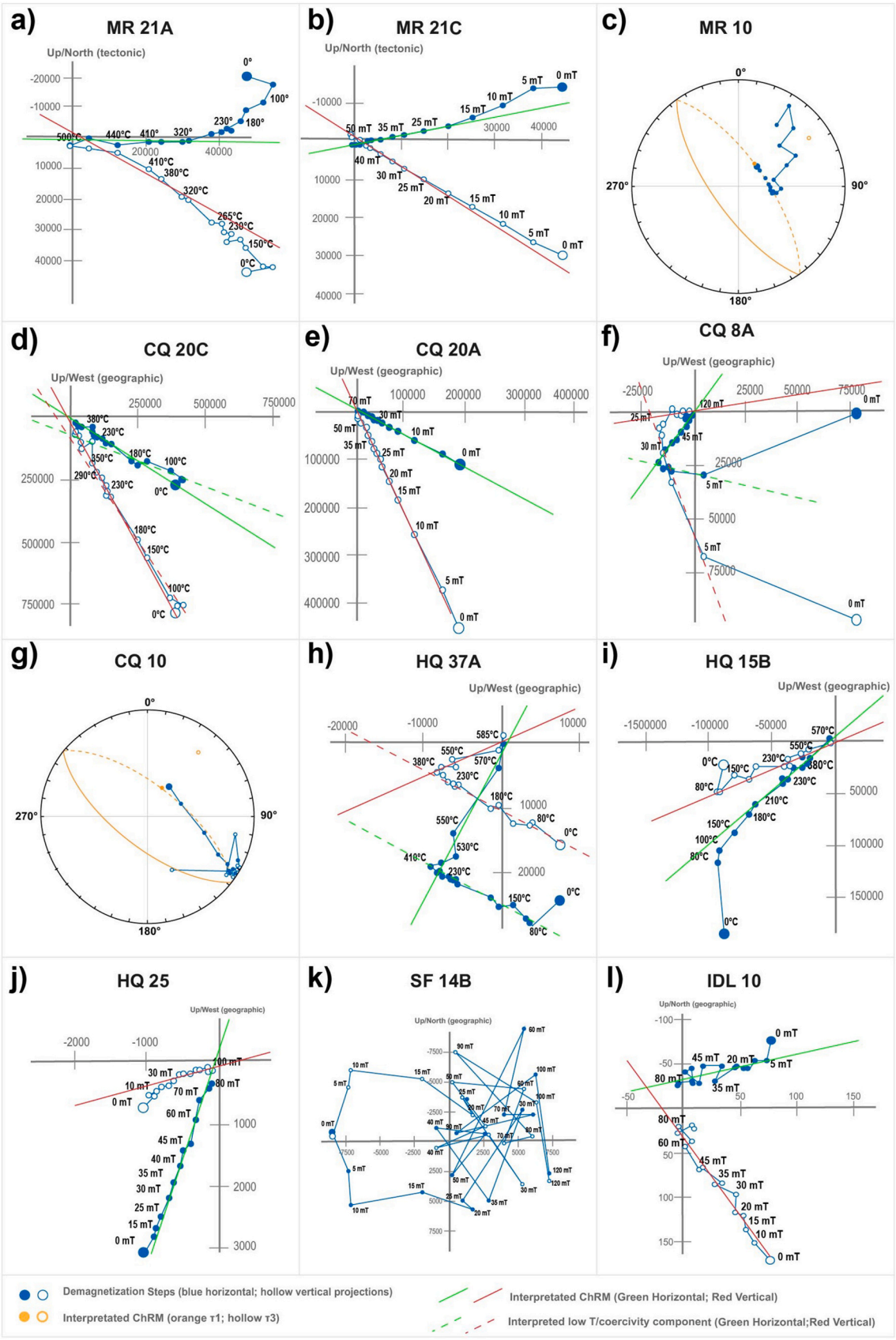

Fig. 9. Orthogonal vector and equal-area plots of the indicated sheeted dyke and pillow lava samples from Josephine Ophiolite (respectively IDL and SF) and Mount Diablo Ophiolite (respectively CQ & HQ and MR). Alternative field (mT) and thermal (°C) demagnetization steps are indicated. The pillow lava samples are on tectonic reference frame, and sheeted dykes are on geographic reference frame.

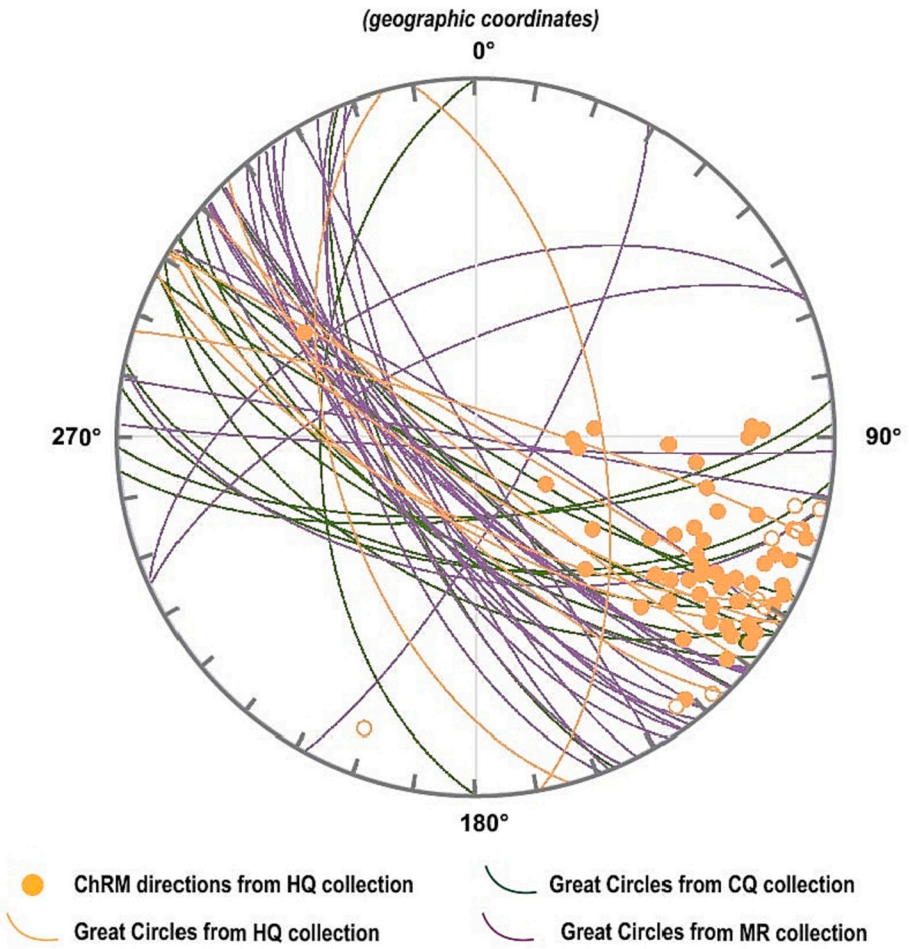

Fig. 10. The great circles between the overprint directions of HQ, CQ, and MR and presumed primary magnetization.

have been associated with some motion parallel to the North American margin, but without major vertical axis rotation of the whole Californian forearc region relative to North America. If such a rotation occurred, as suggested by (Ingersoll and Schweickert, 1986), the reconstructed distances between the Californian ophiolites decrease, which in combination with the constrained spreading direction would allow for lower spreading rates. The scenarios discussed below may thus be considered maximum estimated spreading rates.

Within the uncertainties, we chose two ridge-transform configurations: one with the minimum required transforms (Fig. 12a), and one with the minimum required spreading rate to satisfy the age distribution in the ophiolites (Fig. 12b). The minimum-transform scenario requires two transform faults. A western band of (reconstructed) ophiolites between Elder Creek in the north and San Simeon and Pt Sal in the south can be explained by spreading with high rates of ~18 cm/a between 168 and 161 Ma. A first transform fault is then required between this system and the Smartville ophiolite, which is too young to fit the pattern, but the spreading rate would satisfy the age difference between the Smartville and Josephine ophiolites. A second transform may be inferred between the Josephine and Wild Rogue Wilderness ophiolites.

A scenario with considerably slower spreading rates is obtained by rotating the ophiolites 5–10° clockwise, which is within the uncertainties of our reconstruction. In that case, the ophiolites of southern California may have been separated from the northwest Californian ophiolites by a transform fault (Fig. 12b). In this case, the age distribution is explained by a spreading rate of ~6 cm/a between 170 and 159 Ma. More detailed geochronological analyses will help obtain tighter constraints on these spreading rates.

5.2. Ophiolite kinematics as constraint on plate models

Our analysis suggests that the Californian forearc ophiolites formed by paleo-spreading directions that were nearly parallel to the adjacent subduction zone to the west. Such a spreading geometry is presently active in the Andaman Sea adjacent to the Sunda-Burma subduction zone (Curray, 2005; Morley, 2017). Trench-parallel spreading is also proposed to have occurred in the latest Cretaceous to Paleocene between India and Arabia forming the Bela and Muslim Bagh ophiolites of Pakistan (Gaina et al., 2015; Gnos et al., 1998). The Philippine Sea Plate also underwent trench-parallel spreading above the nascent Mariana-Izu-Bonin subduction zone (Casey and Dewey, 1984; Dewey and Casey, 2011). As well exemplified by the systems on either side of India, trench-parallel spreading is best explained by partitioning of oblique subduction. In those systems, oblique subduction may lead to a forearc sliver bounded by a trench on the foreland side and a transform fault on the hinterland side, and oceanic crust on ophiolites may form in pull-apart basins along extensional stepovers.

Our analysis of the ophiolites of California may thus provide a novel constraint on the kinematic history of the Cordilleran orogen and on Panthalassa plate tectonic evolution. On the one hand, our analysis predicts that for a period of perhaps 10 Ma, a dextral strike-slip system was present between the forearc, to which the ophiolites belong, and the North American continent. If our analysis is correct, then this system must have continued into the Intermontane belt of Canada. The spreading direction and rate of the ophiolites pose constraints on the northward motion component of the subducting Panthalassa plate relative to North America in the Jurassic. The Canadian Cordillera contains intra-oceanic arc remnants, in the Wrangellia superterrane,

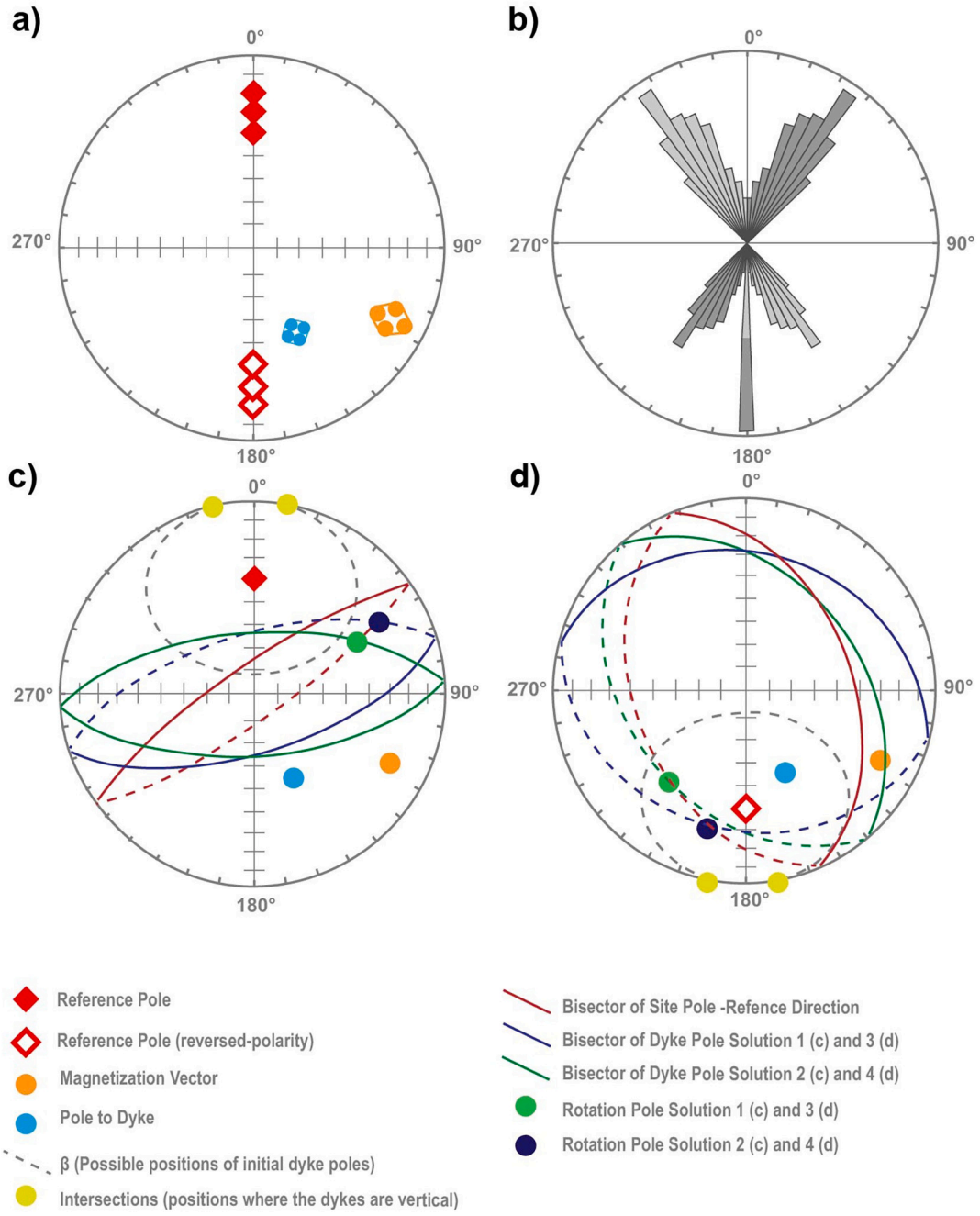

Fig. 11. (a) Plots indicating the input data of the net tectonic rotation analysis: characteristic remanent magnetization of sheeted dyke sequence in geographic coordinates, the average orientation of the dykes and the estimated original inclination (declination standard set to 0) with their error ranges. (b) Rose diagram showing the distribution of the permissible initial dyke orientations calculated for the values given in figure a. (c & d) The NTR Analysis for the preferred inclination, showing the calculated initial dyke poles and the associated rotation poles. The values for initial dyke strike and tilt correlation of the required rotations are given in Table 8. The preferred solution is solution 2 of Figure d. See text for further explanation.

that formed at an intra-oceanic subduction system west of North America contemporaneously, and at similar latitudes as the Californian ophiolites (Jones et al., 1977; Nokleberg et al., 2001). A detailed restoration of the plates of the eastern Panthalassa requires a far more detailed analysis of orogenic architecture and evolution of the Canadian Cordillera than we provide in this paper, but the spreading rate, direction, and duration constrained from forearc ophiolites may be compared to paleolatitudinal motion rates constrained from these intra-oceanic arcs. Ultimately, the subduction zones along and west of North America in the Mesozoic partitioned convergence between the Farallon Plate – connected to a Panthalassa plate motion chain - and North America – connected to an Indo-Atlantic plate motion chain (Boschman et al., 2021). Systematic reconstructions of the kinematics of ophiolites such as those obtained from the Middle to Late Jurassic Californian ophiolites will be helpful in constraining the marginal oceans and arcs, an important bridge towards plate kinematic reconstruction of the lost plates of the Panthalassa Ocean.

5.3. *Jurassic Californian ophiolites as remnants of a coherent forearc oceanic lithosphere*

Much of our understanding of forearc ophiolite systems comes from systems that have demonstrably coherent lithospheric slabs. These are notably the Sema'il Ophiolite of Oman, which is continuously exposed

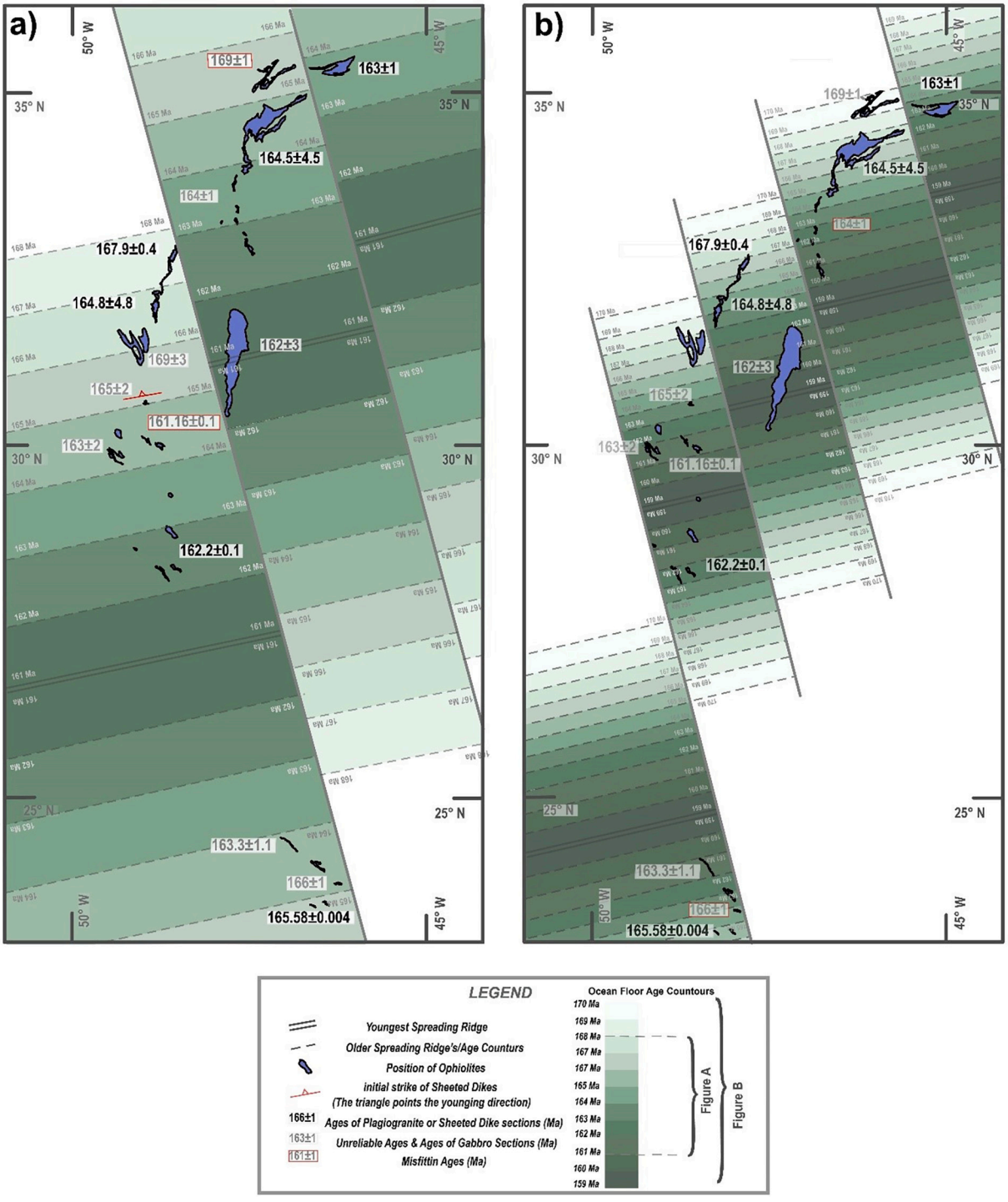

Fig. 12. (a) The ridge-transform configuration with minimum transform faults and a slip rate of ~ 18 cm/a; and (b) the ridge-transform configuration with minimum transform faults and a slip rate of ~ 6 cm/a, in which the ophiolites are 10° rotated. See text for further explanation.

over hundreds of kilometers (e.g., Nicolas et al., 2000) or from dredging and bore hole samples rare exposures of modern forearcs such as of the Philippine Sea Plate (Stern et al., 2012). Most ophiolite systems, including the Californian Ophiolites, however, are strongly dismembered through tectonic processes and erosion. This makes it difficult to establish whether regional variations in geochemical composition and age represent lateral variations within a single plate (system), or are a superposition of allochthonous fragments with markedly different plate tectonic histories. The Californian ophiolites have been instrumental in the development of the concepts of subduction initiation, supra-subduction zone ophiolite formation, and subsequent geochemical evolution (Shervais et al., 2004; Stern and Bloomer, 1992; Wakabayashi and Dilek, 2003; Wakabayashi and Shimabukuro, 2022). Our analysis shows that the assumption that the Jurassic ophiolites of California were derived from a forearc plate system, separated by a single ridge-transform system during formation, is kinematically sound. The vast majority of the original forearc lithosphere must have been eroded and the remaining ophiolitic klippen were displaced during the Cenozoic strike-slip deformation of California. Our reconstruction aids reviving these ophiolites as a natural laboratory to study the evolution of forearc plate systems spanning ~1000 km along trench strike.

Our analysis opens further opportunity to evaluate the initiation setting of the Franciscan subduction zone. Dickinson et al. (1996b) and Ingersoll and Schweickert (1986) suggested that the Coast Range Ophiolite formed in a back-arc setting behind the Klamath Mts – Blue Ridge Mts – Sierra Nevada arc system during the terminal convergence of the latter with North America, during a subduction polarity reversal (Fig. 1a). Our analysis favors such a scenario. This would be comparable to the reconstruction of a subduction polarity reversal that followed upon the collision of the Woyla intra-oceanic arc with Sundaland, on Sumatra, in the Cretaceous, and the coeval initiation of the Sunda subduction zone and the associated Andaman Ophiolites in the original back-arc basin (Advokaat et al., 2018; Bandyopadhyay et al., 2021; Plunder et al., 2020). In the Sumatra-Andaman system, the time span between the onset of the new and arrest of the old subduction zone is on the order of 10 Ma (Bandyopadhyay et al., 2021; Plunder et al., 2020), which is similar as in the case of California. Our reconstruction provides a spatial and kinematic context for future studies that aim to study subduction termination and initiation using the western USA geological records of the Jurassic as a case study.

6. Conclusions

In this paper, we tested whether the isolated Jurassic ophiolite klippen of California may be remnants of a single oceanic lithospheric sheet that was eroded and tectonically dismembered. To this end, we first reviewed the age constraints on the ophiolitic crust, which formed by sea floor spreading in a supra-subduction zone or back-arc basin environment between ~160 and 170 Ma. We then reviewed kinematic constraints on the deformation history of the western United States since the Jurassic formation of the ophiolites around 170 Ma, from the Canadian to the Mexican border. We used these constraints to reconstruct the position of the ophiolites relative to each other prior to dismemberment during Cenozoic displacements along the San Andreas Fault Zone, and to evaluate the positions of the Jurassic ophiolites relative to North America corrected for Cenozoic Basin and Range extension, and Mesozoic to Paleogene orogeneses. The kinematic reconstruction reveals that during the Jurassic, the ophiolites spanned a 1000 km distance parallel to the western North American margin. Previous geological constraints show that until ~150–160 Ma, the ophiolite belt may have still been converging with the north American margin as result of inboard subduction recorded in the Klamath Mountains, Blue Mountains, and Sierra Nevada arcs, but since 150 Ma must have been part of the western North American forearc.

We then performed a paleomagnetic analysis of the sheeted dyke and pillow lava sections of the Mt. Diablo ophiolite. We showed that the pillow lavas and part of the sheeted dyke sections were strongly overprinted, but we recovered a primary magnetization from approximately half of the sheeted dyke sections. We performed a net tectonic rotation analysis that reveals a solution in which the dykes are restored to vertical at a realistic latitude for the Californian forearc in the Jurassic that accurately predicts the modern orientation of the ophiolite. This solution shows a paleo-ridge strike of ~260–080°, near-perpendicular to the reconstructed orientation of the western US subduction zone in the paleomagnetic reference frame. With this reconstructed ridge orientation, we showed that the age distribution of the ophiolites can be explained by a single ridge-transform system if it accommodated a spreading rate of 18 cm/a. This is a maximum estimate: if the Californian ophiolites rotated relative to north America before the ~150–160 Ma arrest of convergence, lower spreading rates are required.

Our analysis shows that kinematic restoration of the ophiolite belt in combination with paleomagnetic analysis of sheeted dyke sections provides novel constraints on the reconstruction of orogenic history, as well as on the motions of paleo-tectonic plates that have been lost to subduction. Our results show that the plate that subducted beneath the western North American forearc in the Jurassic must have had a northward motion component relative to stable North America of up to 6–7 cm/a. In addition, we show that even the highly dismembered and scattered ophiolite klippen of California that were dismembered by the faults of the San Andreas Fault Zone, maintain their original coherence. Variations between these ophiolite klippen may thus be considered temporal and/or spatial within-plate variations that can be helpful to interpret oceanic lithospheric evolution and dynamics. The reconstruction in our paper provides the original spatial context for those studies.

Supplementary data to this article can be found online at https://doi.org/10.1016/j.earscirev.2022.104275.

Declaration of Competing Interest

The authors declare that they have no known competing financial interests or personal relationships that could have appeared to influence the work reported in this paper.

Data availability

The data is privded in the attached files (AP4 & AP5)

Acknowledgements

NL, AQ, and DJJvH acknowledge NWO Vici grant 865.17.001 to DJJvH. We thank Joshua Goodwin (California Geological Survey) for discussion and logistical support. We thank Marco Maffione and Lydian Boschman for discussion. This paper benefited from constructive reviews of Paul Kapp and an anonymous reviewer.

Appendix A. Appendix

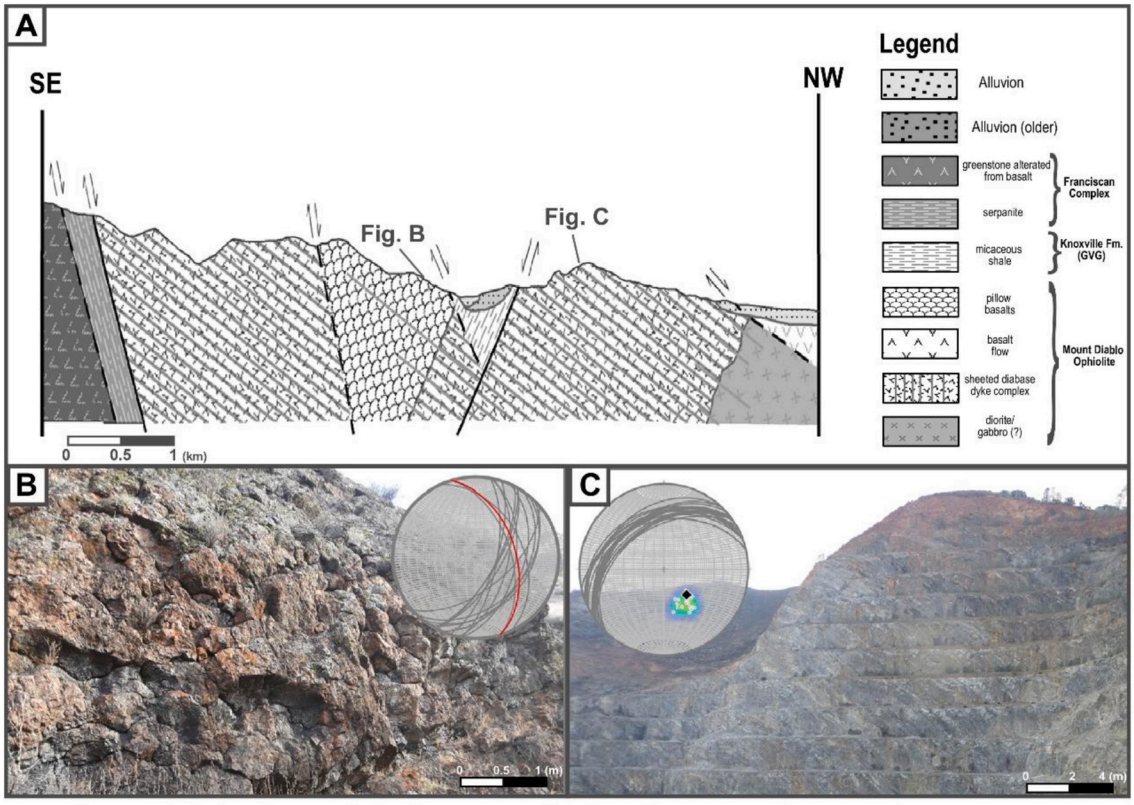

AP 1; (a) NW-SE cross section of Mount Diablo Ophiolite showing the contact relation of sampled rocks [(adapted from Williams (1984)].; (b) Picture of Pillows from Mitchell Rock area with a streonet showing the pillow orientations. The red great circle is the bedding of Mitchel Rock analyzed rocks. (c) Picture of sheeted dykes from Cemex Quarry with a stereonet showing the dyke orientations and magma flow direction from AMS Analysis (black diamond).

AP 2; Google Earth Picture of sampling sides of pillow lava (MR) and sheeted dyke sections (CQ &HQ).

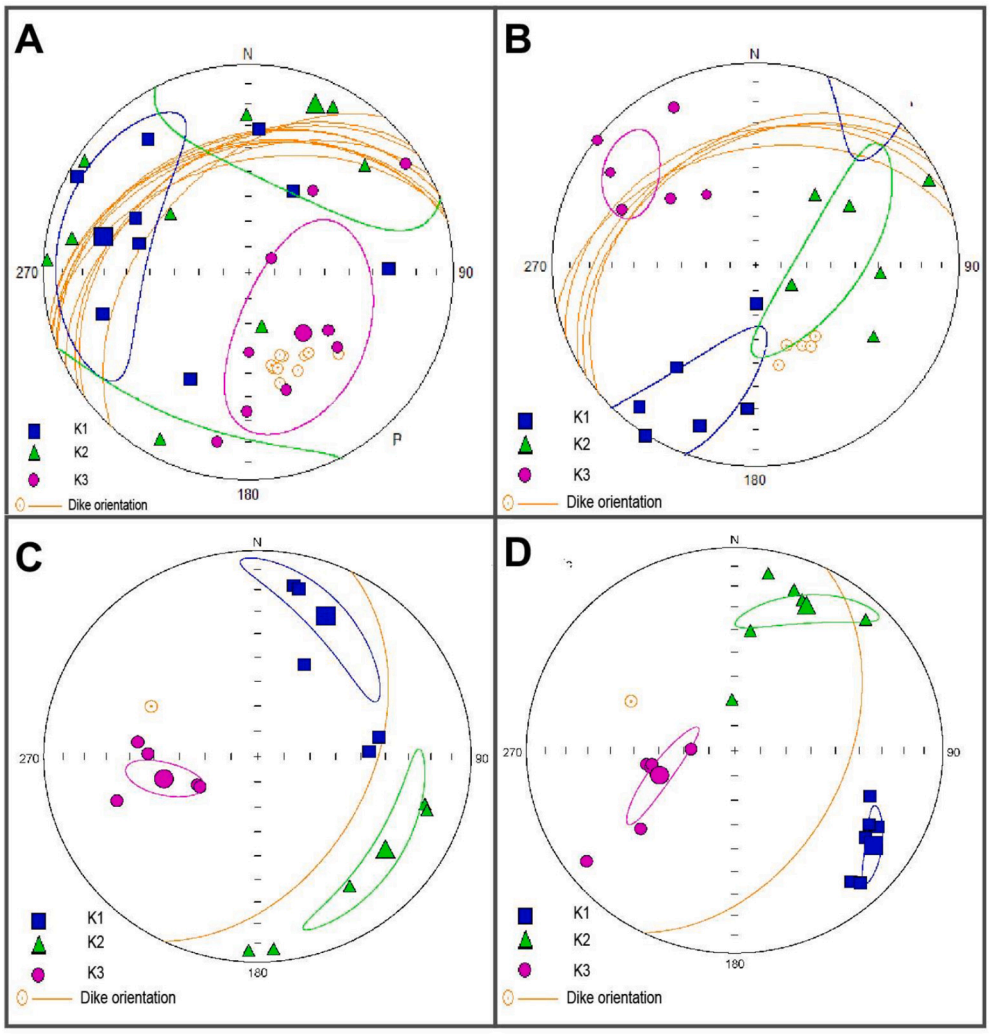

AP3; Orientation of maximum, minimum and average magnetic susceptibilities and dyke (with great circles) (a) of 10 dyke samples of Mount Diablo Ophiolite that have a mean direction indicating magma flow parallel to dyke; (b) of 6 dyke samples of Mount Diablo Ophiolite have mean directions indicating magma flow perpendicular to dyke; (c, d) of 10 dyke samples of Josephine Ophiolite that have mean directions indicating magma flow parallel to the dyke.

References

Abbott, P.L., Kies, R.P., Kerr, D.R., 1983. Right-slip offset of the Eocene Ballena River Valley across the Elsinore Fault Zone, Southern California. Ciencias Mar. 9, 87–94. https://doi.org/10.7773/cm.v9i2.423.

Advokaat, E.L., Bongers, M.L.M., Rudyawan, A., BouDagher-Fadel, M.K., Langereis, C.G., van Hinsbergen, D.J.J., 2018. Early cretaceous origin of the Woyla Arc (Sumatra, Indonesia) on the Australian plate. Earth Planet. Sci. Lett. 498, 348–361. https://doi.org/10.1016/j.epsl.2018.07.001.

Allerton, S., 1989. Distortions, rotations and crustal thinning at ridge-transform intersections. Nature 340, 626–628. https://doi.org/10.1038/340626a0.

Allerton, S., Vine, F.J., 1987. Spreading structure of the Troodos ophiolite, Cyprus: some paleomagnetic constraints. Geology 15, 593. https://doi.org/10.1130/0091-7613(1987)15<593:SSOTTO>2.0.CO;2.

Allmendinger, R.W., 1992. Fold and thrust tectonics of the western United States exclusive of the accreted terranes. In: The Cordilleran Orogen. Geological Society of America, Boulder, Colorado 80301, pp. 583–608. https://doi.org/10.1130/DNAG-GNA-G3.583.

Anczkiewicz, R., Platt, J.P., Thirlwall, M.F., Wakabayashi, J., 2004. Franciscan subduction off to a slow start: evidence from high-precision Lu–Hf garnet ages on high grade-blocks. Earth Planet. Sci. Lett. 225, 147–161. https://doi.org/10.1016/j.epsl.2004.06.003.

Armstrong, R.L., 1968. Sevier orogenic belt in Nevada and Utah. Geol. Soc. Am. Bull. 79, 429–458.

Atwater, T., 1989. Plate tectonic history of the northeast Pacific and western North America. In: The Eastern Pacific Ocean and Hawaii. Geological Society of America, North America, pp. 21–72. https://doi.org/10.1130/DNAG-GNA-N.21.

Atwater, T., Stock, J., 1998. Pacific-North America Plate Tectonics of the Neogene Southwestern United States: an update. Int. Geol. Rev. 40, 375–402. https://doi.org/10.1080/00206819809465216.

Balgord, E.A., Yonkee, W.A., Wells, M.L., Gentry, A., Laskowski, A.K., 2021. Arc tempos, tectonic styles, and sedimentation patterns during evolution of the North American Cordillera: constraints from the retroarc detrital zircon archive. Earth-Sci. Rev. 216, 103557 https://doi.org/10.1016/j.earscirev.2021.103557.

Bandyopadhyay, D., Ghosh, B., Guilmette, C., Plunder, A., Corfu, F., Advokaat, E.L., Bandopadhyay, P.C., van Hinsbergen, D.J.J., 2021. Geochemical and geochronological record of the Andaman Ophiolite, SE Asia: from back-arc to forearc during subduction polarity reversal? Lithos 380–381, 105853. https://doi.org/10.1016/j.lithos.2020.105853.

Bartley, J.M., Glazner, A.F., Coleman, D.S., Kylander-Clark, A., Mapes, R., Friedrich, A. M., 2007. Large Laramide dextral offset across Owens Valley, California, and its possible relation to tectonic unroofing of the southern Sierra Nevada. Spec. Pap. Geol. Soc. Am. 434, 129–148. https://doi.org/10.1130/2007.2434(07).

Beebe, W.J., 1986. A Paleomagnetic Study of the Southern Coast Range Ophiolite, California, and Tectonic Implications. (Doctoral Diss. Univ. California, St. Barbar).

Bird, P., 1998. Kinematic history of the Laramide orogeny in latitudes 35°-49°N, western United States. Tectonics 17, 780–801. https://doi.org/10.1029/98TC02698.

Boschman, L.M., Garza, R.S.M., Langereis, C.G., van Hinsbergen, D.J.J., 2018a. Paleomagnetic constraints on the kinematic relationship between the Guerrero terrane (Mexico) and North America since early cretaceous time. Bull. Geol. Soc. Am. 130, 1131–1142. https://doi.org/10.1130/B31916.1.

Boschman, L.M., van Hinsbergen, D.J.J., Langereis, C.G., Flores, K.E., Kamp, P.J.J., Kimbrough, D.L., Ueda, H., van de Lagemaat, S.H.A., van der Wiel, E., Spakman, W., 2021. Reconstructing lost plates of the Panthalassa Ocean through paleomagnetic data from circum-Pacific accretionary orogens. Am. J. Sci. 321, 907–954. https://doi.org/10.2475/06.2021.08.

Boschman, L.M., van Hinsbergen, D.J.J., Kimbrough, D.L., Langereis, C.G., Spakman, W., 2018b. The dynamic history of 220 million years of subduction below Mexico: a correlation between slab geometry and overriding plate deformation based on geology, paleomagnetism, and seismic tomography. Geochem.Geophys. Geosyst. 19, 4649–4672. https://doi.org/10.1029/2018GC007739.

Boschman, L.M., van Hinsbergen, D.J.J., Torsvik, T.H., Spakman, W., Pindell, J.L., 2014. Kinematic reconstruction of the Caribbean region since the early jurassic. Earth-Sci. Rev. 138, 102–136. https://doi.org/10.1016/j.earscirev.2014.08.007.

Buising, A.V., Walker, J.P., 1995. Preliminary palinspastic paleogeographic reconstructions for the Greater San Francisco Bay Area, 15Ma-5 Ma. In: Sagines, E. M., Anderson, D.W., Buising, A.B. (Eds.), 1995 Recent Geol. Stud. San Fr. Bay Area Pacific Sect. S.E.P.M. 76, pp. 141–160.

Butler, P.R., Troxel, B.W., Verosub, K.L., 1988. Late Cenozoic history and styles of deformation along the southern Death Valley fault zone,California. Bull. Geol. Soc. Am. 100, 402–410. https://doi.org/10.1130/0016-7606(1988)100<0402:LCHASO>2.3.CO;2.

Bürgmann, R., Hilley, G., Ferretti, A., Novali, F., 2006. Resolving vertical tectonics in the San Francisco Bay Area from permanent scatterer InSAR and GPS analysis. Geology 34, 221. https://doi.org/10.1130/G22064.1.

Burnham, K., 2009. Predictive model of San Andreas fault system paleogeography, Late Cretaceous to early Miocene, derived from detailed multidisciplinary conglomerate correlations. Tectonophysics 464, 195–258. https://doi.org/10.1016/j.tecto.2007.11.056.

Camp, V.E., Hanan, B.B., 2008. A plume-triggered delamination origin for the Columbia River Basalt Group. Geosphere 4, 480. https://doi.org/10.1130/GES00175.1.

Campbell, R.H., Yerkes, R.F. (Eds.), 1976. Pac. Sect., Am. Assoc. of Pet. Geol., Los Angeles, Calif. 541–558.

Casey, J.F., Dewey, J.F., 1984. Initiation of subduction zones along transform and accreting plate boundaries, triple-junction evolution, and forearc spreading centres—implications for ophiolitic geology and obduction. Geol. Soc. LondonSpec. Publ. 13, 269–290. https://doi.org/10.1144/GSL.SP.1984.013.01.22.

Cassel, E.J., Stockli, D.F., Smith, M.E., Jicha, B.R., Singer, B.S., 2020. Accelerating exhumation in the Eocene North American Cordilleran hinterland: implications from detrital zircon (U-Th)/(He-Pb) double dating. GSA Bull. 132, 198–214. https://doi.org/10.1130/B35160.1.

Cather, S.M., 1999. Implications of Jurassic, cretaceous, and Proterozoic piercing lines for Laramide oblique-slip faulting in New Mexico and rotation of the Colorado Plateau. Geol. Soc. Am. Bull. 111, 849–868. https://doi.org/10.1130/0016-7606(1999)111<0849:IOJCAP>2.3.CO;2.

Cather, S.M., Harrison, R.W., Lueth, V., Giles, K., Lucas, S., Kues, B., Myers, R., Ulmer-Scholle, D., 2002. In: Lower Paleozoic isopach maps of southern New Mexico and their implications for Laramide and ancestral Rocky Mountain tectonism. 53rd Annu. F. Conf. Guideb, pp. 85–101.

Cather, S.M., Karlstrom, K.E., Timmons, J.M., Heizler, M.T., 2006. Palinspastic reconstruction of Proterozoic basement-related aeromagnetic features in north-central New Mexico: implications for Mesoproterozoic to late Cenozoic tectonism. Geosphere 2, 299–323. https://doi.org/10.1130/GES00045.1.

Chapin, C.E., 2012. Origin of the Colorado Mineral Belt. Geosphere 8, 28–43. https://doi.org/10.1130/GES00694.1.

Chapman, A.D., 2017. The Pelona–Orocopia–Rand and related schists of southern California: a review of the best-known archive of shallow subduction on the planet. Int. Geol. Rev. 59, 664–701. https://doi.org/10.1080/00206814.2016.1230836.

Chapman, A.D., Ernst, W.G., Gottlieb, E., Powerman, V., Metzger, E.P., 2015. Detrital zircon geochronology of Neoproterozoic-Lower Cambrian passive-margin strata of the White-Inyo Range, east-central California: implications for the Mojave-Snow Lake fault hypothesis. Bull. Geol. Soc. Am. 127, 926–944. https://doi.org/10.1130/B31142.1.

Chapman, A.D., Jacobson, C.E., Ernst, W.G., Grove, M., Dumitru, T., Hourigan, J., Ducea, M.N., 2016. Assembling the world's type shallow subduction complex: detrital zircon geochronologic constraints on the origin of the Nacimiento block, Central California Coast Ranges. Geosphere 12, 533–557. https://doi.org/10.1130/GES01257.1.

Chapman, A.D., Luffi, P.I., Saleeby, J.B., Peterson, S., 2011. Metamorphic evolution, partial melting and rapid exhumation above an ancient flat slab: insights from the San Emigdio Schist, southern California. J. Metamorph. Geol. 29, 601–626. https://doi.org/10.1111/j.1525-1314.2011.00932.x.

Chávez-Cabello, G., Aranda-Gómez, J.J., Molina-Garza, R.S., Cossío-Torres, T., Arvizu-Gutiérrez, I.R., González-Naranjo, G.A., 2007. The San Marcos fault: a Jurassic multireactivated basement structure in northeastern México. In: Geology of Mexico: Celebrating the Centenary of the Geological Society of México. Geological Society of America. https://doi.org/10.1130/2007.2422(08).

Choi, S.H., Shervais, J.W., Mukasa, S.B., 2008. Supra-subduction and abyssal mantle peridotites of the Coast Range ophiolite,California. Contrib. Mineral. Petrol. 156, 551–576. https://doi.org/10.1007/s00410-008-0300-6.

Clennett, E.J., Sigloch, K., Mihalynuk, M.G., Seton, M., Henderson, M.A., Hosseini, K., Mohammadzaheri, A., Johnston, S.T., Müller, R.D., 2020. A quantitative tomotectonic plate reconstruction of Western North America and the Eastern Pacific Basin. Geochem. Geophys. Geosyst. 21 https://doi.org/10.1029/2020GC009117.

Clarke, S.H., 1973. The Eocene point of rocks sandstone: provenance, mode of deposition and implications for the history of offset along the San Andreas fault in central California. University of California, Berkeley.

Cloos, M., 1985. Thermal evolution of convergent plate margins: thermal modeling and reevaluation of isotopic AR-ages for Blueschists in the franciscan complex of California. Tectonics 4, 421–433. https://doi.org/10.1029/TC004i005p00421.

Colgan, J.P., Stanley, R.G., 2016. The Point Sal-Point Piedras Blancas correlation and the problem of slip on the San Gregorio-Hosgri fault, Central California Coast Ranges. Geosphere 12, 971–984. https://doi.org/10.1130/GES01289.1.

Constenius, K.N., 1996. Late Paleogene extensional collapse of the Cordilleran foreland fold and thrust belt. Bull. Geol. Soc. Am. 108, 20–39. https://doi.org/10.1130/0016-7606(1996)108<0020:LPECOT>2.3.CO;2.

Cromwell, G., Johnson, C.L., Tauxe, L., Constable, C.G., Jarboe, N.A., 2018. PSV10: a global data set for 0–10 Ma time-averaged field and paleosecular variation studies. Geochem.Geophys. Geosyst. 19, 1533–1558. https://doi.org/10.1002/2017GC007318.

Cummings, M.L., Evans, J.G., Ferns, M.L., Lees, K.R., 2000. Stratigraphic and structural evolution of the middle Miocene synvolcanic Oregon-Idaho graben. Geol. Soc. Am. Bull. 112, 668–682. https://doi.org/10.1130/0016-7606(2000)112<668:SASEOT>2.0.CO;2.

Curray, J.R., 2005. Tectonics and history of the Andaman Sea region. J. Asian Earth Sci. 25, 187–232. https://doi.org/10.1016/j.jseaes.2004.09.001.

Currie, B.S., 2002. Structural configuration of the Early Cretaceous Cordilleran foreland-basin system and Sevier thrust belt, Utah and Colorado. J. Geol. 110, 697–718. https://doi.org/10.1086/342626.

Day, H.W., Bickford, M.E., 2004. Tectonic setting of the Jurassic Smartville and Slate Creek complexes, northern Sierra Nevada,California. Bull. Geol. Soc. Am. 116, 1515–1528. https://doi.org/10.1130/B25416.1.

DeCelles, P.G., 1994. Late Cretaceous-Paleocene synorogenic sedimentation and kinematic history of the Sevier thrust belt, northeast Utah and southwest Wyoming. Geological Society of America Bulletin 106 (1), 32–56.

DeCelles, P.G., 2004. Late Jurassic to Eocene evolution of the Cordilleran. Am. J. Sci. 304, 105–168.

DeCelles, P.G., Coogan, J.C., 2006. Regional structure and kinematic history of the Sevier fold-and-thrust belt, Central Utah. Bull. Geol. Soc. Am. 118, 841–864. https://doi.org/10.1130/B25759.1.

Deenen, M.H.L., Langereis, C.G., van Hinsbergen, D.J.J., Biggin, A.J., 2014. Erratum: Geomagnetic secular variation and the statistics of palaeomagnetic directions. Geophys. J. Int. 197, 643. https://doi.org/10.1093/gji/ggu021.

Deenen, M.H.L., Langereis, C.G., van Hinsbergen, D.J.J., Biggin, A.J., 2011. Geomagnetic secular variation and the statistics of palaeomagnetic directions. Geophys. J. Int. 186, 509–520. https://doi.org/10.1111/j.1365-246X.2011.05050.x.

DeGraaff-Surpless, K., Graham, S.A., Wooden, J.L., McWilliams, M.O., 2002. Detrital zircon provenance analysis of the Great Valley Group, California: evolution of an arc-forearc system. Bull. Geol. Soc. Am. 114, 1564–1580. https://doi.org/10.1130/0016-7606(2002)114<1564:DZPAOT>2.0.CO;2.

Dewey, J.F., 1976. Ophiolite obduction. Tectonophysics 31, 93–120. https://doi.org/10.1016/0040-1951(76)90169-4.

Dewey, J.F., Casey, J.F., 2011. The origin of obducted large-slab ophiolite complexes. Arc-Continent Collision,Springer 4, 431–444. https://doi.org/10.1007/978-3-540-88558-0.

Dickinson, W.R., 2008. Accretionary Mesozoic-Cenozoic expansion of the Cordilleran continental margin in California and adjacent Oregon. Geosphere 4, 329–353. https://doi.org/10.1130/GES00105.1.

Dickinson, W.R., Ducea, M., Rosenberg, L.I., Greene, H.G., Graham, S.A., Clark, J.C., Weber, G.E., Kidder, S., Ernst, W.G., Brabb, E.E., 2005. Net dextral slip, Neogene San Gregorio–Hosgri fault zone, coastal California: geologic evidence and tectonic implications. Geological Society of America Special Paper 391, 1–43. https://doi.org/10.1130/0-8137-2391-4.1.

Dickinson, W.R., Hopson, C.A., Saleeby, J.B., 1996a. Alternate origins of the Coast Range Ophiolite (California). GSA Today 6, 1–10.

Dickinson, W.R., Lawton, T.F., 2001a. Carboniferous to Cretaceous assembly and fragmentation of Mexico. Geol. Soc. Am. Bull. 113, 1142–1160. https://doi.org/10.1130/0016-7606(2001)113<1142:CTCAAF>2.0.CO;2.

Dickinson, W.R., Lawton, T.F., 2001b. Tectonic setting and sandstone petrofacies of the Bisbee basin (USA–Mexico). J. S. Am. Earth Sci. 14, 475–504.

Dickinson, W.R., Schweickert, R., Ingersoll, R., 1996b. Coast Range ophiolite as backarc/intraarc basin lithosphere. GSA Today 6, 2–3.

Dickinson, W.R., Soreghan, M., Gehrels, G., 2000. Geodynamic interpretation of Paleozoic tectonic trends oriented oblique to the Mesozoic Klamath-Sierran continental margin in California. In: Geological Society of America Special Paper. Geological Society of America, pp. 209–246. https://doi.org/10.1130/0-8137-2347-7.209.

Dilek, Y., Furnes, H., 2011. Ophiolite genesis and global tectonics: geochemical and tectonic fingerprinting of ancient oceanic lithosphere. Geol. Soc. Am. Bull. 123, 387–411. https://doi.org/10.1130/B30446.1.

Dixon, T.H., Xie, S., 2018. A kinematic model for the evolution of the Eastern California Shear Zone and Garlock Fault, Mojave Desert,California. Earth Planet. Sci. Lett. 494, 60–68. https://doi.org/10.1016/j.epsl.2018.04.050.

Dokka, R.K., Travis, J., 1990a. Role of the eastern California shear zone in accommodating Pacific-North American plate motion. Geophys. Res. Lett. 17, 1323–1326.

Dokka, R.K., Travis, C.J., 1990b. Late Cenozoic strike-slip faulting in the Mojave Desert, California. Tectonics 9, 311–340. https://doi.org/10.1029/TC009i002p00311.

Doubrovine, P.V., Steinberger, B., Torsvik, T.H., 2012. Absolute plate motions in a reference frame defined by moving hot spots in the Pacific, Atlantic, and Indian oceans. J. Geophys. Res. Solid Earth 117. https://doi.org/10.1029/2011JB009072.

du Bray, E., John, D.A., 2011. Petrologic, tectonic, and metallogenic evolution of the Ancestral Cascades magmatic arc, Washington, Oregon, and northern California. Geosphere 7, 1102. https://doi.org/10.1130/GES00669.1.

Dumitru, T.A., Ernst, W.G., Hourigan, J.K., McLaughlin, R.J., 2015. Detrital zircon U-Pb reconnaissance of the franciscan subduction complex in northwestern California. Int. Geol. Rev. 57, 767–800. https://doi.org/10.1080/00206814.2015.1008060.

Dumitru, T.A., Hourigan, J.K., Elder, W.P., Ernst, W.G., Joesten, R., Ingersoll, R.V., Lawton, T.F., Graham, S.A., 2018. In: New, much younger ages for the Yolla Bolly terrane and a revised time line for accretion in the Franciscan subduction complex, California. Tectonics, Sediment. Basins, Proven. A Celebr. Career William R. Dickinson, pp. 339–366.

Dumitru, T.A., Wakabayashi, J., Wright, J.E., Wooden, J.L., 2010. Early Cretaceous transition from nonaccretionary behavior to strongly accretionary behavior within the franciscan subduction complex. Tectonics 29. https://doi.org/10.1029/2009TC002542.

Edelman, S.H., Sharp, W.D., 1989. Terranes, early faults, and pre-Late Jurassic amalgamation of the western Sierra Nevada metamorphic belt,California. Geol. Soc. Am. Bull. 101, 1420–1433. https://doi.org/10.1130/0016-7606(1989)101<1420:TEFAPL>2.3.CO;2.

Ernst, W.G., 2011. Accretion of the Franciscan Complex attending Jurassic-Cretaceous geotectonic development of northern and Central California. Geol. Soc. Am. Bull. 123, 1667–1678. https://doi.org/10.1130/B30398.1.

Ernst, W.G., 1980. Mineral paragenesis in Franciscan metagraywackes of the Nacimiento Block, a subduction complex of the Southern California Coast Ranges. J. Geophys. Res. 85, 7045. https://doi.org/10.1029/JB085iB12p07045.

Ernst, W.G., Snow, C.A., Scherer, H.H., 2008. Contrasting early and late Mesozoic petrotectonic evolution of northern California. Geol. Soc. Am. Bull. 120, 179–194. https://doi.org/10.1130/B26173.1.

Evarts, R.C., Sharp, W.D., Phelps, D.W., 1992. The Del Puerto Canyon remnant of the Great Valley ophiolite: geochemical and age constraints on its formation and evolution. Bull. Am. Assoc. Pet. Geol. 76, 418.

Erslev, E.A., Schmidt, C.J., Chase, R.B., 1993. Thrusts, back-thrusts and detachment of Rocky Mountain foreland arches. SPECIAL PAPERS-GEOLOGICAL SOCIETY OF AMERICA 280, 339–358.

Evarts, R.C., Schiffman, P., 1983. Submarine hydrothermal metamorphism of the Del Puerto ophiolite,California. Am. J. Sci. 283, 289–340.

Faulds, J.E., Henry, C.D., Hinz, N.H., 2005. Kinematics of the northern Walker Lane: An incipient transform fault along the Pacific–North American plate boundary. Geology 33 (6), 505–508.

Faulds, J., Henry, C.D., Spencer, J., Titley, S., 2008. Ectonic influences on the spatial and temporal evolution of the Walker Lane: an incipient transform fault along the evolving Pacific-North American plate boundary. Ores Orogenes. Circum-Pacific Tectonics, Geol. Evol. Ore DeposArizona Geol. Soc. Dig.22 22, 437–470.

Fitz-Díaz, E., Hudleston, P., Tolson, G., 2011. Comparison of tectonic styles in the Mexican and Canadian Rocky Mountain fold-thrust belt. Geol. Soc. Spec. Publ. 349, 149–167. https://doi.org/10.1144/SP349.8.

Fitz-Díaz, E., Lawton, T.F., Juárez-Arriaga, E., Chávez-Cabello, G., 2018. The Cretaceous-Paleogene Mexican orogen: structure, basin development, magmatism and tectonics. Earth Sci. Rev. 183, 56–84. https://doi.org/10.1016/j.earscirev.2017.03.002.

Ford, E., Caskey, S.J., Wagner, D.L., Fleck, R.J., 2003. Miocene volcanic rocks at Burdell Mountain and implications for slip along the East Bay Fault System. Geol. Soc. Am. Abstr. with Programs 73.

Foster, D.A., Doughty, P.T., Kalakay, T.J., Fanning, C.M., Coyner, S., Grice, W.C., Vogl, J., 2007. Kinematics and timing of exhumation of metamorphic core complexes along the Lewis and Clark fault zone, northern Rocky Mountains,USA. Spec. Pap. Geol. Soc. Am. 434, 207–232. https://doi.org/10.1130/2007.2434(10).

Foster, D.A., Grice, W.C., Kalakay, T.J., 2010. Extension of the Anaconda metamorphic core complex: 40Ar/39Ar thermochronology and implications for Eocene tectonics of the northern Rocky Mountains and the Boulder batholith. Lithosphere 2, 232–246. https://doi.org/10.1130/L94.1.

Furnes, H., Dilek, Y., 2022. Archean versus Phanerozoic oceanic crust formation and tectonics: Ophiolites through time. Geosyst. Geoenviron. 1, 100004 https://doi.org/10.1016/j.geogeo.2021.09.004.

Gaina, C., van Hinsbergen, D.J.J., Spakman, W., 2015. Tectonic interactions between India and Arabia since the Jurassic reconstructed from marine geophysics, ophiolite geology, and seismic tomography. Tectonics 34, 875–906. https://doi.org/10.1002/2014TC003780.

Gans, P.B., Miller, E.L., Gurgel, K., 1983. In: Tyle of mid-Tertiary extension in east-central Nevada. Geol. excursions overthrust belt Metamorph. core complexes Intermt. Reg. Utah Geol. Miner. Surv. Spec. Stud. 59, pp. 107–139.

Gaschnig, R.M., Vervoort, J.D., Lewis, R.S., Tikoff, B., 2011. Isotopic evolution of the Idaho Batholith and Challis Intrusive Province, Northern US Cordillera. J. Petrol. 52, 2397–2429. https://doi.org/10.1093/petrology/egr050.

Geist, D., Richards, M., 1993. Origin of the Columbia Plateau and Snake River plain: deflection of the Yellowstone plume. Geology 21, 789. https://doi.org/10.1130/0091-7613(1993)021<0789:OOTCPA>2.3.CO;2.

Gerritsen, D., Vaes, B., van Hinsbergen, D.J.J., 2022. Influence of data filters on the position and precision of paleomagnetic poles: what is the optimal sampling strategy? Geochem. Geophys. Geosyst. 23 e2021GC010269.

Giorgis, S., McClelland, W., Fayon, A., Singer, B.S., Tikoff, B., 2008. Timing of deformation and exhumation in the western Idaho shear zone. McCall, Idaho. Bull. Geol. Soc. Am. 120, 1119–1133. https://doi.org/10.1130/B26291.1.

Giorgis, S., Tikoff, B., McClelland, W., 2005. Missing Idaho arc: transpressional modification of the 87Sr/86Sr transition on the western edge of the Idaho batholith. Geology 33, 469–472. https://doi.org/10.1130/G20911.1.

Gnos, E., Khan, M., Mahmood, K., Khan, A.S., Shafique, N.A., Villa, I.M., 1998. Bela oceanic lithosphere assemblage and its relation to the Reunion hotspot. Terra Nov. 10, 90–95. https://doi.org/10.1046/j.1365-3121.1998.00173.x.

Goldfinger, C., Legg, M., Torres, M., 2000. New mapping and submersible observations of recent activity on the San Clemente Fault. Eos (Trans. Am. Geophys. Union) 81 (48), 1069.

Gourmelen, N., Dixon, T.H., Amelung, F., Schmalzle, G., 2011. Acceleration and evolution of faults: an example from the Hunter Mountain-Panamint Valley fault zone,Eastern California. Earth Planet. Sci. Lett. 301, 337–344. https://doi.org/10.1016/j.epsl.2010.11.016.

Graham, S.A., 1978. Role of Salinian Block in Evolution of San Andreas Fault System, California. Am. Assoc. Pet. Geol. Bull. 62, 2214–2231. https://doi.org/10.1306/C1EA53C3-16C9-11D7-8645000102C1865D.

Graham, S.A., Dickinson, W.R., 1978. Evidence for 115 kilometers of right slip on the San Gregorio-Hosgri fault trend. Science 199 (4325), 179–181.

Graham, S.A., Stanley, R.G., Bent, J.V., Carter, J.B., 1989. Oligocene and Miocene paleogeography of Central California and displacement along the San Andreas fault. Geol. Soc. Am. Bull. 101, 711–730. https://doi.org/10.1130/0016-7606(1989)101<0711:OAMPOC>2.3.CO;2.

Griscom, A., Jachens, R.C., Raymer, M.J., Ellsworth, W.L., 1990. Tectonic implications of gravity and magnetic models along east-west seismic profiles across the Great Valley near Coalinga. Coalinga, California. Earthq (May, 2), 69–78.

Guest, B., Niemi, N., Wernicke, B., 2007. Stateline fault system: a new component of the Miocene-Quaternary Eastern California shear zone. Bull. Geol. Soc. Am. 119, 1337–1346. https://doi.org/10.1130/0016-7606(2007)119[1337:SFSANC]2.0.CO.

Guilmette, C., Smit, M., van Hinsbergen, D., Gurer, D., Maffione, M., Rabeau, O., Savard, D., 2018. Forced subduction initiation recorded in the sole and crust of the 2 Semail ophiolite of Oman. Nat. Geosci. 11, 688–695.

Hacker, B.R., Mosenfelder, J.L., Gnos, E., 1996. Rapid emplacement of the Oman ophiolite: thermal and geochronologic constraints. Tectonics 15, 1230–1247. https://doi.org/10.1029/96TC01973.

Hagstrum, J.T., Jones, D.L., 1998. JonesPaleomagnetism, paleogeographic origins, and uplift history of the Coast Range ophiolite at Mount Diablo,California. J. Geophys. Res. Solid Earth 103, 597–603. https://doi.org/10.1029/97jb02785.

Hagstrum, J.T., Murchey, B.L., 1996. Paleomagnetism of Jurassic radiolarian chert above the Coast Range ophiolite at Stanley Mountain, California, and implications for its paleogeographic origins. Bull. Geol. Soc. Am. 108, 643–652. https://doi.org/10.1130/0016-7606(1996)108<0643:POJRCA>2.3.CO;2.

Hamilton, W., Myers, W.B., 1966. Cenozoic tectonics of the western United States. Rev. Geophys. 4, 509. https://doi.org/10.1029/RG004i004p00509.

Harper, G.D., 2003. Fe-Ti basalts and propagating-rift tectonics in the Josephine Ophiolite. Bull. Geol. Soc. Am. 115, 771–787. https://doi.org/10.1130/0016-7606(2003)115<0771:FBAPTI>2.0.CO;2.

Harper, G.D., Grady, K., Coulton, A.J., 1996. Origin of the amphibolite “sole” of the Josephine ophiolite: emplacement of a cold ophiolite over a hot arc. Tectonics 15, 296–313. https://doi.org/10.1029/95TC02525.

Harper, G.D., Grady, K., Wakabayashi, J., 1990. In: A structural study of a metamorphic sole beneath the Josephine ophiolite, western Klamath terrane, California-Oregon, pp. 379–396. https://doi.org/10.1130/SPE255-p379.

Harper, G.D., Saleeby, J.B., Heizler, M., 1994. Formation and emplacement of the Josephine ophiolite and the Nevadan orogeny in the Klamath Mountains, California-Oregon: U/Pb zircon and 40 Ar/ 39 Ar geochronology. J. Geophys. Res. Solid Earth 99, 4293–4321. https://doi.org/10.1029/93JB02061.

Hatem, A.E., Dolan, J.F., 2018. A Model for the Initiation, Evolution, and Controls on Seismic Behavior of the Garlock Fault, California. Geochemistry, Geophys. Geosystems 19, 2166–2178. https://doi.org/10.1029/2017GC007349.

Hébert, R., Bezard, R., Guilmette, C., Dostal, J., Wang, C.S., Liu, Z.F., 2012. The Indus-Yarlung Zangbo ophiolites from Nanga Parbat to Namche Barwa syntaxes, southern Tibet: first synthesis of petrology, geochemistry, and geochronology with incidences on geodynamic reconstructions of Neo-Tethys. Gondwana Res. 22, 377–397. https://doi.org/10.1016/j.gr.2011.10.013.

Hill, M. L., Dibblee, T. W., Jr., 1953. San Andreas, Garlock, and Big Pine faults, California: a study of the character, history, and tectonic significance of their displacements. Geological Society of America Bulletin 64 (4), 443–458.https://doi.org/10.1130/0016-7606(1953)64[443:SAGABP]2.0.CO;2.

Hildebrand, R.S., 2013. Mesozoic assembly of the North American cordillera. Spec. Pap. Geol. Soc. Am. 495, 1–42. https://doi.org/10.1130/2013.2495(a).

Hildebrand, R.S., 2009. Did westward subduction cause Cretaceous-Tertiary orogeny in the North American Cordillera? Geol. Soc. Am. 457.

Hooper, P.R., Camp, V.E., Reidel, S.P., Ross, M.E., 2007. He origin of the Columbia River flood basalt province: plume versus nonplume models. Geol. Soc. Am. Spec. Pap. 430, 635–668.

Hopson, C.A., Mattinson, J.M., Pessagno, E.A., Luyendyk, B.P., 2008. California Coast Range ophiolite: composite Middle and Late Jurassic oceanic lithosphere. Spec. Pap. Geol. Soc. Am. 438, 1–101. https://doi.org/10.1130/2008.2438(01).

Hopson, C.A., Mattinson, J.M., Pessagno, E.A.J., 1981. Coast Range Ophiolite, western California. In: Ernst, W.G. (Ed.), Geotecton. Dev. California. Prentice Hall, Englewood Cliffs, New Jersey, pp. 418–510.

Hull, D.M., Pessagno, E.A., 1994. Upper Jurassic Radiolarian biostratigraphy of Stanley Mountain, Southern California Coast Ranges. Geobios 27, 309–315. https://doi.org/10.1016/S0016-6995(94)80149-5.

Ingersoll, R.V., 2019. Forearc strike-slip displacement as an alternative to subduction erosion, with examples from Mexico and California (Sinistral Nacimiento fault). Can. J. Earth Sci. 56, 1285–1296. https://doi.org/10.1139/cjes-2018-0205.

Ingersoll, R.V., Schweickert, R.A., 1986. A plate-tectonic model for late Jurassic Ophiolite Genesis, Nevadan orogeny and forearc initiation, northern California. Tectonics 5, 901–912. https://doi.org/10.1029/TC005i006p00901.

Isozaki, Y., Aoki, K., Nakama, T., Yanai, S., 2010. New insight into a subduction-related orogen: a reappraisal of the geotectonic framework and evolution of the Japanese Islands. Gondwana Res. 18, 82–105. https://doi.org/10.1016/j.gr.2010.02.015.
Isozaki, Y., Maruyama, S., Furuoka, F., 1990. Accreted oceanic materials in Japan. Tectonophysics 181, 179–205. https://doi.org/10.1016/0040-1951(90)90016-2.
Jachens, R.C., Langenheim, V.E., Matti, J.C., 2002. Relationship of the 1999 Hector Mine and 1992 Landers fault ruptures to offsets on neogene faults and distribution of late Cenozoic basins in the eastern California shear zone. Bull. Seismol. Soc. Am. 92, 1592–1605. https://doi.org/10.1785/0120000915.
Jacobson, C.E., Grove, M., Pedrick, J.N., Barth, A.P., Marsaglia, K.M., Gehrels, G.E., Nourse, J.A., 2011. Late Cretaceous-early Cenozoic tectonic evolution of the southern California margin inferred from provenance of trench and forearc sediments. Bull. Geol. Soc. Am. 123, 485–506. https://doi.org/10.1130/B30238.1.
Jacobson, C.E., Oyarzabal, F.R., Haxel, G.B., 1996. Subduction and exhumation of the Pelona-Orocopia-Rand schists, southern California. Geology 24, 547. https://doi.org/10.1130/0091-7613(1996)024<0547:SAEOTP>2.3.CO;2.
Jarboe, N.A., Koppers, L., Tauxe, L., Minnett, R., Constable, C., 2012. The online MagIC Database: data archiving, compilation, and visualization for the geomagnetic, paleomagnetic and rock magnetic communities. n AGU Fall Meet. Abstr. 2012.
Jayko, A.S., Blake, M.C., Harms, T., 1987. Attenuation of the Coast Range Ophiolite by extensional faulting, and nature of the Coast Range "Thrust", California. Tectonics 6, 475–488. https://doi.org/10.1029/TC006i004p00475.
Johnston, S.M., Kylander-Clark, A.R.C., Chapman, A.D., 2018. Detrital zircon geochonology and evolution of the Nacimiento block late Mesozoic forearc basis, central California coast in Ingersoll.
Johnston, S.T., 2008. The cordilleran ribbon continent of North America. Annu. Rev. Earth Planet. Sci. 36, 495–530. https://doi.org/10.1146/annurev.earth.36.031207.124331.
Johnston, S.T., 2001. The Great alaskan Terrane Wreck: reconciliation of paleomagnetic and geological data in the northern Cordillera. Earth Planet. Sci. Lett. 193, 259–272. https://doi.org/10.1016/S0012-821X(01)00516-7.
Jones, D.L., Silberling, N.J., Hillhouse, J., 1977. Wrangellia - a Displaced Terrane in Northwestern North America. Can. J. Earth Sci. 14, 2565–2577. https://doi.org/10.1139/e77-222.
Kapp, P., DeCelles, P.G., 2019. Mesozoic-Cenozoic geological evolution of the Himalayan-Tibetan orogen and working tectonic hypotheses. Am. J. Sci. 319, 159–254. https://doi.org/10.2475/03.2019.01.
Karlstrom, K.E., Daniel, C.G., 1993. Restoration of Laramide right-lateral strike slip in northern New Mexico by using Proterozoic piercing points: tectonic implications from the Proterozoic to the Cenozoic. Geology 21, 1139–1142. https://doi.org/10.1130/0091-7613(1993)021<1139:ROLRLS>2.3.CO;2.
Kidder, S., Ducea, M.N., 2006. High temperatures and inverted metamorphism in the schist of Sierra de Salinas,California. Earth Planet. Sci. Lett. 241, 422–437. https://doi.org/10.1016/j.epsl.2005.11.037.
Kirschvink, J.L., 1980. The least-squares line and plane and the analysis of palaeomagnetic data. Geophys. J. Int. 62, 699–718. https://doi.org/10.1111/j.1365-246X.1980.tb02601.x.
Kistler, R.W., Wooden, J.L., Premo, W.R., Morton, D.M., 2014. Pb-Sr-Nd-O isotopic characterization of Mesozoic rocks throughout the northern end of the Peninsular Ranges batholith: isotopic evidence for the magmatic evolution of oceanic arc–continental margin accretion during the Late Cretaceous of southern California. In: Geological Society of American Memoir. Geological Society of America, pp. 263–316. https://doi.org/10.1130/2014.1211(07).
Knapp, J., Heizler, M.T., 1990. Thermal history of Crystalline Nappes of the Maria Fold and Thrust Belt, West Central Arizona. J. Geophys. Res. 95, 20049–20073.
Kosanke, S.B., 2000. The geology, geochronology, structure and geochemistry of the Wild Rogue wilderness remnant of the Coast Range ophiolite, Southwest Oregon: implications for the magmatic and tectonic evolution of the Coast Range ophiolite (Doctoral dissertation). State Univ. New York, Albany.
Koymans, M.R., Hinsbergen, D.J.J., Pastor-Galán, D., Vaes, B., Langereis, C.G., 2020. Towards FAIR paleomagnetic data management through Paleomagnetism.Org 2.0. Geochem. Geophys. Geosyst. 21 https://doi.org/10.1029/2019GC008838.
Koymans, M.R., Langereis, C.G., Pastor-Galán, D., van Hinsbergen, D.J.J., 2016. Paleomagnetism.Org: an online multi-platform open source environment for paleomagnetic data analysis. Comput. Geosci. 93, 127–137. https://doi.org/10.1016/j.cageo.2016.05.007.
Lahren, M.M., Schweickert, R.A., 1989. Proterozoic and lower Cambrian miogeoclinal rocks of Snow Lake pendant, Yosemite-Emigrant wilderness, Sierra Nevada, California: evidence for major early cretaceous dextral translation. Geology 17, 156. https://doi.org/10.1130/0091-7613(1989)017<0156:PALCMR>2.3.CO;2.
LaMaskin, T.A., Rivas, J.A., Barbeau, D.L., Schwartz, J.J., Russell, J.A., Chapman, A.D., 2022. A crucial geologic test of late Jurassic exotic collision versus endemic re-accretion in the Klamath Mountains Province, western United States, with implications for the assembly of western North America. GSA Bull. 134, 965–988. https://doi.org/10.1130/B35981.1.
Langenheim, V.E., Jachens, R.C., Graymer, R.W., Colgan, J.P., Wentworth, C.M., Stanley, R.G., 2013. Fault geometry and cumulative offsets in the central Coast Ranges, California: evidence for northward increasing slip along the San Gregorio-San Simeon-Hosgri fault. Lithosphere 5, 29–48. https://doi.org/10.1130/L233.1.
Lawton, T.F., Amato, J.M., Machin, S.E., Gilbert, J.C., Lucas, S.G., 2020. Transition from late Jurassic rifting to middle Cretaceous dynamic foreland, southwestern US and northwestern Mexico. Bulletin 132, 2489–2516.
Lease, R.O., McQuarrie, N., Oskin, M., Leier, A., 2009. Quantifying dextral shear on the Bristol-Granite mountains fault zone: successful geologic prediction from kinematic compatibility of the Eastern California Shear Zone. J. Geol. 117, 37–53. https://doi.org/10.1086/593320.
MacDonald, W.D., 1980. Net tectonic rotation, apparent tectonic rotation, and the structural tilt correction in paleomagnetic studies. J. Geophys. Res. Solid Earth 85, 3659–3669. https://doi.org/10.1029/JB085iB07p03659.
Maffione, M., Thieulot, C., van Hinsbergen, D.J.J., Morris, A., Plümper, O., Spakman, W., 2015a. Dynamics of intraoceanic subduction initiation: 1. Oceanic detachment fault inversion and the formation of supra-subduction zone ophiolites. Geochem.Geophys. Geosyst. 16, 1753–1770. https://doi.org/10.1002/2015GC005746.
Maffione, M., van Hinsbergen, D.J.J., 2018. Reconstructing Plate Boundaries in the Jurassic Neo-Tethys from the East and West Vardar Ophiolites (Greece and Serbia). Tectonics 37, 858–887. https://doi.org/10.1002/2017TC004790.
Maffione, M., Van Hinsbergen, D.J.J., Koornneef, L.M.T., Guilmette, C., Hodges, K., Borneman, N., Huang, W., Ding, L., Kapp, P., 2015b. Forearc hyperextension dismembered the south Tibetan ophiolites. Geology 43, 475–478. https://doi.org/10.1130/G36472.1.
Mankinen, E.A., Gromme, C.S., Williams, K.M., 1991. Concordant paleolatitudes from ophiolite sequences in the northern California Coast Ranges, U.S.A. Tectonophysics 198, 1–21. https://doi.org/10.1016/0040-1951(91)90127-E.
Martini, M., Solari, L., López-Martínez, M., 2014. Correlating the Arperos Basin from Guanajuato, Central Mexico, to Santo Tomás, southern Mexico: implications for the paleogeography and origin of the Guerrero terrane. Geosphere 10, 1385–1401. https://doi.org/10.1130/GES01055.1.
Matthews, V.I., 1976. Correlation of Pinnacles and Neenach Volcanic Formations and Their Bearing on San Andreas Fault Problem. Am. Assoc. Pet. Geol. Bull. 60. https://doi.org/10.1306/C1EA3A82-16C9-11D7-8645000102C1865D.
Mattinson, J.M., Hopson, C.A., Wright, J.E., Shervais, J.W., 2008. New high-precision CA-TIMS U-Pb zircon plateau ages for the Point Sal and San Simeon ophiolite remnants, California Coast Ranges. Spec. Pap. Soc. Am. 438, 103.
McCrory, P.A., Wilson, D.S., 2013. A kinematic model for the formation of the Siletz-Crescent forearc terrane by capture of coherent fragments of the Farallon and Resurrection plates. Tectonics 32, 718–736. https://doi.org/10.1002/tect.20045.
McDowell, F. W., Lehman, D. H., Gucwa, P. R., Fritz, D., Maxwell, J. C., 1984. Glaucophane schists and ophiolites of the northern California Coast Ranges: Isotopic ages and their tectonic implications. Geological Society of America Bulletin 95 (11), 1373–1382.https://doi.org/10.1130/0016-7606(1984)95<1373:GSAOOT>2.0.CO;2.
McLaughlin, R.J., Ohlin, H.N., 1984. In: Tectonostratigraphic framework of the Geysers-Clear Lake region, California, pp. 221–254.
McCulloh, T.H., 1981. Middle Tertiary Laumontite Isograd Offset 37 Km by Left-Lateral Strike-Slip on Santa Ynez Fault, California. Am. Assoc. Pet. Geol. Bull. 65, 956.
McFadden, P.L., McElhinny, M.W., 1988. The combined analysis of remagnetization circles and direct observations in palaeomagnetism. Earth Planet. Sci. Lett. 87, 161–172. https://doi.org/10.1016/0012-821X(88)90072-6.
McLaughlin, R.J., Blake, M.C., Griscom, A., Blome, C.D., Murchey, B., 1988. Tectonics of formation, translation, and dispersal of the Coast Range Ophiolite of California. Tectonics 7, 1033–1056. https://doi.org/10.1029/TC007i005p01033.
McLaughlin, R.J., Sliter, W.V., Sorg, D.H., Russell, P.C., Sarna-Wojcicki, A.M., 1996. Large-scale right-slip displacement on the East San Francisco Bay Region fault system, California: implications for location of late Miocene to Pliocene Pacific plate boundary. Tectonics 15, 1–18. https://doi.org/10.1029/95TC02347.
McQuarrie, N., Wernicke, B., 2005. An animated tectonic reconstruction of southwestern North America since 36 Ma. Geosphere 1, 147. https://doi.org/10.1130/GES00016.1.
McWilliams, M.O., Howell, D.G., 1982. Exotic terranes of western California. Nature 297, 215–217.
Memeti, V., Gehrels, G.E., Paterson, S.R., Thompson, J.M., Mueller, R.M., Pignotta, G.S., 2010. Evaluating the Mojave-Snow Lake fault hypothesis and origins of central Sierran metasedimentary pendant strata using detrital zircon provenance analyses. Lithosphere 2, 341–360. https://doi.org/10.1130/L58.1.
Miller, J., Miller, R., Wooden, J., Harper, G., 2003. Geochronologic links between the Ingalls ophiolite. In: North Cascades, Washington and the Josephine Ophiolite, Klamath Mts., Oregon and California: Geological Society of America Abstracts with Programs, p. 113.
Miller, R.B., Mattinson, J.M., Funk, S.A.G., Hopson, C.A., Treat, C.L., 1993. In: Tectonic evolution of Mesozoic rocks in the southern and central Washington Cascades, pp. 81–98.
Moores, E.M., Kellogg, L.H., Dilek, Y., 2000. Tethyan ophiolites, mantle convection, and tectonic "historical contingency": a resolution of the "ophiolite conundrum". Spec. Pap. Geol. Soc. Am. 349, 3–12. https://doi.org/10.1130/0-8137-2349-3.3.
Morley, C.K., 2017. Cenozoic rifting, passive margin development and strike-slip faulting in the Andaman Sea: a discussion of established v. new tectonic models. GeolSoc. London, Mem. 47, 27–50. https://doi.org/10.1144/M47.4.
Morris, A., Anderson, M.W., Omer, A., Maffione, M., van Hinsbergen, D.J.J., 2017. Rapid fore-arc extension and detachment-mode spreading following subduction initiation. Earth Planet. Sci. Lett. 478, 76–88. https://doi.org/10.1016/j.epsl.2017.08.040.
Morris, A., Anderson, M.W., Robertson, A.H.F., 1998. Multiple tectonic rotations and transform tectonism in an intraoceanic suture zone, SW Cyprus. Tectonophysics 299, 229–253. https://doi.org/10.1016/S0040-1951(98)00207-8.
Morris, A., Maffione, M., 2016. Is the Troodos ophiolite (Cyprus) a complete, transform fault-bounded Neotethyan ridge segment? Geology 44, 199–202. https://doi.org/10.1130/G37529.1.
Mulcahy, S.R., Starnes, J.K., Day, H.W., Coble, M.A., Vervoort, J.D., 2018. Early onset of Franciscan subduction. Tectonics 37, 1194–1209. https://doi.org/10.1029/2017TC004753.
Mullender, T.A.T., Frederichs, T., Hilgenfeldt, C., de Groot, L.V., Fabian, K., Dekkers, M. J., 2016. Automated paleomagnetic and rock magnetic data acquisition with an in-

line horizontal “2G” system. Geochem.Geophys. Geosyst. 17, 3546–3559. https://doi.org/10.1002/2016GC006436.
Müller, R.D., Cannon, J., Qin, X., Watson, R.J., Gurnis, M., Williams, S., Pfaffelmoser, T., Seton, M., Russell, S.H.J., Zahirovic, S., 2018. GPlates: building a virtual Earth through deep time. Geochem.Geophys. Geosyst. 19, 2243–2261. https://doi.org/10.1029/2018GC007584.
Nadin, E.S., Saleeby, J.B., 2008. Disruption of regional primary structure of the sierra Nevada batholith by the kern canyon fault system, California. Spec. Pap. Geol. Soc. Am. 438, 429–454. https://doi.org/10.1130/2008.2438(15).
Nicolas, A., Boudier, F., Ildefonse, B., Ball, E., 2000. Accretion of Oman and United Arab Emirates ophiolite—discussion of a new structural map. Mar. Geophys. Res. 21, 147–180.
Nokleberg, W.J., Parfenov, L.M., Monger, J.W.H., Norton, I.O., Khanchuk, A.I., Stone, D. B., Scotese, C.R., Scholl, D.W., Fujita, K., 2001. Phanerozoic tectonic evolution of the Circum-North Pacific. US Geol. Surv. Prof. Pap. 1–102.
Ohlin, H.N., McLaughlin, R.J., Moring, B.C., Sawyer, T.L., 2010. Geologic map of the Bartlett Springs Fault Zone in the vicinity of Lake Pillsbury and Adjacent Areas of Mendocino, Lake, and Glenn Counties , California By 94025.
Oldow, J.S., Geissman, J.W., Stockli, D.F., 2008. Evolution and strain reorganization within LateNeogene structural stepovers linking the Central Walker Lane and Northern Eastern California Shear Zone, Western Great Basin. Int. Geol. Rev. 50, 270–290. https://doi.org/10.2747/0020-6814.50.3.270.
Orme, D.A., Surpless, K.D., 2019. The birth of a forearc: the basal Great Valley Group, California, USA. Geology 47, 757–761. https://doi.org/10.1130/G46283.1.
Pálfy, J., Smith, P.L., Mortensen, J.K., 2000. A U-Pb and 40Ar/39Ar time scale for the Jurassic. Can. J. Earth Sci. 37, 923–944. https://doi.org/10.1139/cjes-37-6-923.
Pavlis, T.L., Amato, J.M., Trop, J.M., Ridgway, K.D., Roeske, S.M., Gehrels, G.E., 2019. Subduction polarity in ancient arcs: a call to integrate geology and geophysics to decipher the mesozoic tectonic history of the northern cordillera of North America. GSA Today 29, 4–10. https://doi.org/10.1130/GSATG402A.1.
Pearce, J.A., Lippard, S.J., Roberts, S., 1984. Characteristics and tectonic significance of supra-subduction zone ophiolites. Geol. Soc. LondonSpec. Publ 16, 77–94. https://doi.org/10.1144/GSL.SP.1984.016.01.06.
Pessagno, E.A.J., Hopson, C.A., Mattinson, J.M., Blome, C.D., Luyendyk, B.P., Hull, D., Beebe, W.J., 1996. In: Coast Range Ophiolite and its sedimentary cover (California Coast Ranges): Jurassic stratigraphy and northward tectonic transport. Phiolites Ocean. Crust New Insights from F. Stud. Ocean DrillProgr. Geol. Soc. Am. Spec. Pape, 349, pp. 383–394.
Piccardo, G.B., Padovano, M., Guarnieri, L., 2014. The Ligurian Tethys: Mantle processes and geodynamics. Earth-Sci. Rev. 138, 409–434. https://doi.org/10.1016/j.earscirev.2014.07.002.
Platt, J.P., 1986. Dynamics of orogenic wedges and the uplift of high-pressure metamorphic rocks. Geol. Soc. Am. Bull. 97, 1037. https://doi.org/10.1130/0016-7606(1986)97<1037:DOOWAT>2.0.CO;2.
Platt, J.P., 1975. Metamorphic and deformational processes in the Franciscan Complex, California: some insights from the Catalina Schist terrane. Geol. Soc. Am. Bull. 86, 1337. https://doi.org/10.1130/0016-7606(1975)86<1337:MADPIT>2.0.CO;2.
Plunder, A., Bandyopadhyay, D., Ganerød, M., Advokaat, E.L., Ghosh, B., Bandopadhyay, P., Hinsbergen, D.J.J., 2020. History of subduction polarity reversal during arc-continent collision: constraints from the Andaman Ophiolite and its Metamorphic Sole. Tectonics 39. https://doi.org/10.1029/2019TC005762.
Porkoláb, K., Duretz, T., Yamato, P., Auzemery, A., Willingshofer, E., 2021. Extrusion of subducted crust explains the emplacement of far-travelled ophiolites. Nat. Commun. 12 https://doi.org/10.1038/s41467-021-21866-1.
Pourteau, A., Scherer, E.E., Schorn, S., Bast, R., Schmidt, A., Ebert, L., 2019. Thermal evolution of an ancient subduction interface revealed by Lu–Hf garnet geochronology, Halilbağı Complex (Anatolia). Geosci. Front. 10, 127–148. https://doi.org/10.1016/j.gsf.2018.03.004.
Powell, Robert Edward, 1981. Geology of the Crystalline Basement Complex, Eastern Transverse Ranges, Southern California: Constraints on Regional Tectonic Interpretation. (Doctoral Dissertation). California Institute of Technology. https://resolver.caltech.edu/CaltechETD:etd-07252007-135803.
Powell, R.E., Weldon, R.J., 1992. Evolution of the San Andreas Fault. Annu. Rev. Earth Planet. Sci. 20, 431–468. https://doi.org/10.1146/annurev.ea.20.050192.002243.
Powell, R.E., 1993. Balanced palinspastic reconstruction of pre-late Cenozoic paleogeography, southern California: Geologic and kinematic constraints on evolution of the San Andreas fault system, in The San Andreas Fault System: Displacement, Palinspastic Reconstruction and Geologic Evolution, edited by R.E. Powell, R.J. Weldon II, and J.C. Matfi, Mere. Geol. Soc. Am., 178, 1- 106. https://doi.org/10.1130/MEM178-p1.
Raymond, L.A., 2018. What is Franciscan?: revisited. Int. Geol. Rev. 60, 1968–2030. https://doi.org/10.1080/00206814.2017.1396933.
Reidel, S.P., Camp, V.E., Tolan, T.L., Kauffman, J.D., Garwood, D.L., 2013. Tectonic evolution of the Columbia River flood basalt province. Spec. Pap. Geol. Soc. Am. 497, 293–324. https://doi.org/10.1130/2013.2497(12).
Reidel, S.P., Fecht, K.R., Hutter (Harrold), I.L., Tolan, T.L., Chamness, M.A., 2021. The Olympic-Wallowa lineament: a new look at an old controversy. GSA Bull. 133, 115–133. https://doi.org/10.1130/B35454.1.
Ring, U., Brandon, M.T., 1994. Kinematic data for the Coast Range fault and implications for exhumation of the franciscan subduction complex. Geology 22, 735. https://doi.org/10.1130/0091-7613(1994)022<0735:KDFTCR>2.3.CO;2.
Rioux, M., Bowring, S., Kelemen, P., Gordon, S., Miller, R., Dudás, F., 2013. Tectonic development of the Samail ophiolite: high-precision U-Pb zircon geochronology and Sm-Nd isotopic constraints on crustal growth and emplacement. J. Geophys. Res. Solid Earth 118, 2085–2101. https://doi.org/10.1002/jgrb.50139.
Robertson, A.H., 2002. Overview of the genesis and emplacement of Mesozoic ophiolites in the Eastern Mediterranean Tethyan region. Lithos 65, 1–67. https://doi.org/10.1016/S0024-4937(02)00160-3.
Rodgers, D.W., Hackett, W.R., Ore, H.T., 1990. Extension of the Yellowstone plateau, eastern Snake River Plain, and Owyhee plateau. Geology 18, 1138. https://doi.org/10.1130/0091-7613(1990)018<1138:EOTYPE>2.3.CO;2.
Rollinson, H., 2017. Masirah – the other Oman ophiolite: a better analogue for mid-ocean ridge processes? Geosci. Front. 8, 1253–1262. https://doi.org/10.1016/j.gsf.2017.04.009.
Ross, J.A., Sharp, W.D., 1988. The effects of sub-blocking temperature metamorphism on the K/Ar systematics of hornblendes: 40Ar/39Ar dating of polymetamorphic garnet amphibolite from the Franciscan Complex,California. Contrib. Mineral. Petrol. 100, 213–221. https://doi.org/10.1007/BF00373587.
Rutte, D., Garber, J., Kylander-Clark, A., Renne, P.R., 2020. An Exhumation Pulse from the Nascent franciscan Subduction Zone (California, USA). Tectonics 39. https://doi.org/10.1029/2020TC006305.
Saleeby, J.B., Blake, M.C., Coleman, R.S., 1984. Pb/U zircon ages on thrust plates of west central Klamath Mountains and Coast Ranges, northern California and southern Oregon. EOS (Trans. Am. Geophys. Union) 65, 1147.
Saleeby, J.B., Ducea, M.N., Busby, C.J., Nadin, E.S., Wetmore, P.H., 2008. Chronology of pluton emplacement and regional deformation in the southern Sierra Nevada batholith,California. Spec. Pap. Geol. Soc. Am. 438, 397–427. https://doi.org/10.1130/2008.2438(14).
Saleeby, J.B., Shaw, H.F., Niemeyer, S., Moores, E.M., Edelman, S.H., 1989. U/Pb, Sm/Nd and Rb/Sr geochronological and isotopic study of northern Sierra Nevada ophiolitic assemblages,California. Contrib. Mineral. Petrol. 102, 205–220. https://doi.org/10.1007/BF00375341.
Schellart, W.P., Stegman, D.R., Farrington, R.J., Freeman, J., Moresi, L., 2010. Cenozoic tectonics of Western North America controlled by evolving width of Farallon Slab. Science (80-.) 329, 316–319. https://doi.org/10.1126/science.1190366.
Schmidt, W.L., Platt, J.P., 2018. Subduction, accretion, and exhumation of coherent franciscan blueschist-facies rocks, northern Coast Ranges, California. Lithosphere 10, 301–326. https://doi.org/10.1130/L697.1.
Schwartz, J.J., Snoke, A.W., Cordey, F., Johnson, K., Frost, C.D., Barnes, C.G., LaMaskin, T.A., Wooden, J.L., 2011. Late Jurassic magmatism, metamorphism, and deformation in the Blue Mountains Province, Northeast Oregon. Geol. Soc. Am. Bull. 123, 2083–2111. https://doi.org/10.1130/B30327.1.
Sears, J.W., 2001. Emplacement and denudation history of the Lewis-Eldorado-Hoadley thrust slab in the northern Montana Cordillera, USA: Implications for steady-state orogenic processes. Am. J. Sci. 301, 359–373. https://doi.org/10.2475/ajs.301.4-5.359.
Sharman, G.R., Graham, S.A., Grove, M., Hourigan, J.K., 2013. A reappraisal of the early slip history of the San Andreas fault, Central California, USA. Geology 41, 727–730. https://doi.org/10.1130/G34214.1.
Sharman, G.R., Graham, S.A., Grove, M., Kimbrough, D.L., Wright, J.E., 2015. Detrital zircon provenance of the late Cretaceous-Eocene California forearc: influence of laramide low-angle subduction on sediment dispersal and paleogeography. Bull. Geol. Soc. Am. 127, 38–60. https://doi.org/10.1130/B31065.1.
Sharp, R.V., 1981. Variable rates of late Quaternary strike slip on the San Jacinto fault zone, southern California. J. Geophys. Res. 86, 1754–1762. https://doi.org/10.1029/JB086iB03p01754.
Shervais, J.W., 2001. Birth, death, and resurrection: the life cycle of suprasubduction zone ophiolites. Geochem. Geophys. Geosyst. 2 https://doi.org/10.1029/2000GC000080.
Shervais, J.W., Choi, S.H., Sharp, W.D., Ross, J., Zoglman-Schuman, M., Mukasa, S.B., 2011. Serpentinite matrix mélange: implications of mixed provenance for mélange formation. In: Mélanges: Processes of Formation and Societal Significance. Geological Society of America. https://doi.org/10.1130/2011.2480(01).
Shervais, J.W., Kimbrough, D.L., 1985. Geochemical evidence for the tectonic setting of the Coast Range ophiolite: a composite island arc–oceanic crust terrane in western California. Geology 13, 35. https://doi.org/10.1130/0091-7613(1985)13<35:GEFTTS>2.0.CO;2.
Shervais, J.W., Kimbrough, D.L., Renne, P., Hanan, B.B., Murchey, B., Snow, C.A., Zoglman Schuman, M.M., Beaman, J., 2004. Multi-stage origin of the Coast Range Ophiolite, California: implications for the life cycle of Supra-Subduction Zone Ophiolites. Int. Geol. Rev. 46, 289–315. https://doi.org/10.2747/0020-6814.46.4.289.
Shervais, J.W., Murchey, B.L., Kimbrough, D.L., Renne, P.R., Hanan, B., 2005. Radioisotopic and biostratigraphic age relations in the Coast Range Ophiolite, northern California: implications for the tectonic evolution of the Western Cordillera. Bull. Geol. Soc. Am. 117, 633–653. https://doi.org/10.1130/B25443.1.
Sigloch, K., Mihalynuk, M.G., 2013. Intra-oceanic subduction shaped the assembly of Cordilleran North America. Nature 496, 50–56. https://doi.org/10.1038/nature12019.
Sims, J.D., 1993. In: Chapter 6: Chronology of displacement on the San Andreas fault in central California: Evidence from reversed positions of exotic rock bodies near Parkfield, California, pp. 231–256. https://doi.org/10.1130/MEM178-p231.
Snavely, P.D., MacLeod, N.S., Wagner, H.C., 1968. Tholeiitic and alkalic basalts of the Eocene Siletz River Volcanics, Oregon Coast Range. Am. J. Sci. 266, 454–481. https://doi.org/10.2475/ajs.266.6.454.
Snortum, E., Day, J.M.D., 2020. Forearc origin for Coast Range Ophiolites inferred from osmium isotopes and highly siderophile elements. Chem. Geol. 550, 119723 https://doi.org/10.1016/j.chemgeo.2020.119723.
Speed, R.C., Sleep, N.H., 1982. Antler orogeny and foreland basin: a model. Geol. Soc. Am. Bull. 93, 815. https://doi.org/10.1130/0016-7606(1982)93<815:AOAFBA>2.0.CO;2.

Staudigel, H., Gee, J., Tauxe, L., Varga, R.J., 1992. Shallow intrusive directions of sheeted dikes in the Troodos ophiolite: anisotropy of magnetic susceptibility and structural data. Geology 20, 841. https://doi.org/10.1130/0091-7613(1992)020<0841:SIDOSD>2.3.CO;2.

Stern, R.J., Bloomer, S.H., 1992. Subduction zone infancy: examples from the Eocene Izu-Bonin-Mariana and Jurassic California arcs. Geol. Soc. Am. Bull. 104, 1621–1636. https://doi.org/10.1130/0016-7606(1992)104<1621:SZIEFT>2.3.CO;2.

Stern, R.J., Reagan, M., Ishizuka, O., Ohara, Y., Whattam, S., 2012. To understand subduction initiation, study forearc crust: to understand forearc crust, study ophiolites. Lithosphere 4, 469–483. https://doi.org/10.1130/L183.1.

Stetson-Lee, T.A., 2015. Using kinematics and orientational statistics to interpret deformational events: separating the Ahsahka and Dent shear zones near Orofino, ID 115. https://doi.org/10.13140/RG.2.1.2699.5925.

Stewart, J.H., 1967. Possible large right-lateral displacement along fault and shear zones in the Death Valley-Las Vegas Area, California and Nevada. Bull. Geol. Soc. Am. 78, 131–142. https://doi.org/10.1130/0016-7606(1967)78[131:PLRDAF]2.0.CO;2.

Stewart, J., Ernst, W., 1988. In: Tectonics of the Walker Lane belt, western Great Basin: Mesozoic and Cenozoic deformation in a zone of shear. Metamorph. crustal Evol. West. United States. 7, pp. 683–713.

Suppe, J., 1970. Offset of Late Mesozoic Basement Terrains by the San Andreas Fault System. Geol. Soc. Am. Bull. 81, 3253–3258.

Surpless, K.D., Graham, S.A., Covault, J.A., Wooden, J.L., 2006. Does the Great Valley Group contain Jurassic strata? Reevaluation of the age and early evolution of a classic forearc basin. Geology 34, 21. https://doi.org/10.1130/G21940.1.

Surpless, K.D., Gulliver, K.D.H., 2018. Provenance analysis of the Ochoco basin, Central Oregon: a window into the late cretaceous paleogeography of the northern U. SCordillera. Spec. Pap. Geol. Soc. Am. 540, 235–266. https://doi.org/10.1130/2018.2540(11).

Takahahshi, E., Nakajima, K., Wright, T.L., 1998. Origin of the Columbia River basalts: melting model of a heterogeneous plume head. Earth Planet. Sci. Lett. 162, 63–80. https://doi.org/10.1016/S0012-821X(98)00157-5.

Tauxe, L., Gee, J.S., Staudigel, H., 1998. Flow directions in dikes from anisotropy of magnetic susceptibility data: the bootstrap way. J. Geophys. Res. Solid Earth 103, 17775–17790. https://doi.org/10.1029/98JB01077.

Tauxe, L., Shaar, R., Jonestrask, L., Swanson-Hysell, N.L., Minnett, R., Koppers, A.A.P., Constable, C.G., Jarboe, N., Gaastra, K., Fairchild, L., 2016. PmagPy: Software package for paleomagnetic data analysis and a bridge to the Magnetics Information Consortium (MagIC) Database. Geochem.Geophys. Geosyst. 17, 2450–2463. https://doi.org/10.1002/2016GC006307.

Titus, S.J., Davis, J.R., 2021. Problems with net tectonic rotation for dikes and suggestions for alternative approaches. Geochem. Geophys. Geosyst. 22 https://doi.org/10.1029/2020GC009395.

Torsvik, T.H., Van der Voo, R., Preeden, U., Mac Niocaill, C., Steinberger, B., Doubrovine, P.V., van Hinsbergen, D.J.J., Domeier, M., Gaina, C., Tohver, E., Meert, J.G., McCausland, P.J.A., Cocks, L.R.M., 2012. Phanerozoic polar wander, palaeogeography and dynamics. Earth-Sci. Rev. 114, 325–368. https://doi.org/10.1016/j.earscirev.2012.06.007.

Tosdal, R.M., 1990. Constraints on the tectonics of the Mule Mountains Thrust Southeast California and Southwest Arizona. J. Geophys. Res. 95, 20025–20048.

Truex, J.N., 1976. Santa Monica and Santa Ana Mountains—relation to Oligocene Santa Barbara basin. AAPG Bulletin 60 (1), 65–86.

Unruh, J.R., Dumitru, T.A., Sawyer, T.L., 2007. Coupling of early Tertiary extension in the Great Valley forearc basin with blueschist exhumation in the underlying franciscan accretionary wedge at Mount Diablo,California. Bull. Geol. Soc. Am. 119, 1347–1367. https://doi.org/10.1130/B26057.1.

van der Meer, D.G., Spakman, W., Van Hinsbergen, D.J.J., Amaru, M.L., Torsvik, T.H., 2010. Towards absolute plate motions constrained by lower-mantle slab remnants. Nat. Geosci. 3, 36–40. https://doi.org/10.1038/ngeo708.

van der Meer, D.G., Torsvik, T.H., Spakman, W., van Hinsbergen, D.J.J., Amaru, M.L., 2012. Intra-Panthalassa Ocean subduction zones revealed by fossil arcs and mantle structure. Nat. Geosci. 5, 215–219.

van der Meer, D.G., van Hinsbergen, D.J.J., Spakman, W., 2018. Atlas of the underworld: Slab remnants in the mantle, their sinking history, and a new outlook on lower mantle viscosity. Tectonophysics 723, 309–448. https://doi.org/10.1016/j.tecto.2017.10.004.

van Hinsbergen, D.J.J., Maffione, M., Koornneef, L.M.T., Guilmette, C., 2019. Kinematic and paleomagnetic restoration of the Semail ophiolite (Oman) reveals subduction initiation along an ancient Neotethyan fracture zone. Earth Planet. Sci. Lett. 518, 183–196. https://doi.org/10.1016/j.epsl.2019.04.038.

van Hinsbergen, D.J.J., Schouten, T.L.A., 2021. Deciphering paleogeography from orogenic architecture: constructing orogens in a future supercontinent as thought experiment. Am. J. Sci. 321, 955–1031. https://doi.org/10.2475/06.2021.09.

van Hinsbergen, D.J.J., Torsvik, T.H., Schmid, S.M., Maţenco, L.C., Maffione, M., Vissers, R.L.M., Gürer, D., Spakman, W., 2020. Orogenic architecture of the Mediterranean region and kinematic reconstruction of its tectonic evolution since the Triassic. Gondwana Res. https://doi.org/10.1016/j.gr.2019.07.009.

Vedder, J.G., McLean, H., Stanley, R.G., Wiley, T.J., 1991. Paleogeographic implications of an erosional remnant of Paleogene rocks southwest of the Sur-Nacimiento Fault Zone, southern Coast Ranges,California. Geol. Soc. Am. Bull. 103, 941–952. https://doi.org/10.1130/0016-7606(1991)103<0941:PIOAER>2.3.CO;2.

Wagner, D.L., Fleck, R.J., McLaughlin, R.J., Sarna-Wojcicki, A.M., Calhan, K.B., Bezore, S., 2005. New constraints on the age and distribution of Cenozoic volcanics north of San Pablo Bay, California: implications for displacement along faults inboard of the San Andreas fault. In: Geological Society of America Abstracts with Programs 37, p. 83.

Wahrhafting, C.W., 1984. Structure of the Marin Headlands Block, California: A progress report. In: Blake Jr., M.C. (Ed.), Fr. Geol. North. Calif. Los Angeles, California, Pacific Sect. Soc. Econ. Paleontol. Mineral. 43, pp. 31–50.

Wakabayashi, J., 2022. Along-strike variation in accretion, non-accretion, and subduction erosion recorded in rocks of the Jurassic-Neogene Convergent Plate margin of California. Front. Earth Sci. 10 https://doi.org/10.3389/feart.2022.818171.

Wakabayashi, J., 2021b. Subduction and exhumation slip accommodation at depths of 10–80 km inferred from field geology of exhumed rocks: evidence for temporal-spatial localization of slip. In: Plate Tectonics, Ophiolites, and Societal Significance of Geology: A Celebration of the Career of Eldridge Moores. Geological Society of America, pp. 257–296. https://doi.org/10.1130/2021.2552(12).

Wakabayashi, J., 2021a. Field and petrographic reconnaissance of Franciscan complex rocks of Mount Diablo, California: imbricated ocean floor stratigraphy with a roof exhumation fault system. In: Regional Geology of Mount Diablo, California: Its Tectonic Evolution on the North America Plate Boundary. Geological Society of America, pp. 155–178. https://doi.org/10.1130/2021.1217(09).

Wakabayashi, J., 2015. Anatomy of a subduction complex: architecture of the franciscan complex, California, at multiple length and time scales. Int. Geol. Rev. 57, 669–746. https://doi.org/10.1080/00206814.2014.998728.

Wakabayashi, J., 1999a. Subduction and the rock record: concepts developed in the Franciscan Complex,California. Spec. Pap. Geol. Soc. Am. 338, 123–133. https://doi.org/10.1130/0-8137-2338-8.123.

Wakabayashi, J., 1999b. Distribution of displacement on and evolution of a young transform fault system: the northern San Andreas fault system, California. Tectonics 18, 1245–1274. https://doi.org/10.1029/1999TC900049.

Wakabayashi, J., 1992. Nappes, tectonics of Oblique Plate convergence, and metamorphic evolution related to 140 million years of continuous subduction, Franciscan Complex,California. J. Geol. 100, 19–40. https://doi.org/10.1086/629569.

Wakabayashi, J., Dilek, Y., 2003. What constitutes 'emplacement' of an ophiolite?: Mechanisms and relationship to subduction initiation and formation of metamorphic soles. Geol. Soc. LondonSpec. Publ. 218, 427–447. https://doi.org/10.1144/GSL.SP.2003.218.01.22.

Wakabayashi, J., Dumitru, T.A., 2007. 40Ar/39Ar ages from coherent, high-pressure metamorphic rocks of the Franciscan Complex, California: revisiting the timing of metamorphism of the world's type subduction complex. Int. Geol. Rev. 49, 873–906. https://doi.org/10.2747/0020-6814.49.10.873.

Wakabayashi, J., Ghatak, A., Basu, A.R., 2010. Suprasubduction-zone ophiolite generation, emplacement, and initiation of subduction: a perspective from geochemistry, metamorphism, geochronology, and regional geology. Geol. Soc. Am. Bull. 122, 1548–1568. https://doi.org/10.1130/B30017.1.

Wakabayashi, J., Hengesh, J.V., Sawyer, T.L., 2004. Four-dimensional transform fault processes: progressive evolution of step-overs and bends. Tectonophysics 392, 279–301. https://doi.org/10.1016/j.tecto.2004.04.013.

Wakabayashi, J., Shimabukuro, D.H., 2022. The contrasting geologic record of inferred "hot" intraoceanic and "cold" continental margin subduction initiation. In: From the Guajira Desert to the Apennines, and from Mediterranean Microplates to the Mexican Killer Asteroid: Honoring the Career of Walter Alvarez. Geological Society of America. https://doi.org/10.1130/2022.2557(11).

Wallace, C.A., Lidke, D.J., Schmidt, R.G., 1990. Faults of the central part of the Lewis and Clark line and fragmentation of the late cretaceous foreland basin in west-Central Montana. Geol. Soc. Am. Bull. 102, 1021–1037. https://doi.org/10.1130/0016-7606(1990)102<1021:FOTCPO>2.3.CO;2.

Weil, A.B., Yonkee, A., Schultz, M., 2016. Tectonic evolution of a Laramide transverse structural zone: Sweetwater Arch, south Central Wyoming. Tectonics 35, 1090–1120. https://doi.org/10.1002/2016TC004122.

Weil, A.B., Yonkee, A., Sussman, A., 2010. Reconstructing the kinematic evolution of curved mountain belts: a paleomagnetic study of Triassic red beds from the Wyoming salient, Sevier thrust belt, U.S.A. Geol. Soc. Am. Bull. 122, 3–23. https://doi.org/10.1130/B26483.1.

Wells, R., Bukry, D., Friedman, R., Pyle, D., Duncan, R., Haeussler, P., Wooden, J., 2014. Geologic history of Siletzia, a large igneous province in the Oregon and Washington Coast Range: correlation to the geomagnetic polarity time scale and implications for a long-lived Yellowstone hotspot. Geosphere 10, 692–719. https://doi.org/10.1130/GES01018.1.

Wernicke, B., 1981. Low-angle normal faults in the Basin and Range Province: nappe tectonics in an extending orogen. Nature 291, 645–648.

Wernicke, B., Burchfiel, B., Lipman, P., Zoback, M., 1992. Cenozoic extensional tectonics of the US Cordillera. Geol. North Am. 3, 553–582.

Wesnousky, S.G., 2005. Active faulting in the Walker Lane. Tectonics 24, n/a-n/a. https://doi.org/10.1029/2004TC001645.

Williams, K.M., 1984. Geologic map and cross sections of the Coast Range Ophiolite at Mount Diablo, Contra Costa County, California. https://doi.org/10.3133/ofr84553.

Williams, K.M., 1983. The Mount Diablo Ophiolite, Contra Costa County. San Jose State University, California.

Williams, T.A., Graham, S.A., 2013. Controls on forearc basin architecture from seismic and sequence stratigraphy of the Upper Cretaceous Great Valley Group, Central Sacramento Basin,California. Int. Geol. Rev. 55, 2030–2059. https://doi.org/10.1080/00206814.2013.817520.

Woodward, L.A., Anderson, O.J., Lucas, S.G., 1997. Mesozoic stratigraphic constraints on Laramide right slip on the east side of the Colorado Plateau. Geology 25, 843–846. https://doi.org/10.1130/0091-7613(1997)025<0843:MSCOLR>2.3.CO;2.

Wu, J.T.-J., Wu, J., Okamoto, K., 2022. Intra-oceanic arc accretion along Northeast Asia during Early Cretaceous provides a plate tectonic context for North China craton

destruction. Earth-Sci. Rev. 226, 103952 https://doi.org/10.1016/j.earscirev.2022.103952.
Wyld, S.J., 2002. Structural evolution of a Mesozoic backarc fold-and-thrust belt in the U. S. Cordillera: new evidence from northern Nevada. Bull. Geol. Soc. Am. 114, 1452–1468. https://doi.org/10.1130/0016-7606(2002)114<1452:SEOAMB>2.0.CO;2.
Wyld, S. J., Wright, J. E., 1988. The Devils Elbow ophiolite remnant and overlying Galice Formation: new constraints on the Middle to Late Jurassic evolution of the Klamath Mountains, California. Geological Society of America Bulletin 100 (1), 29–44. 10.1130/0016-7606(1988)100<0029:TDEORA>2.3.CO;2.
Wyld, S.J., Wright, J.E., 2001. New evidence for cretaceous strike-slip faulting in the United States cordillera and implications for terrane-displacement, deformation patterns, and plutonism. Am. J. Sci. 301, 150–181. https://doi.org/10.2475/ajs.301.2.150.
Xenophontos, C., Bond, G.C., 1978. Petrology, sedimentation and paleogeography of the Smartville terrane (Jurassic) - bearing on the genesis of the Smartville ophiolite. In: Howell, B., MacDougall, I. (Eds.), Mesozoic paleogeography West United States. Soc Econ Paleontol. Mineral, pp. 291–302.
Yonkee, W.A., Eleogram, B., Wells, M.L., Stockli, D.F., Kelley, S., Barber, D.E., 2019. Fault Slip and Exhumation History of the Willard Thrust Sheet, Sevier Fold-Thrust Belt, Utah: Relations to Wedge Propagation, Hinterland Uplift, and Foreland Basin Sedimentation. Tectonics 38, 2850–2893. https://doi.org/10.1029/2018TC005444.
Yonkee, A., Weil, A.B., 2010. Reconstructing the kinematic evolution of curved mountain belts: internal strain patterns in the Wyoming salient, Sevier thrust belt, U.S.A. Geol. Soc. Am. Bull. 122, 24–49. https://doi.org/10.1130/B26484.1.
Yonkee, W.A., Weil, A.B., 2015. Tectonic evolution of the Sevier and Laramide belts within the north American Cordillera orogenic system. Earth-Sci. Rev. 150, 531–593. https://doi.org/10.1016/j.earscirev.2015.08.001.
Yule, J.D., Saleeby, J.B., Barnes, C.G., Snoke, A.W., 2006. A rift-edge facies of the late Jurassic Rogue-Chetco arc and Josephine ophiolite, Klamath Mountains,Oregon. Spec. Pap. Soc. Am 410, 53.
Zahirovic, S., Müller, R.D., Seton, M., Flament, N., 2015. Tectonic speed limits from plate kinematic reconstructions. Earth Planet. Sci. Lett. 418, 40–52. https://doi.org/10.1016/j.epsl.2015.02.037.
Zijderveld, J.D.A., 1967. A. C. Demagnetization of rocks: analysis of results. In: Collinson, D.W., Creer, K.M., Runcorn, S.K. (Eds.), Methods in Palaeomagnetism. Elsevier, New York, pp. 254–286.